ISTANBUL TECHNICAL UNIVERSITY ★ GRADUATE SCHOOL OF SCIENCE ENGINEERING AND TECHNOLOGY

AN EXPERIMENTAL INVESTIGATION OF HIGH PURITY SINGLE WALLED CARBON NANOTUBES AS TRANSPARENT ELECTRODE MATERIALS

M.Sc. THESIS

Mozhgan LAKI

Department of Nano Science and Nano Engineering

Nano Science and Nano Engineering Graduate Program

MAY 2015

**ISTANBUL TECHNICAL UNIVERSITY ★ GRADUATE SCHOOL OF SCIENCE
ENGINEERING AND TECHNOLOGY**

**AN EXPERIMENTAL INVESTIGATION
OF HIGH PURITY SINGLE WALLED CARBON NANOTUBES
AS TRANSPARENT ELECTRODE MATERIALS**

M.Sc. THESIS

**Mozhgan LAKI
(513121010)**

Department of Nano Science and Nano Engineering

Nano Science and Nano Engineering Graduate Program

Thesis Advisor: Assoc. Dr. Elif Ülkü ARICI

MAY 2015

İSTANBUL TEKNİK ÜNİVERSİTESİ ★ FEN BİLİMLERİ ENSTİTÜSÜ

**TEK DUVARLI KARBON NANOTÜP SAFLAŞTIRMASI
VE GEÇİRGEN ELEKTROT OLUŞTURULMASI KONUSUNDA DENEYSEL
ÇALIŞMALAR**

YÜKSEK LİSANS TEZİ

**Mozhgan LAKI
(513121010)**

Nano Bilim ve Nano Mühendislik Anabilim Dalı

Nano Bilim ve Nano Mühendislik Programı

Tez Danışmanı: Assoc. Dr. Elif Ülkü ARICI

MAYIS 2015

Mozhgan Iaki, a **M.Sc.** student of ITU **Graduate School of Science, Engineering and Technology** student ID` **513121010**, successfully defended the **thesis** entitled "**AN EXPERIMENTAL INVESTIGATION OF HIGH PURITY SINGLE WALLED CARBON NANOTUBES AS TRANSPARENT ELECTRODE MATERIALS**", which he/she prepared after fulfilling the requirements specified in the associated legislations, before the jury whose signatures are below.

Thesis Advisor :   **Assoc. Dr. Elif Ülkü ARICI**   ....
İstanbul Technical University

Jury Members :   **Prof. Dr. Nilgün YAVUZ**   ....
İstanbul Technical University

                         Prof. Dr. Serap GÜNEŞ   ....
Yildiz Technical University

Date of Submission : 4 MAY 2015
Date of Defense   : 25 MAY 2015

To my family and my love,

x

FOREWORD

I would like to express my deepest gratitude to my advisor Assoc. Prof. Dr. Elif Ülkü Arıcı for the continuous support during my research, for their motivation, enthusiasm and knowledge. I would like to thank Prof. Dr. Nilgün Karatepe YAVUZ and Prof. Dr. Üner ÇOLAK for giving me the opportunity to work in their project.
I would also like to thank Ahmet GULTEKIN, Amin TABATABAEI, and Ridvan ERGUN for their invaluable technical supports.
Lastly and most importantly, I thank my parents who have supported me all through my life and in all times, good and bad.

February 2015   Mozhgan LAKI
                                                                          (Nano Engineering)

TABLE OF CONTENTS

ABBREVIATIONS

AZO   :Aluminum Doped Zinc Oxide
AFM   : Atomic force microscopy
BHJ   : Bulk-heterojunction device
CMC   : Critical micellar concentration
CNPs   : Carbon nanoparticles
CNT   : Carbon nanotubes
CVD   : Chemical Vapor Deposition
DMF   : Dimethyl formamide
DOC   : Sodium deoxycholate
DSSC   : Dye-sensitized solar cell
EDS   : Energy dispersive spectroscopy
FTO   : Fluorine doped tin oxide
HOMO   : Highest occupied molecular orbital
HOPG   : Highly Oriented Pyrolitic Graphite
ITO   : Tin-doped indium-oxide
LUMO   : Lowest unoccupied molecular orbital
MOCVD   : Metal organic chemical vapor deposition
MOMBD   : Metal organic molecular beam deposition
MWCNT   : Multi-walled carbon nanotubes
NIR   : Near-infrared spectroscopy
NMP   : N-Methyl-2-pyrrolidone
OPV   : Organic Photovoltaic
PEDOT: PSS : Poly(3,4-ethylenedioxythiophene) Polystyrene sulfonate
PET   : Polyethylene terephthalate
PLD   : Pulsed laser deposition
RBM   : Radial breathing mode
SC   : Sodium cholate
SDBS   : Sodium dodecylbenzene sulfonate
SDeC   : Sodium deoxy cholate
SDS   : Sodium dodecyl sulfate
SEM   : Scanning electron microscope
SS   : Steroid-based surfactants
SWCNT   : Single Walled Carbon Nanotubes
TCOs   : Transparent and conducting oxides
TEM   : Transmission electron microscopy
TGA   : Thermogravimetric analysis
UVO   : Ultraviolet Ozone Cleaner

LIST OF TABLES

LIST OF FIGURES

AN EXPERIMENTAL INVESTIGATION OF HIGH PURITY SINGLE WALLED CARBON NANOTUBES AS TRANSPARENT ELECTRODE MATERIALS

SUMMARY

Thin films of carbon nanotubes (CNTs) are suitable alternatives to indium tin oxide, the mostly used transparent electrode for opto-electronic devices and solar cells. A big advantage of CNTs is their thin film preparation from solution together with high flexibility.

A three step chemical method using suitable surfactants in acidic media has been applied to purify and to dope carbon nanotubes synthesized by CVD method. A purity of more than 98 wt. % is verified by thermal gravimetric analysis, X-ray and Raman spectroscopy. We prepared afterwards highly transparent and continuous fine mesh structured CNT thin films using different surfactants via spin coating. The balance between thin film morphology and conductivity is controlled by the molecular interactions between the surfactants and CNT bundles. These interactions have been classified by contact angle measurements. Surfactants having strong interactions with CNT walls can form easily large-scale thin films, but the replacement of the insulating surfactant and doping of the CNTs electrode is more effective, when the molecular interactions are weak. Therefore, electrochemical properties of the prepared CNT electrodes are characterized using cyclic voltammetry, for comparison.

Our studies demonstrate that CNT thin film preparation using SDS (Sodium dodecyl sulphate) leads to better performing CNT electrodes in comparison to electrodes investigated using DOC (Sodium deoxycholate), NMP (N-Methyl-2-pyrrolidone) and SDBS (Sodium dodecylbenzene sulfonate) as surfactants.

YÜKSEK SAFLIKTA TEK CİDARLI KARBON NANOTÜPLERİ ŞEFFAF ELEKTRODU MALZEMELERİ OLARAK DENEYSEL İNCELENMESİ

ÖZET

Dünya ekonomisi hızla büyüdükçe, enerji tüketimi çok hızlı bir şekilde artmaktadır Bu enerjinin büyük bir kısmı bilindiği üzere fosil yakıtlardan sağlanmaktadır. fosil yakıtlar atmosferdeki CO_2 derişimini arttırmakta ve dolayısıyla gerek çevre gerek iklim üzerinde olumsuz etkiler yaratmaktadır. Bu olumsuz etkiler dünya genelinde sıcaklık ortalamasının 1900'lü yıllara oranla yaklaşık 1 derece artmasına ve iklimsel dengelerin değişmesine yol açmıştır. Bu nedenlerle, tüm dünyada petrol ve doğal gaza daha az bağımlı, çevre-dostu yenilenebilir enerji kaynaklarının geliştirilmesi ve günlük hayatımıza uyarlanması arayışı içine girilmiştir.

Her yıl Dünya yüzeyine düşen güneş enerjisi, tüm dünyanın yıllık enerji tüketiminin 15.000 katıdır. Bu devasa enerji kaynağından yararlanabilmek, enerji probleminin çözümü için en ideal yoldur. Güneş panelleri, gürültüsüz, zehirli artıklar üretmeyen, sera gazı yayımı olmayan, kurulduktan sonra bakım gerektirmeyen bir teknoloji olduğu gibi, elektrik enerjisi istendiğinde, son kullanıcının yakınında üretilebilmekte ve taşıma kayıplarını ve masraflarını da ortadan kaldırmaktadır.

Günei enerjisi teknolojilerin bir kısmı güneş enerjisini ısı enerjisine dönüştüren kollektör sistemleri olup, diğer önemli teknoloji ise, güneş enerjisini elektrik enerkisine çeviren fotovoltaik sistemlerdir.

Güneş pilleri olarakta adlandırılan bu cihazlarda, yarıiletken malzemelerin ışığı soğurması ile oluşan eksitonların (elektron-boşluk çifti), iki elektrot arasında oluşan elektrik alanında ayrışması (dissaziation) ve elektronların katoda, pozitif yük taşıyan boşlukların ise anoda yönlenmesi ile elektrik akımı üretilir.

Klasik silikon kökenli güneş pilleri üretiminde; kullanılan ileri teknoloji, malzemenin saflaştırılması ve kristallenmesi için gereken yüksek ısı (1500-1800 C), ince tabaka oluşturulurken kaybolan malzeme ve benzeri nedenlerden dolayı harcanan enerji yüksektir. Seri üretime geçildiğinden, inorghanik güneş pillerinde maliyetler giderek azalmıştır. Enerji dönüşüm verimi yaklaşık olarak % 15-%17 civarındadır.

organik güneş pillerin dönüşümün temel basamakları, güneş ışığının soğurulması, yük ayrışması, yük transportu ve yüklerin toplanmasıdır. Konjuge polimerlerde π-bağlarını oluşturan delokalize Pz – orbitalleri, gerçekte iki farklı orbital meydana getirmektedirler: düşük enerjili bağlayıcı orbitaller (π) ve yüksek enerjili karşıt bağlayıcı orbitaller (π^*). Bu iki orbital arasındaki enerji farkı organik yarıiletken malzemenin enerji bant aralığına (Eg) karşılık gelir.

Bant aralığı değerleri 0,5 eV' tan 4 eV'a kadar değişen yarı iletken konjuge polimerler, çoğunluğu görünür bölge ışığından etkilenir. Işık, yeterli bir enerji ile molekül tarafından soğurulduğunda, bir elektron temel hal enerji bandından (HOMO) uyarılmış hal enerji bandına (LUMO) geçer.yani, enerji bant aralığına eşit veya daha büyük enerjide ışığın soğurulması ile π^*-orbitallerinde elektron ve π-

orbitallerinde elektron boşluğu meydana getirilmektedir. İletkenlik bandındaki elektronları ve valans bandındaki elektron boşluklarının serbest olunur. Eksitonun ayrışması, metal kontak ile organik yarıiletken ara yüzeyinde veya farklı elektron akseptör veya donör özellikteki molekül ara yüzeyinde gerçekleşebilir. Yarıiletken polimer ve fulleren türevlerinin harmanlanması ile oluşturulan katmanlarda. Elektron ilgisi daha yüksek olan malzeme diğerinin iletkenlik bandından (ELUMO, Donör) elektron alabilir, bu nedenle de akseptör olarak adlandırılır. Düşük iyonlaşma potansiyeline (I_P) sahip malzeme ise temas halinde bulunduğu yarıiletkenin değerlik bandından (V_B) elektron boşluğu alabilir, bu nedenle boşluk iletken malzeme ya da elektron donör malzeme olarak adlandırılmaktadır. Yüklerin transferinin, iyonlaşma potansiyeli düşük olan donör ve elektron ilgisi (E_A) yüksek olan akseptörün ara yüzeyinde meydana gelir. Organik güneş pili, iş fonksiyonu farklı iki metal elektrot arasına yapılan aygıtlardır. Bu elektrotlardan bir tanesi anot diğeri de katottur. Katot elektron alarak indirgenen malzemeyi anot ise elektron vererek yükseltgenen malzemeyi ifade eder. Elektrik alanının ayırdığı yükler çoğunlukta oldukları bölgelere gittikten sonra elektron, elektron alıcısı olan katoda, boşluk ise anoda doğru çekilir ve böylelikle elektrik alanının ayırdığı bu yükler devrede dolanarak akıma katılmış olurlar.

İdeal morfoloji, eksiton difüzyon mesafesinin 10 nm civarı olduğu varsayılırsa, iç içe geçmiş donör/akseptör ağ yapısının 10 nm'lik bir nanomorfolojiye sahip olmasını gerektirir. Böylece, olabildiğince uzun donör/akseptör ara yüzeyinde, donör polimerin ışıkla etkileşimi sayesinde oluşan eksitonlar, ara yüzeyde etkili bir şekilde ayrışırlar. Diğer yandan, ayrışmış yüklerin elektrotlara ulaştırılabilmesi için hem donör hem de akseptör ağının mümkün olduğunca kesintisiz bir şekilde zıt elektrotlara yönlenmesi gerekmektedir. Bütün bu senaryo, hacim heteroeklem güneş pillerinde nano-morfolojinin ne kadar önemli olabileceğini göstermektedir.

Organik güneş pilleri Yarı-iletken polimerler, sıvı kristaller, fulleren türevi 1-(3-metoksikarbonil) propil 1-1 fenil-[6,6]-metanofulleren (PCBM) gibi organik çözeltilerden ince film oluşturabilen malzemeler, püskürtme, dönel-kaplama (spin-coating) teknolojisi, esnek veya sert elektrot tabakaları üzerine hazırlanabilirler, ve bu teknolojinin getirdiği avantajlarla (üretim maliyeti düşük, her türlü elektrot üzerine kaplanabilen, esnek, hafif, seri üretime uygun, boyutları kullanım alanına göre rahatlıkla uyarlanabilen) özdeşleşirken, küçük organik moleküller vakum işleminin getirdiği avantajlarla (az malzeme sarfı, üretim kontrolü kolay teknoloji) yanı sıra, hafif ve esnek olmaları da anılırlar. Ucuz üretim teknolojisinin, güneş pillerinin, günlük hayatta kullanılmasına (Laptop charger, mobile charger,...) imkan verir.

Organik güneş pilleri, verimliliği arttırıldığı takdirde, gerek düşük maliyetleri, gerekse esnek, hafif, katlanabilir yapıları nedeniyle bazı kulanım alanlarında, inorganik güneş pillerinin yerini alabilir.

Organik güneş pillerinde en kritik faktör, uluslararası birçok araştırma grubunun da üzerinde çalıştığı, maliyet artışı olmadan enerji dönüşüm verimliliğinin arttırılması konusudur.

Opto-elektronik cihazlarda ve güneş pillerinde elektrot olarak genelde indium çinko oksit (ITO) kaplı cam tabakalar kullanılır. Indium kaynaklarının az olması nedeniyle, bu malzeme gün geçtikce, pahalılaşmaktadır. Karbon nanotüp (CNT) ince filmleri, şeffaf elektrot ITO) yerine kullanılabilecek en uygun alternatiflerdir.

CNT'lerın en büyük avantajı yüksek esneklikte ince film oluşturmasıdır. Ayrıca bu filmlerin çözeltiden hazırlanması, maliyeti düşürür.

Sentez sonrasında SWNTlerde 1:3 oranında metalik NT oluşmaktadır. 2:3 oranında ise p- tipi yarıiletkenlik özelliğine sahip SWNT oluşmaktadır. Metalik SWNTler ışık geçirgen iken, p-tipi olanlar ışığı (......nm)de soğurur. Ancak, instristik olarak p-tipi iletkenliğe sahip CNT yüzeyleri çok düşük miktarda katkı maddeleri (HNO_3 vs.) kullanılarak % 85 - % 90 oranında ışık geçirgen, iletken tabakalar oluşturmak mümkündür.

 CNT katkılanması hem serbest yük miktarını arttırdığından hem de tüpler arasındaki direnci azalttığından, CNT iletkenliğini katkılayıcı derişimine bağlı olarak, yarı-iletken CNTleri metalik CNTlere dönüştürür.

CVD yöntemi ile sentezlenmiş karbon nanotüpleri, asidik ortam içinde uygun yüzey aktif maddeler kullanılarak ve dört aşamalı kimyasal yöntemiyle saflaştırmak ve doplama uygulanır. Isıl ağırlık analiz metodu (TGA) , X-ışını (X-Ray) ve Raman ölçümleri kullanılarak saflaştırma yönteminin dört basamakları sonunda % 98 üzeri saf CNT ağırlığına ulaşım, doğrulanır. Çözelti, püskürtme, dönel kaplama (spin-coating), daldırmalı kaplama (dip-coating) yöntemleriyle olabileceği gibi, kimyasal buharlaştırma yöntemiyle de, CNT ince filmleri hazırlanmaktadır. CNT ince film hazırlanmasında risk teşkil eden faktörler, morfolojide kararlılık, az pürüzlü yüzeylerin oluşturulması, kontrollü ve homojen p-tipi kararlı katkılanma, homojen optik/elektriksel geçirgenlik olabilir esnek veya sert elektrot tabakaları üzerine hazırlanabilirler esnek veya sert elektrot tabakaları üzerine hazırlanabilirler esnek veya sert elektrot tabakaları üzerine hazırlanabilirler esnek veya sert elektrot tabakaları üzerine hazırlanabilirler. bu calışma da çözeltı çok şeffaf ve sürekli ince örgü spin kaplama üzerinden farklı yüzey aktif kullanan CNT ince filmler yapılandırılmış hazırlanan. spin kaplama yontemıle ve farklı yüzey aktif maddeler kullanarak son derece şeffaf ve gayet iyi gözenekli yapılı CNT ince filmler hazırlandı. İnce film morfolojisi ve iletkenlik arasındaki denge, yüzey aktif maddeler ve CNT demetleri arasındaki moleküler etkileşimler tarafından kontrol edilir. Bu etkileşimler temas açısı ölçümleri tarafından sınıflandırılmıştır. CNT duvarları ile güçlü etkileşimlere sahip olan yüzey aktif maddeler, kolayca büyük ölçekli ince filmler oluştururlar. Ancak moleküler etkileşimler zayıf olduğundan, yalıtkan yüzey aktif madde değiştirilmesi ve CNT elektrot doping daha etkilidir. Bu nedenle, elde CNT elektrotların elektro-kimyasal özellikleri, karşılaştırma amacıyla, çevrimsel voltametre karakterize edilir. Çalışmalarımız göstermektedir ki, SDS (sodyum dodesil sülfat) ile hazırlanmış CNT ince film elektrotları, DOC (sodyum deoksikolat), NMP (N-metil-2-pirolidon) ve SDBS (sodyum dodesilbenzen sülfonat), yüzey aktif madde olarak kullanılarak CNT elektrotlar, kıyasla daha iyi performans yol açtığını göstermektedir.

1. INTRODUCTION

1.1   Photovoltaic

Photovoltaic devices or solar cells are very simple devices which convert radiation, in the visible wavelength range (400-750nm), into electricity. The majority of commercially available solar cells work on what is known as a p-n junction and consist entirely of a junction between ntype and p-type semiconductors. These semiconductors have different Fermi Energies (E_F). When a junction is formed by putting these two semiconductors together, holes diffuse from the p-type to the n-type semiconductor and vice versa for electrons. The diffusion of these majority carriers unscreen the ionized acceptors in the p-type and the ionized donors in the n-type semiconductor. in Figure 1.1 The difference in Fermi energies in a n- and p-type semiconductor has shown.this energies diffrence cause the diffusion of free carriers. These carriers unscreen ionized acceptors which uncover an electric field, ϵ , opposite the direction of diffusion. The region near the junction where there is an electric field is known as the depletion region, since it has no free carriers, or the space charge region.
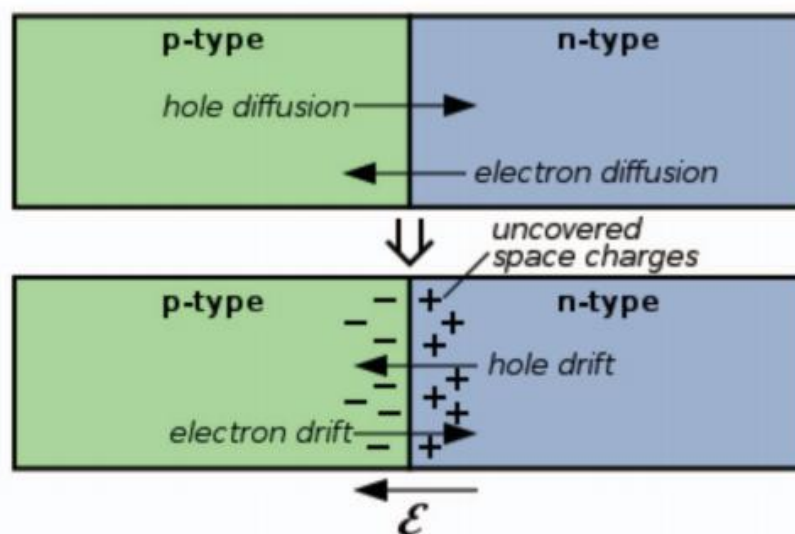
Figure 1.1: The difference in Fermi energies in a n- and p-type semiconductor.

The region where this electric field is present is known as the depletion region (because there are effectively no free carriers) or the space-charge region (SCR) and the potential difference in the region is known as the built-in voltage (V_{bi}). The distance the SCR extends into the semiconductor layer is directly related to the dopant density of that semiconductor. Traditional p-n junction solar cells require doped semiconductor material that can be very expensive to produce in sufficient purity.

A photon possessing an energy less than the bandgap of the absorber layer will pass through the material without absorption. A photon with an energy much greater than the bandgap will be weakly interacting, due to the relatively small density of states at higher energies. A photon with an energy equal to or slightly larger than the bandgap of the absorber layer can create an electron-hole pair by promoting an electron from the valence to the conduction band. If this pair is generated in the quasi-neutral region of the p/n-junction, then the electron and hole will diffuse randomly until eventually recombining. If, however, the electron and hole is generated within a diffusion length of the depletion region, then the electric field will separate the pair, causing electrons to go down the potential towards the n-type semiconductor while holes flow up the potential towards the p-type semiconductor. Shown in fgure 1.2. Collection of these charges and flow through a circuit yields a current. There are thus three different processes that must occur for a photocurrent to be generated. (1) A photon must be absorbed.(2) An exciton pair must be dissociated.(3) The respective carriers must propagate through the junction to the contacts.
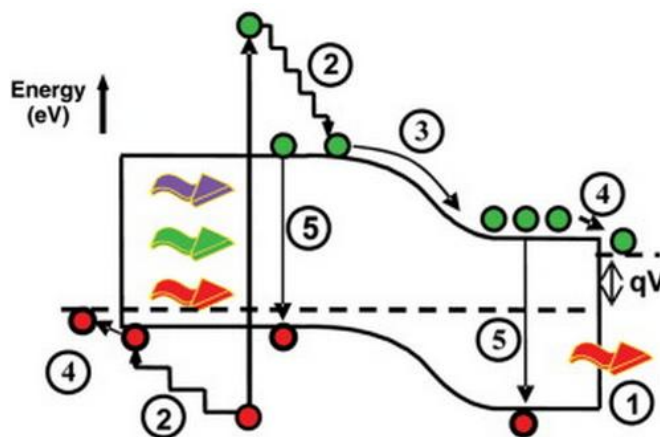
Figure 1.2 : Loss processes in a solar cell: (1) nonabsorption of below-bandgap photons; (2) lattice thermalization loss; (3) , (4) junction and contact voltage losses; (5) recombination loss.[1]

To compare and analyze a solar cell's efficiency standard conditions must be chosen, as the intensity of solar radiation fluctuates depending on time of day, latitude and weather. To compensate for the changing angle of the sun a system called air mass values is used. Air mass values (AM) are used to determine the angle the sun is from the Earth's surface and thus the amount of atmosphere that the light has had to traverse, as seen in the Figure 1.3
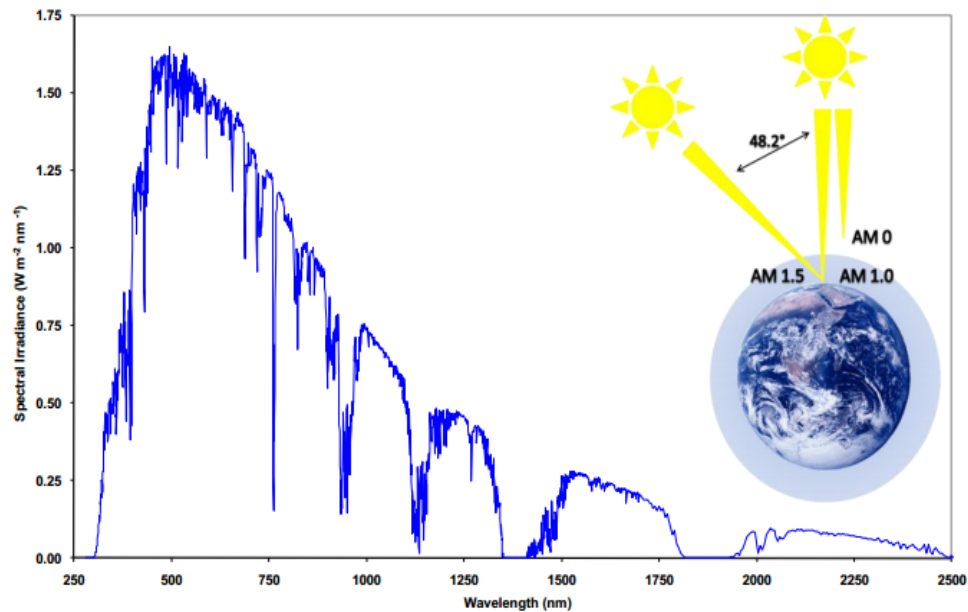
Figure 1.3 : AM 1.5 solar spectrum (Inset: air mass schematic showing; AM 0, AM
      1.0 and AM 1.5)

When the window layer and absorber layer are made from the same material which has been n- and p-doped, then the cell is known as a homojunction. If, however, the window layer is a different material than the absorber layer, the device is known as a heterojunction. Heterojunctions have an advantage over homojunctions because the window layer may be chosen to have a wider bandgap than the absorber layer. This means than the window layer is totally transparent to any photons which would be absorbed by the absorber layer. In a homojunction, the difference in doping results in a difference in the Fermi energy between the window and absorber layers. In a heterojunction, the difference in Fermi energies is determined by the work functions (energy required to remove an electron from E_F) and bandgaps of the materials. Therefore, a heterojunction doesn't necessarily require any external doping or modifications of any kind to set up a SCR [2]. A complete working junction could be formed simply by bringing together the window and absorber layers and adding

contacts to each side (Figure 1.4). Heterojunctions do have two distinct disadvantages. The first is that since the window and absorber layers are composed of different materials, they most likely exhibit atomic disregistry from the mismatch of lattice parameters. If this dis-registry is large enough, it can induce strain and form defects, which act as recombination sites, reducing the efficiency of the device. The second is that for a wide bandgap window layer and narrow bandgap absorber layer (such as a CdS/CdTe junction), discontinuities in the conduction and valence band develop due to the difference in bandgaps between the materials.
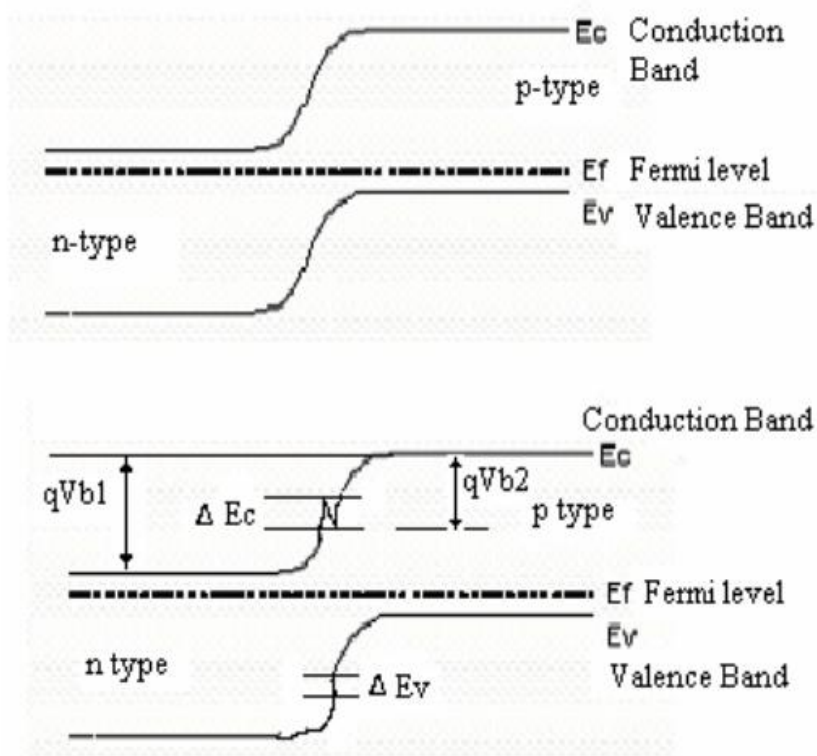
Figure 1.4: Band Alignments in Homojunction (top) and Heterojunction (bottom)

This extended band gap will allow better current generation from high energy photons. Further series resistance can also be lower for a heterojunction if the window layer is able to be heavily doped. The only modification to the p-n junction to turn it into a solar cell is the addition of suitable contacts. One of the contacts would have to be semi-transparent to permit the light; or alternatively it could also be a metal grid that only covered a small part of the device. When the front contact used is a semi-transparent oxide, the material used is classified as transparent conducting oxide (TCO). The back contact need only be chemically and physically compatible with the adjacent material. concerning to figure1.5, it can be seen that the n-type

material is facing the light. So light passes through the n-type material and reaches the p-type material.
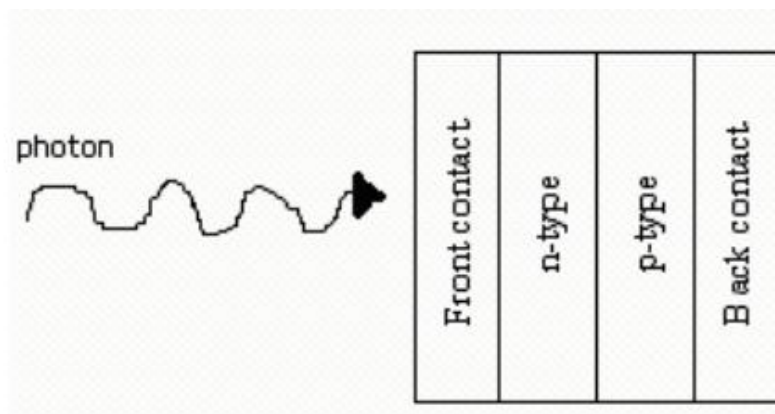
Figure1.5: Basic Structure of a Solar Cell.

The p-type material is indicated to as absorber so it should be able of absorb the photons with energy equal or greater than it's band gap. n-type material should be large band gap devices, to prevent optical losses, And they should be as thin as possible to permit most of the light to enter the p-type material. Solar cells can be manufactured in a variety of ways and with a variety of materials. as shown in Table 1.1 Solar cells can be categorized into three main types.

Table 1.1: Different Types of Materials Used to Make Solar Cells

Crystalline	Thin Film	Other
Cyrstalline Silicon	Amorphous Silicon (a-Si)	Quantum dot solar cels
	Thin Film Silicon	Dye sensitized photochemical cells
Gallium Arsenide (GeAs) and Aloys	Copper Indium Diselenide (CIS)	Polymer Cells
	Cadmium Telluride (CdTe)	Photoelectrochimical Cells

1.2   Organic photovoltaics

Organic photovoltaics are devices based on semiconducting organic molecular and polymeric materials. The organic, polymer-based photovoltaic elements have introduced for obtaining cheap and easy methods to produce electricity from sunlight with using flexible polymers. Because of these polymers high band gaps, OPVCs have lower efficiencies when compared to inorganic photovoltaic cells. Materials which have a delocalized π electron system can absorb sunlight, create

5

photogenerated charge carriers, and transport these charge carriers. For example, phthalocyanine and perylene have commonly sue in thin film organic solar cells. [3] Phthalocyanine is a p-type, hole conducting material that works as electron donor, whereas perylene and its derivatives show an n-type, electron conducting behavior and serve as electron-acceptor material
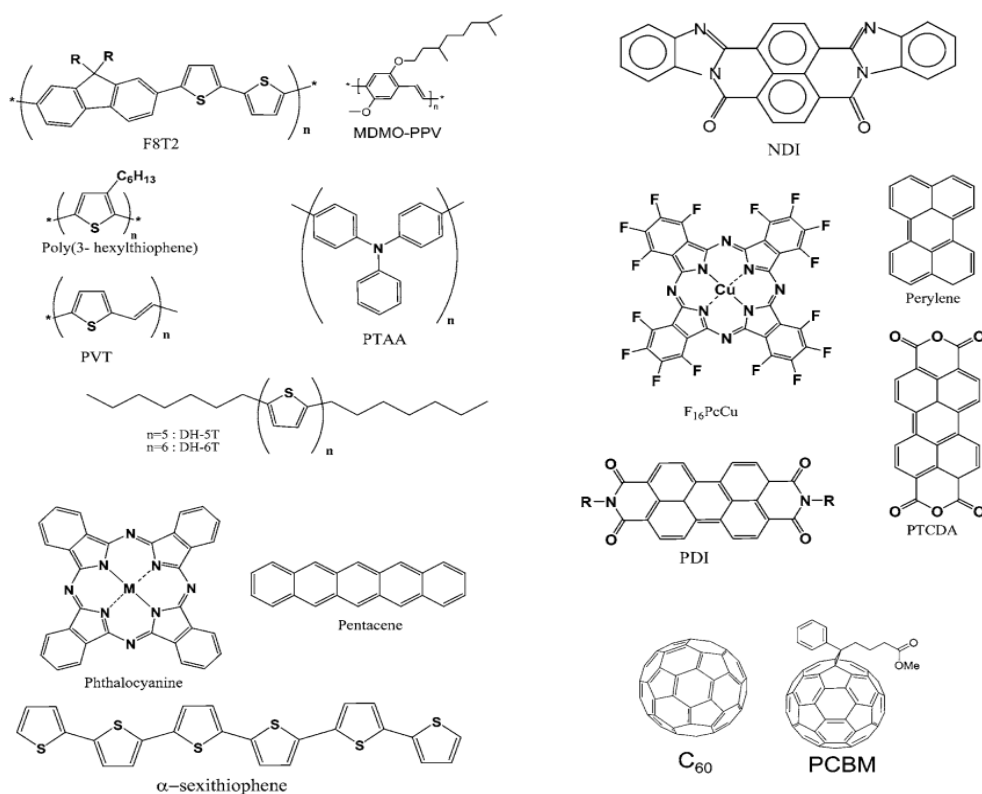
Figure 1.6: Common organic semiconducting materials including donor materials and acceptor materials.

One difference between inorganic and organic semiconductors is the charge carrier mobility. The primary photoexcitation's in organic materials do not directly and quantitatively lead to free charge carriers. In inorganic semiconductors have 3D crystal lattice structures that result in high carrier mobilities , while organic semiconductors only have ordering along the molecular stalk through overlapping π orbitals and as a result require a "hopping" type mechanism to facilitate charge propagation from one molecular unit or polymer chain to another as shown in figure 1.7. This hopping mechanism results in charge carrier mobilities, which are strongly dependent on the layer morphology.
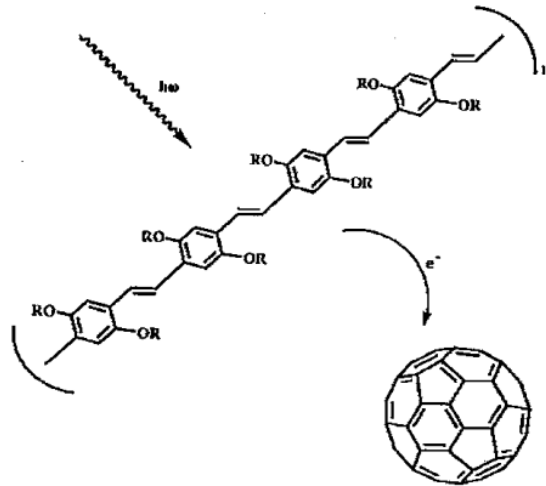
Figure 1. 7 : Illustration of the photoinduced charge transfer with a sketch of the energy level [3]

For efficient photovoltaic devices, the created charges need to be transported to the appropriate electrodes within their lifetime. The charge carriers need a driving force to reach the electrodes. when the delocalized electron is excited from its highest occupied molecular orbital (HOMO) to the lowest unoccupied molecular orbital (LUMO) it can move along the conjugated backbone of the molecule. The difference in energies between the LUMO and HOMO levels of a molecule is its band gap.

$$EG = E(LUMO) - E(HOMO) \tag{1.1}$$

This internal electrical field determines the maximum open circuit voltage (V_{oc}). Materials are selected as electron-donating and electron-accepting based on their HOMO and LUMO levels with respect to one another. It is possible for one organic material to be an acceptor to another organic material while that same material is a donor to yet another organic material. Donor and Acceptor organic materials are analogous to p- and n-type inorganic materials, respectively. An electron-donating material, or Donor, has a high HOMO level or low ionization potential. While an electron-accepting material, or Acceptor, has a low LUMO level or high electron dependence. The location of the HOMO and LUMO bands, their relationship to the ionization potential and electron affinity is shown in figure1.8. The complete four-step photocurrent generation process starting from an absorbed photon and ending with charges collected at the electrodes is depicted in figure 1. 8.

a) The absorption of a photon results in an exciton,

b) the exciton diffuses towards the donor - acceptor interface (the heterojunction)

c) the bound electron hole pair disassociates into free carriers, and

d) the free carriers transport towards the electrodes for collection.

Each of these steps has its corresponding loss mechanism, namely, non-absorbed photons in step a, exciton decay in step b, geminate recombination of the bound pair in step c, and bimolecular recombination in step d. Loss mechanisms are also indicated:

(1) non-absorbed photons,

(2) exciton decays,

(3) geminate recombination's of the bound pair

(4) bimolecular recombination's.
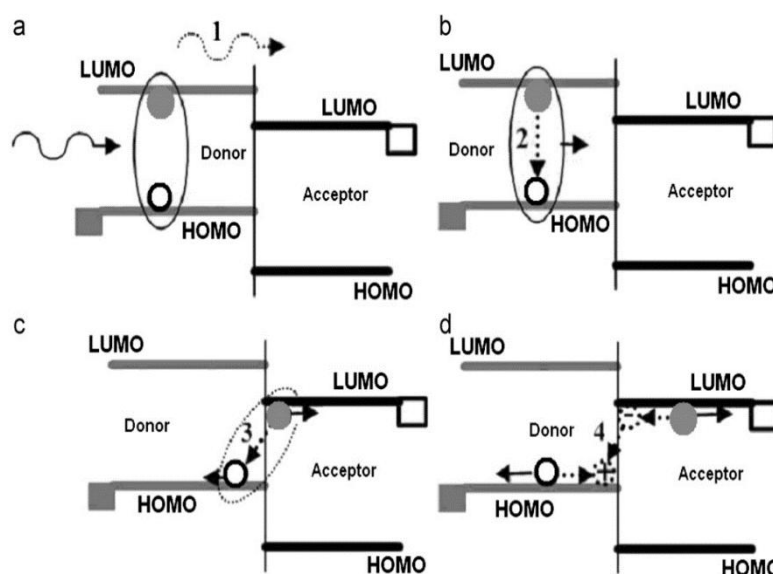
Figure 1. 8: The scheme of the operative sequence of an OPVC.[4]

There are different types of D–A interface structures. in 1985 at Kodak laboratories where Tang developed a two layer organic photovoltaic (OPV) using semiconducting molecules to function as a donor and acceptor [5] and the power conversion efficiency was over 1%. The simple bilayer cells are made via sandwiching two layers of organic electronic materials between two metallic conductors, typically a layer of indium tin oxide (ITO) with high work function and a layer of low work function metal such as Al, Mg, or Ca. The organic layer with higher EA and IP is the acceptor, and the other organic layer is the donor. The basic structure of such cell is illustrated in Figure 1.9 the geometry of this type guarantees directional photoinduced charge transfer across the interface. After the exciton dissociation, both

types of charge carriers travel in different layers. Therefore, the chance for recombination is significantly reduced. The limiting factor on this type of heterojunction cells is the short length of the interfacial area.
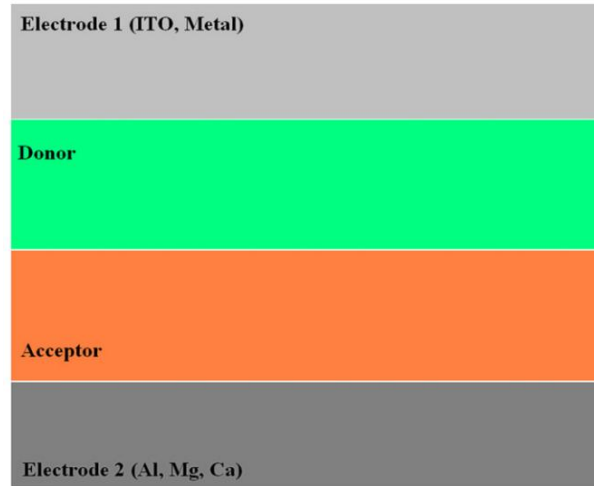
Figure 1. 9: The basic structure of a simple bilayer heterojunction**.**[4]

A new structure based on the mixture of the electron donor and acceptor material is prepared to increase the interfacial area length and thus to improve exciton dissociation efficiency. This mixture of materials spin coated on the surface to form a heterojunction layer, also called as bulk heterojunction as illustrated Figure 1.10. Devices employing the BHJ active layer have a donor-acceptor interface that is distributed throughout the photoactive layer, although ultrafast charge transfer helps with exciton dissociation and a strong electrical due to asymmetric electrodes helps separated excitons move towards collecting electrodes there is no promise that a pathway exists between the point of dissociation and collection. The availability and formation of pathways has to do with the nanoscale morphology. The excitons generated may reach the D–A interface more readily for efficient disassociations. The electrons then move to the acceptor domains and are carried through the device to be collected by one electrode, while the holes are pulled toward the opposite direction to be collected atthe other side. BHJs have higher quantum efficiencies compared to the bilayer heterojunction, because in BHJ it is more likely for an exciton to find a D–A interface within its diffusion length.
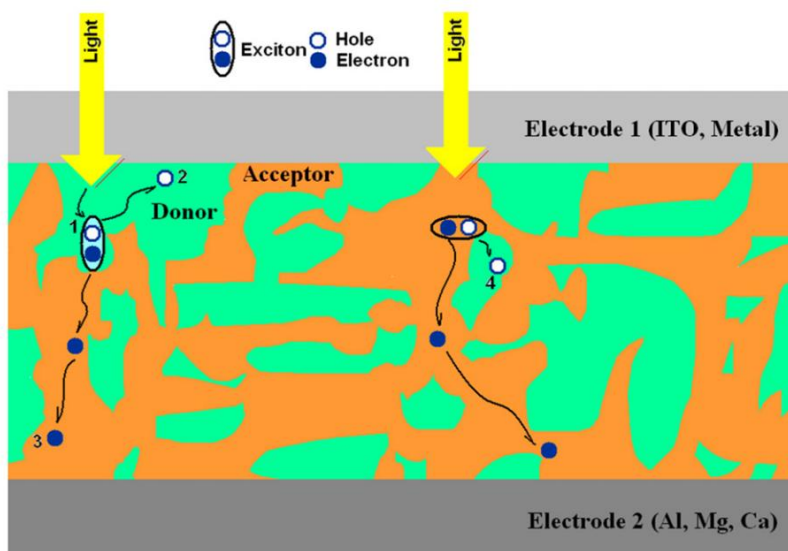
Figure 1.10: The structure of a BHJ. (1) exciton created by incident light diffusing towards a D–A interface; (2) hole drifting towards electrode; (3) electron moving towards electrode;(4) hole trapped in an isolated island of organic molecule. [4]

Among different polymers, the buckminster fullerene C_{60} drew a lot of attention because of its' strong electron acceptor properties. It's based on experiments in bulk heterojunction cells that when C_{60} is mixed with hole conducting materials, photoconductivity increases under illumination.[3] . C_{60} shows a tendency to crystallize in the polymer mixture. This leads to the development of PCBM, a derivative of $C6_0$ (Figure 1. 11). The increased solubility of PCBM resulted in the formation of smaller crystallites in the blend.
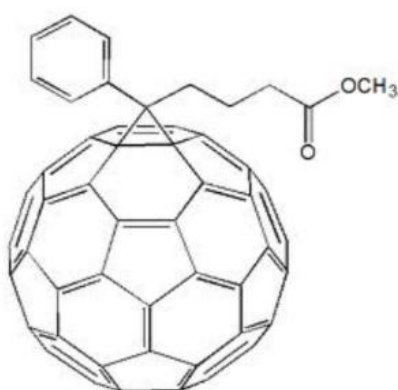
Figure 1. 11: Electron-conducting acceptor polymer, a soluble derivative of C_{60}, namely PCBM (1-(3-methoxycarbonyl) propyl-1-phenyl[6,6]C_{61})

For the electron donor material, PPV derivatives were widely used until the development of P3HT (poly-3- hexylthiophene) (Figure 1. 12). As being able to absorb photons at longer wavelength compared to PPV derivatives, it draws attention

as a partner for PCBM in organic solar cells. The most important finding was that slow drying of the P3HT: PCBM layer leads to increase mobilities, thus prevents the buildup of space charge inside the device.
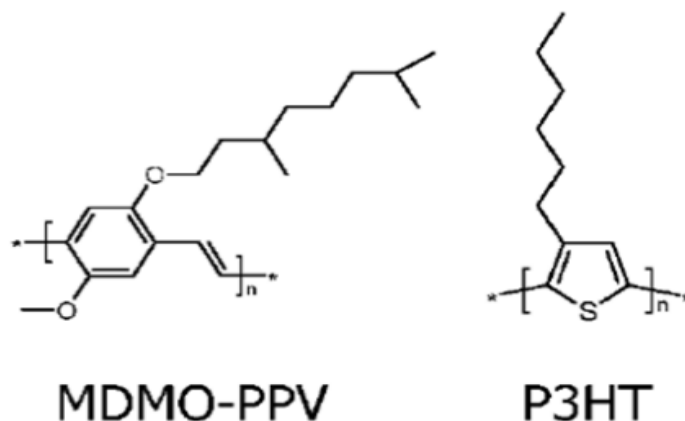
Figure 1.12: Some commonly used conjugated polymers are shown .Two important representatives of hole-conducting donor type polymers are MDMO-PPV (poly [2-methoxy-5- (3,7-dimethyloctyloxy)] -1,4 phenylenevinylene), P3HT (poly(3 hexylthiophene-2,5-diyl)

Typical cell architecture for polymer-fullerene bulk heterojunction solar cell is shown in the Figure 1.13 the absorbing and charge separating bulk heterojunction layer (active layer) with thickness approximately 100 nm is sandwiched between two charge selective electrodes. A transparent bilayer electrode comprises poly (3,4-ethylene dioxylene thiophene) –polystyrene sulfuric acid (PEDOT: PSS) on transparent conducting oxide, indium-tin oxide (ITO) glass for collecting the holes and a lower work function metal (e.g. Al) for collecting the electrons.

One of the early problems in bulk heterojunction organic solar cells is the possible short circuits between electrodes based on the fabrication of the thin polymer layer. These short circuits can cause from the gaps in the layers or from the morphology. This problem is solved by spin casting another polymer layer between the anode contact ant the active polymer layer. Most common buffer polymer is poly-(3,4-ethylenedioxythiophene):poly-(styrenesulphonic acid) (PEDOT:PSS). Along with acting as an electron blocking layer, a thin semiconductor PEDOT:PSS layer works to prevent electron leakage from the bulk heterojunction acceptor to the anode, to help extracting the photo generated holes and to planarize the contact surface.
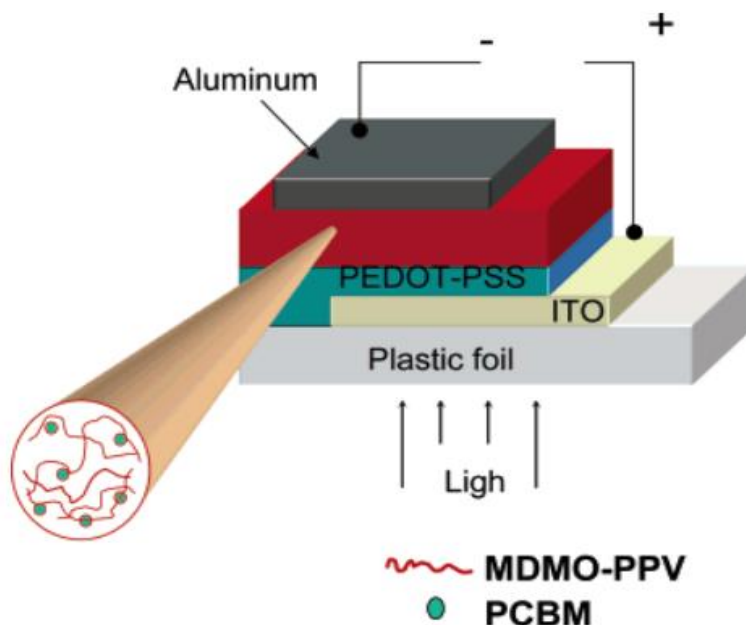
Figure 1. 13: Bulk heterojunction configuration in organic solar cells

1.3 Materials for Transparent Electrodes

Transparent and conducting electrodes are the essential elements of many optoelectronic devices applications, including solar cells, flat panel displays, touch panels, organic light emitting diodes, electroluminescent lighting and many others. Remarkable research has been carried out on various types of transparent and conducting oxides (TCOs) to perfect the materials for achieving high conducting and transparent electrodes. To date, the industry standard in TCO is ITO, or tin-doped indium-oxide. This material boasts a low resistivity of $\sim 10^{-4}$ $\Omega \cdot$cm and a transmittance of greater than 80%. However, ITO has the drawback of being expensive. Indium, the film's primary metal, is rare and its price fluctuates due to market demand. For this reason, TCOs for photovoltaic applications have been fabricated from both inorganic and organic materials. Alternative inorganic films typically are made up of a layer of fluorine doped tin oxide (FTO); aluminum doped zinc oxide (AZO). Doped metal oxides for use as transparent conducting layers in photovoltaic devices are typically grown on a glass substrate. This glass substrate, apart from providing a support that the oxide can grow on, has the additional benefit of blocking most infrared wavelengths greater than 2 µm and converting it to heat in the glass layer. TCO films can be deposited on a substrate through various deposition methods, including metal organic chemical vapor deposition (MOCVD), metal organic molecular beam deposition (MOMBD), spray pyrolysis and pulsed laser

12

deposition (PLD), however conventional fabrication techniques typically involve magnetron sputtering of the film. The sputtering process is very inefficient, with only 30 % of planar target material available for deposition on the substrate. For AZO or ZnAl sputtering target material is sufficiently inexpensive that recovery of materials use is of no concern but for limited resources of available indium for ITO, alternative solutions have to be sort out. Also organic films are being developed using carbon nanotube networks and graphene, which can be fabricated to be highly transparent to infrared light, along with networks of polymers such as poly(3,4-ethylenedioxythiophene) and its derivatives. Intrinsically conductive polymers like polyanilines, polypyrrols and polythiophenes become conductive by removing an electron from their conjugated π-orbitals via doping.

The electrical conductivity results from the delocalization of electrons along the polymer backbone - hence the term "synthetic metals". For three decades, conductive polymers have been an area of intense research and in the year 2000 Alan Heeger, Alan MacDiarmid, and Hideki Shirakawa received the Nobel Prize in Chemistry "for the discovery and development of conductive polymers. Conductive polymers were reported in the mid the 20th century as derivatives of polyaniline. However, the process ability of poly aniline in thin films was so difficult, that today mostly investigated conductive polymers are derivatives of polyacetylene, polypyrrole or polythiophenes. By manipulating the band structure, polythiophenes have been modified to achieve a HOMO-LUMO separation (bandgap) that is large enough to make them transparent to visible light. Doping Poly(3,4-ethylenedioxythiophene) (PEDOT) with poly(styrene sulfonate) as shown in figure 1.14 can improve the properties over the unmodified PEDOT. This PEDOT:PSS compound has become the industry leader in transparent conductive polymers. PEDOT:PSS is water soluble making processing easier. PEDOT:PSS has a conductivity ranging from 400 to 600 S/cm while still transmitting ~80% of visible light. Treatment in air at 100 °C for over 1000 hours will result in a minimal change in conductivity. Recently, it was reported that the conductivity of PEDOT:PSS can be improved to be more than 3000 S/cm [6,7].
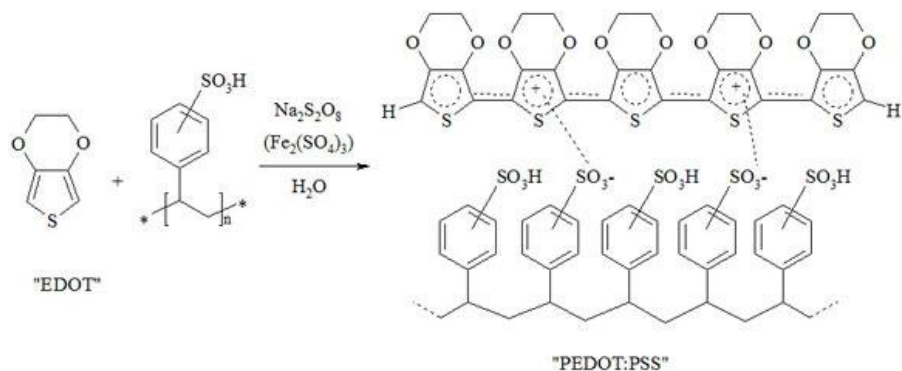
Figure 1.14 : Poly (3,4-ethylenedioxythiophene) PEDOT doped with poly(styrene 3sulfonate) chemical formula

The two-dimensional allotrope of carbon graphene is an emerging material currently being researched for TCO.In figure 1.15 a single sheet of graphene shown.
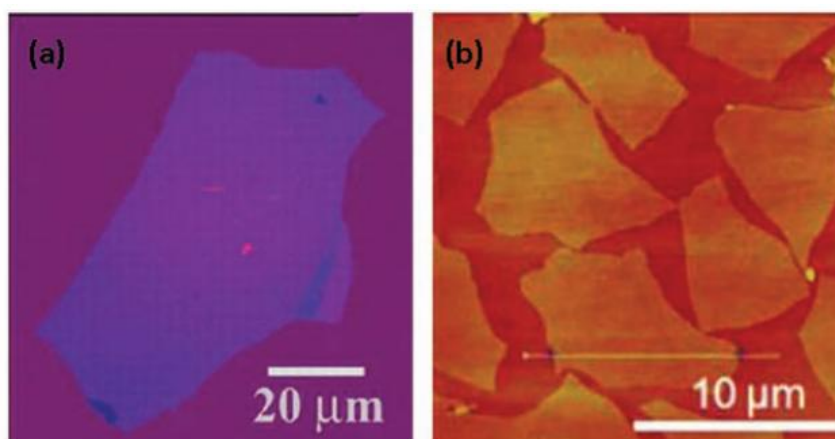
Figure 1.15 : (a) A large, single sheet of graphene (b) A random network of graphene sheets.

The special properties of graphene lead to unique. A pure single-layer graphene chip is a 0 eV bandgap semiconductor with a width up to ~50 μm and thickness of 0.34 nm, fit to the interlayer spacing of graphite. Charge carriers in an individual graphene sheet delocalize over the entire sheet and can travel thousands of interatomic distances without scattering. Since graphene is a zero-gap semiconductor with a very high Fermi velocity $V_F=10^6$ m/s, individual graphene sheets have very high in-plane conductivities.[8] they   found that a graphene film exhibits a strong am bipolar electric field effect showing electron/hole concentrations up to 10^{13} /cm^2 and room-temperature mobilities of ~10^4 cm^2/Vs[8]. Graphene can be chemically doped at doping levels of $N_i =10^{12}$ cm^{-2} while maintaining charge carrier mobilities of $\mu=10^5$ cm^2/(V s) or higher. Peumans et al. predicts that the sheet resistance of graphene will vary with the number of layers as $R_{sh} \sim 62.4\Omega/N$ for highly doped graphene, where

N is the number of layers and the transmittance will vary as T ~100 – 2.3N (%).In figure 1.16 and 1.17   transmission and thickness of sheet resistance for different transparent conductors shown.
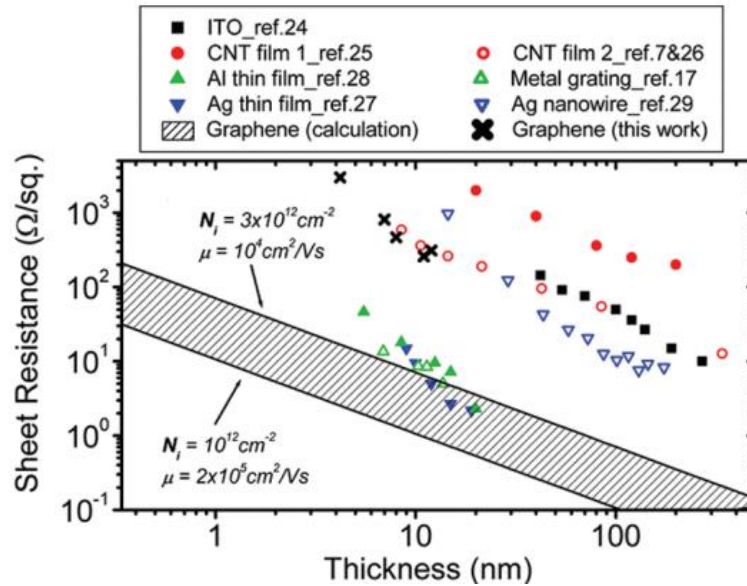
Figure 1.16 : Film thickness dependence of sheet resistance for different transparent conductors
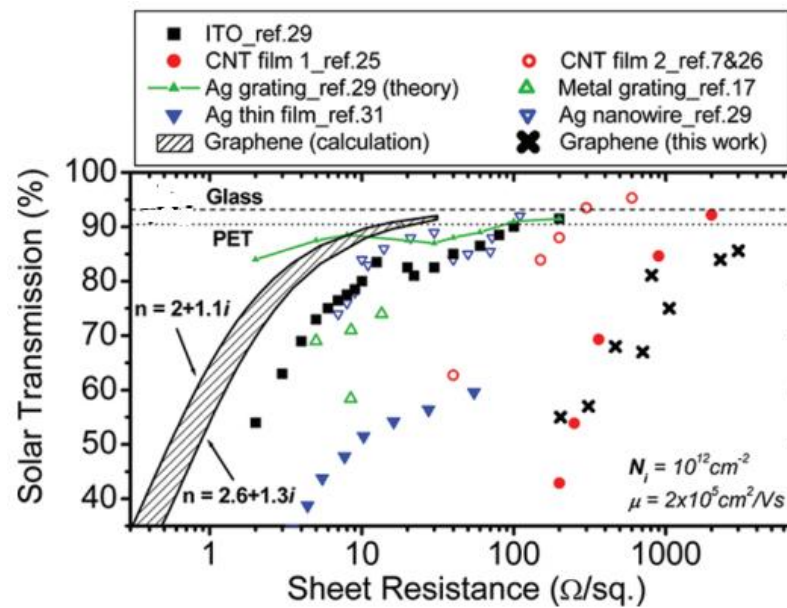
Figure 1.17 : Transmission dependence of sheet resistance for different transparent conductors
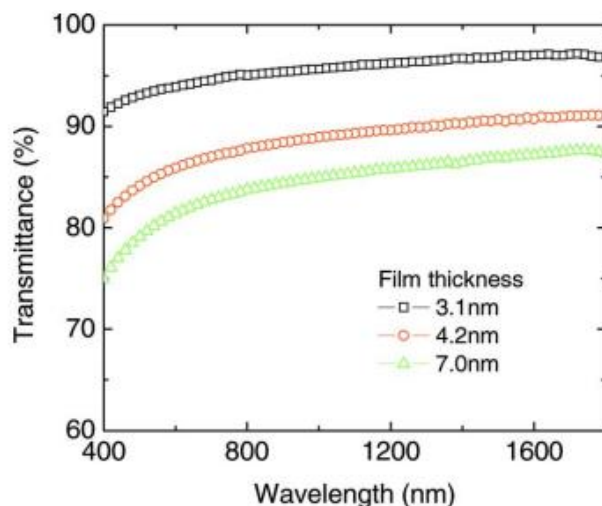
Figure 1.18 : Transmittance as a function of wavelength for graphene films of various thicknesses.

The dependence of transmittance on wavelength is shown in Figure 1.18 for three graphene films with different thicknesses, which were reduced by the hydrazine treatment and argon annealing. The graphene films were reduced by the hydrazine treatment and argon annealing at 400 C^o The optical transparency monotonically decreases for decreasing wavelengths over the spectral range λ=400 – 1800 nm.The sheet resistance of the graphene films shown here is much higher than that of ITO films for the same transparency. This may be because the functionalized graphene is not completely reduced. Bilayer small molecule OPV cells were fabricated on graphene films on quartz and on commercially obtained 130-nm-thick ITO on glass (sheet resistance of <20 Ω/sq) as transparent anode. All organic materials were commercially obtained and then purified using thermal gradient sublimation.

1.4 SWNTs as Transparent Electrodes for Solar Cells

In our laboratory we use SWNTs as organic material for transparent conductive oxide electrode(TCOs). SWNTs are highly-conducting objects with conductivity up to 10^5 S/cm.5 Thin films with randomly distributed SWNTs have been shown to possess high transmittance in the visible range and high conductivity.[8-12]. The performance of transparent films, sheet resistance and optical transmittance highly depends on the nanotube sources, surfactant choices, and fabrication methods.

Figure 1.19 shows the sheet resistance vs SWNT thickness made by spin and spray method. Sheet resistances of around 100 $\Omega sq^{-1}$are obtained at reasonable

transmission, for example, 128 ± 2 Ωsq^{-1} at 90% for DCE, 57 ± 3 Ω sq^{-1} at 65% for H$_2$O:SDS, and 68 ± 5 Ωsq^{-1} at 70% for H$_2$O:SDBS.
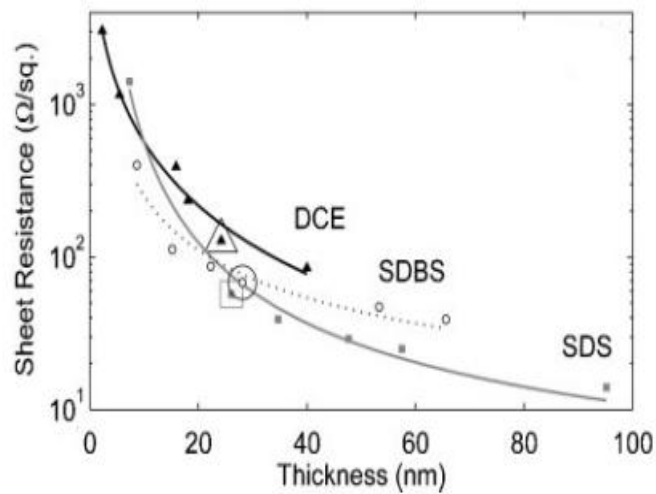
Figure 1.19 : Thickness dependence of the sheet-resistance of thin-film SWCNTs spin-coated from DCE and spray-coated from H$_2$O: SDS or H$_2$O: SDBS [9]

For thin films in the air with the thickness much less than the wavelength, the relation between the transparency and the sheet resistance is decided by the optical conductivity σ_{op} and the DC conductivity σ_{dc}. Typical data are 60% with 50 Ohm/sq, 80% with 150 Ohm/sq, 90% with 300 Ohm/sq, which is in the same range of transparent ITO on PET substrate. Note that the transmittance is highly dependent on the nanotube film thickness, while transmittance for ITO slightly depends on the film thickness. This indicates that the transmittance is determined by the absorption for nanotube films and by the reflectance for ITO film, which we will discuss in the section on optoelectronic properties.

Flexible transparent coating of CNTs on a Polyester foil is shown in figure 1.120 which the multimeter display is to demonstrate the surface resistance in 2-probe configuration. The CNT-coated plastic foil used in Fig. 1.20 shows a transmittance of about 97% and a surface resistivity of 20 kV/sq. After heavy crumpling, an increase in resistivity to 70 kV/sq was observed (right side of figure1.20). ITO will not show this flexibility and fail during this test (even though flexible ITO coatings on a polymer have been reported their flexibility is very limited compared to CNT networks.[13]The stability of devices fabricated on the SWNT/PET films was much greater than devices on ITO/PET during simple bending tests. SWNT devices could be folded over(inducing compressive or tensile strain)down to radii of curvature of

~5 mm with no degradation in power efficiency and radii of ~1 mm with a 20%−25% loss in efficiency.
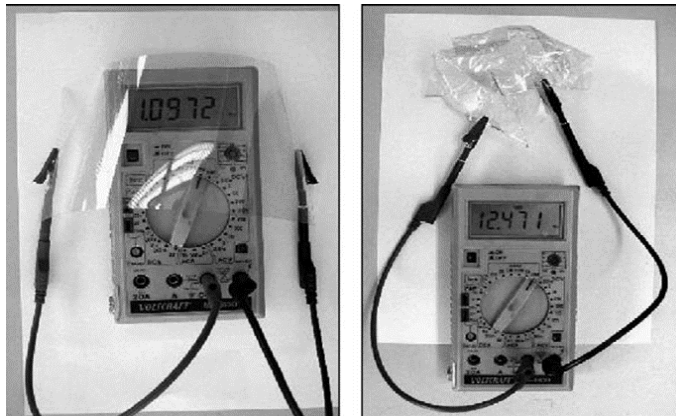
Figure 1.20 : Flexible transparent coating of CNTs on a Polyester foil(left: slightly bent, right: same sample heavily crumpled). The multimeter display is to demonstrate the surface resistance in 2-probe configuration (left: 1 MΩ, right: 12 MΩ).[13]

In figure 1.21 Sheet resistance dependence of transparency at 550nm for laser ablation SWNT film shown.
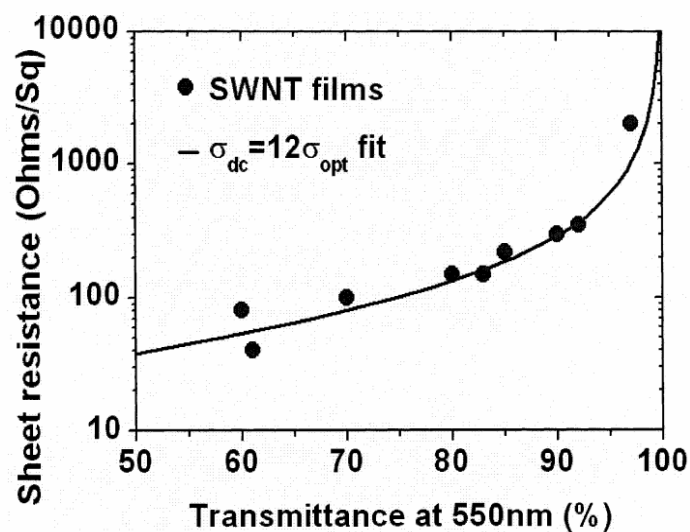
Figure 1.21 : Sheet resistance vs transparency at 550nm for laser ablation SWNT film

2. INVESTIGATION OF MATERIALS

2.1 Carbon Nanotube Structure

Carbon nanotubes (CNTs) were first described by Iijima [17].they discovered hollow tube analogs of the buckyball that contained multiple tubes, or shells, one within another. This new material is called multiwall nanotubes (MWNTs) because of their nanometer-scale diameters. MWNTs are composed of larger-diameter nanotubes surrounded with smaller nanotubes, as shown in Figure 2.1.
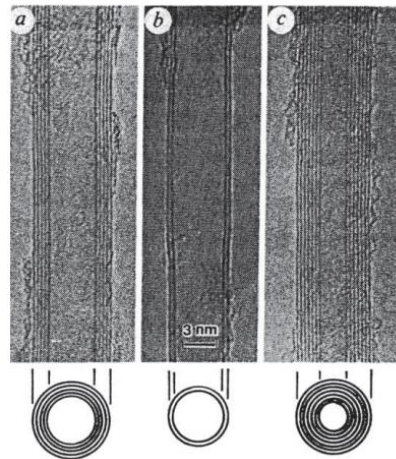
Figure 2.1 : The first electron micrographs to be identified as carbon nanotubes. The images are of MWNTs. In (a) the MWNT has5 shells and a diameter of 6.7 nm. In (b) the MWNT has 2 shells and a diameter of 5.5 nm. In (c) the MWNT has 7 shells and a diameter of 6.5 nm.

In most instances, a CNT is create of a concentric arrangement of many cylinders. Such multi-walled nanotubes (MWNTs) can reach diameters of up to 100 nm. If the CNT composed of just two concentric cylinder is double-walled CNT (DWNTs), which is special case of multi-walled tubes (MWNTs).

The formation of a SWNT can be visualized through the rolling of a graphene sheet. Single-walled nanotubes (SWNTs) possess the simplest geometry and have been observed with diameters ranging from 0.4 to 3 nm.

The SWNTs and MWNTs produced at lower temperatures have a higher amount of defects in the walls and caps there for nanotubes produced at higher temperatures. Carbon nanotubes (CNTs) have attracted the interest of researchers of many fields because of their unique physical, chemical, electronic, and mechanical properties [18]. They are efficient conductors of electrons and heat [19].

Carbon nanotubes are "helical microtubules of graphitic carbon". Carbon nanotubes refer to cylinders of graphene with diameters on the order of nanometers along an (m,n) lattice vector in the graphene plane (figure 2.2) which determined the diameter and chirality[20,21]. Depending on the chirality, SWNTs can be either metals or semiconductors. Depending on the orientation of the graphite sheet (the hexagonal lattice of Carbon atoms), three types of SWCNTs are obtained: "armchair," "chiral," and "zigzag" nanotubes, as shown in figure 2.3. Mathematically, the tube chirality can be defined in terms of a chiral vector C_n ($C_n =ma_1 + na_2$), which also determines the tube diameter d [22]. This vector determines the direction of rolling a graphene sheet, in which a lattice point (m, n) is superimposed with an origin defined as (0, 0). Therefore, the diameter of a carbon tubule can be expressed as:

$$d = \frac{a\sqrt{(m^2 + mn + n^2)}}{\pi}$$

(2.1)

Where ;

$$a = 1.42\sqrt{3A}$$

(2.2)

A corresponds to the lattice constant in the graphite sheet. Note that the C–C distance is 1.42°.
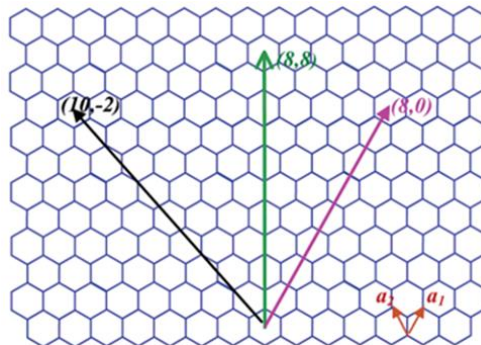
Figure 2.2 : Schematic honeycomb structure of a graphene sheet. Carbon atoms are at the vertices.

(a) Armchair   (b) Zigzag   (c) Chiral
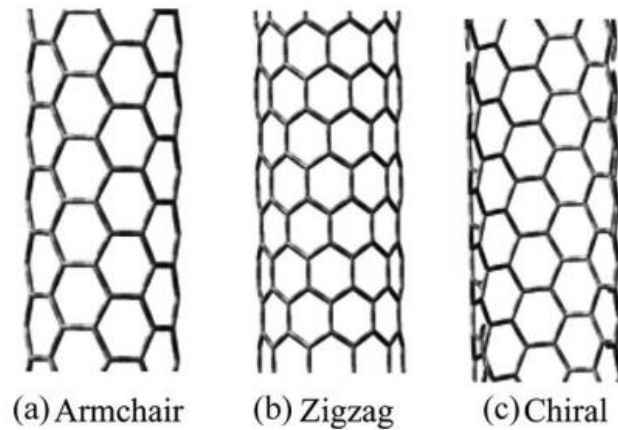
Figure 2.3 : Roll up of a grapheme leading to three different types of carbon nanotube. Armchair (a), zigzag (b), and chiral (c) tubes, respectively.

2.2   SWNT Synthesis Methods

SWNTs can be synthesized from a variety of different materials. In general, three methods described below are well established for the production of SWNTs:

➢ Electric arc-discharge

➢ Catalytic decomposition of gaseous hydrocarbons

➢ Laser ablation

2.2.1 Arc-discharge

Arc-discharge is the easiest and most common method to produce carbon nanotubes which First developed by Iijima in 1991. A schematic of this method is shown in Figure 2.4.
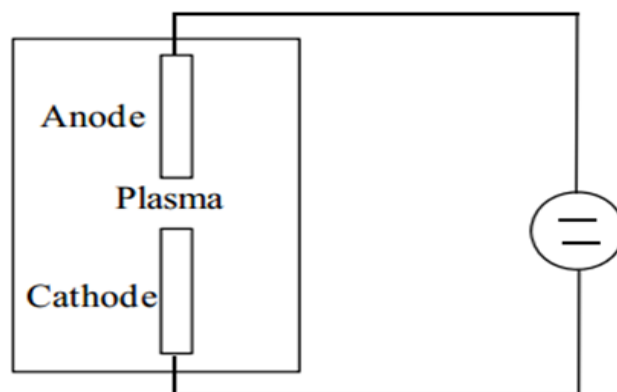
Figure 2.4 : Schematic of Arc discharge method.

a

2.2.2 Laser-ablation

The pulsed laser-ablation process for production of single-wall carbon nanotubes was developed by Guo et al [26, 27]. Nanotubes produced by laser ablation are purer (up to about 90 % pure) than those produced in the arc process. High-power Laser pulses (YAG type) heat the target surface which consists of a mixture of graphite and metal catalyst (Co, Ni) inside a furnace at 1200 $^{\circ}$C, and finely divided nickel and cobalt (metal catalyst) and vaporized the target in a flow of inert gas at temperatures above 3000 °C. A schematic of the laser-ablation process is shown in Figure 2.5.
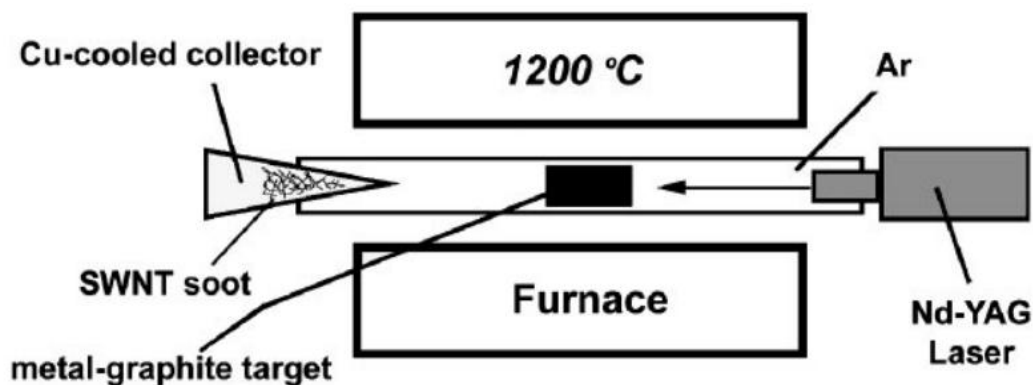
Figure 2.5 : A schematic of the laser-ablation process [28].

Experimental setup for the production of SWNTs and MWNTs using the laser technique. In particular, a high-power laser is focused on a composite graphite target, which is located inside a furnace at 1200C embedded in an Ar atmosphere.

The diameter of SWCNTs decreases with decreasing oven temperature and lower flow rates [29].

The X-ray diffraction and TEM showed that the synthesized nanotubes were remarkably uniform in diameters and that they formed ropes (or bundles) 5–20 nm in diameter and tens to hundreds of micrometers long [30].

The yield and size of SWNTs produced by laser ablation is also similar to those obtained by arc discharge (i.e. > 70% purity, mean diameter of 1.3 nm) but there are two main disadvantage in both method (1) they rely on on the evaporation of carbon atoms from solid graphite targets at temperatures >3000 °C and (2) the resulting SWNTs are tangled which makes subsequent purification processing difficult (2) the nanotubes are garbled which makes difficult the purification and application of the samples [31].

2.2.3 Chemical vapor deposition CVD

CVD methods are favorable for producing nanotube materials at large scales with high quality. A schematic experimental setup for CVD growth is depicted in Fig.2.6
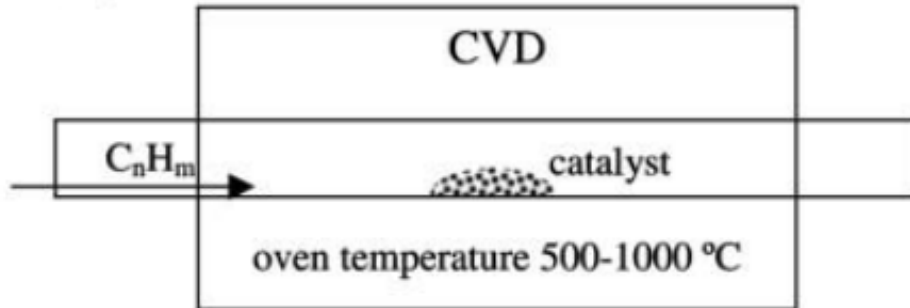
Figure 2.6: Schematic of CVD operated as floating catalyst or substrate catalyst.

Chemical vapor deposition CVD Utilize hydrocarbon gases (commonly benzene, ethanol, acetylene, propylene, methane, ethylene, CO, etc.)as the carbon source for production of both single and multi-walled carbon nanotubes flowing through the tube reactor over a period of time, involves heating a catalyst material(Ni, Co or Fe) to high temperatures (500–1000 C^o) in a tube furnace [32]. The catalytic species are typically transition-metal nanoparticles that are formed on a support material such as porous aluminum oxide (alumina) materials with large surface areas. The saturated metal particle leads to the formation of tubular carbon solids in a sp^2 structure. Tubule formation is preferred over other forms of carbon such as graphitic sheets with open edges because of a low energy form of them [33]

Two general nanotube growth of nanotube in chemical vapor deposition are base growth mode And tip growth mode. Fig 2.7

For MWNT growth, the growth temperature is typically in the range of 550–750 ^{o}C and Iron, nickel or cobalt nanoparticles are often used as catalysts but contain high densities of defects such as pentagons and heptagons on the sidewalls of the multi-walled carbon nanotubes. Growth of single-walled carbon nanotubes with perfect structure was enabled by CVD methods. For grow high quality SWNT materials by CVD, using methane as carbon feedstock and reaction temperatures in the range of 850–1000 C and alumina supported catalyst materials are affective factors. [34–37].

High growth temperatures cause to form SWNTs that have small diameters and thus high strain energies, and allow for nearly defect-free tube structures [38].
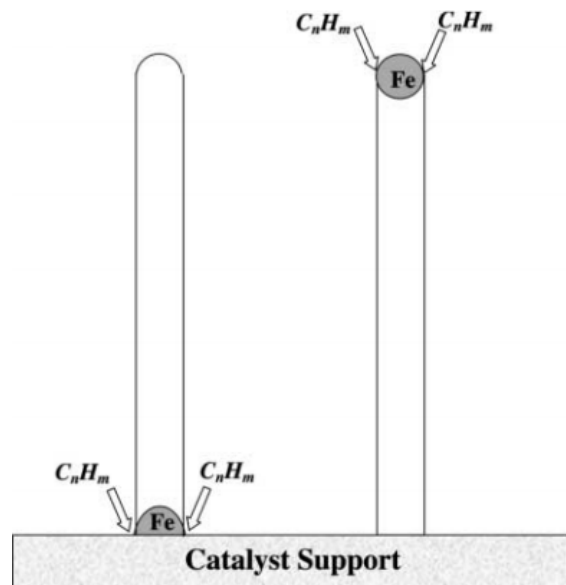
Figure 2.7 : Two general growth modes of nanotube in chemical vapor deposition. Left diagram: base growth mode. Right diagram: tip growth mode

Nanotubes are not ideal structures, but rather contain defects formed during synthesis. Typically, around 1–3 % of the carbon atoms of a nanotube are located at a defect site [39]. A frequently encountered type of defect is the so-called Stone–Wales defect, which is comprised of two pairs of five-membered and seven-membered rings, and is hence referred to as a 7-5-5-7 defect.
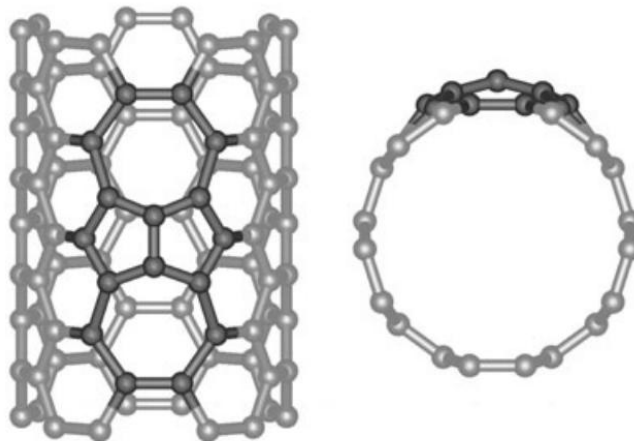
Figure 2.8 : Stone–Wales (or 7-5-5-7) defect on the sidewall of a nanotube.

Control of carbon nanotubes size is critical because the length of CNT significantly affects its mechanical, thermal, chemical, and particularly electronic properties. For a single-walled carbon nanotube (SWNT), the diameter determines the band gap of a semiconducting nanotube and it's directly cause to change the performance of this material in electronics and optics applications [20,21]].

For characterizing diameter distribution, using Raman scattering and TEM observation is so often. Raman spectroscopy is perhaps the most often used method because the frequency of the radial breathing mode (RBM) is resolved the SWNT diameter directly [22].

Because of excitation of the RBM is a resonance process, leaving the actual diameter distribution of bulk SWNT sun clear, Raman spectra contain information from a limited number of SWNTs in the sample. Furthermore, the strong dependence of Raman intensity on diameter and chirality hinders the use of this technique for the accurate estimation of diameter distribution.

TEM and atomic force microscopy (AFM) in this sense are the most reliable methods, despite the complicated sample preparation and time-consuming measurement.

Table 2.1: Advantages and Disadvantages of the synthesis methods in comparison

Methods	Advantage	Disadvantage
Arc- discharge	Growth of CNTs with fewer structural defects	Higher temperature (above 1700 ^{o}C)
	Easy to get	
	Low cost material	Physical- chemical factor influencing the process
	SWNT high purify (1.5 nm- 2 nm)	
	Highly crystalline MWNT (10 nm-20 nm)	
Laser ablation	use for SWNT synthesis	Small amount of SWNT deposition in each synthesis
	High quality (up to 90 %)	
	High purity (1.2 nm- 1.7 nm)	
	CNTs structure is better graphitized	
Chemical vapor deposition	Large scale	High temperature
	Quite pure	
	Economically viable process	
	Easy control of the reaction	

2.3 Purification Methods for CNTs

As-synthesized CNTs prepared by the arc discharge, laser ablation of graphite and chemical vapor deposition (CVD) contain carbonaceous impurities and metal catalyst particles. In general, the main impurities in the soot are graphite (wrapped up) sheets, amorphous carbon, metal catalyst, and the smaller fullerenes. In addition, structural defects, such as dangling bonds, are often found in most types of CNTs. the amount of the impurities commonly increases with the decrease of CNT diameter. The fundamental problems that exist are how to remove impurities; the amount of the impurities commonly increases with the decrease of CNT diameter. As shown in high resolution TEM , mages Figure 2.9.
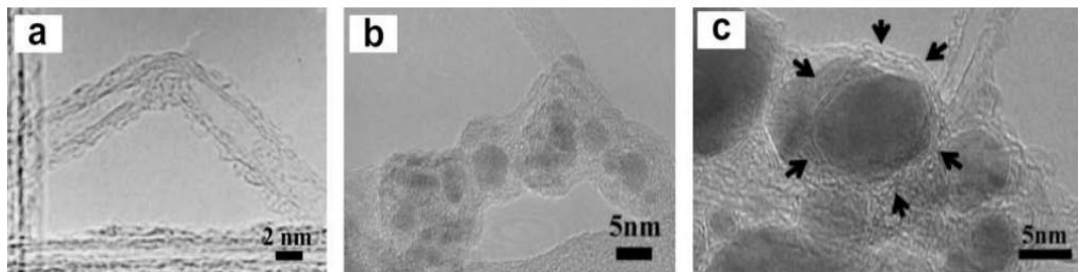
Figure 2.9: TEM images of (a) amorphous carbon and fullerene molecules on the surface of CNTs; (b) metal nanoparticles covered by amorphous carbon layer, (c) metal nanoparticles covered by graphitic carbon multi-layer[40]

These impurities could obviously affect the CNT properties such as physical, chemical, electronic, and mechanical properties. Therefore, high-purity carbon SWCNTs are necessary for obtain the optimal performance of SWCNTs.

Purification methods generally involving separation and elimination processes can be categorized into three major methods:

1.   Physical separation: this produce is based on the use of SWCNT dispersions in a surfactant solution, such as SDS (sodium dodecyl sulphate) or SDBS (Sodium dodecyl benzene sulfonate), which is submitted to separation by filtration [41], centrifugation [42].

2.   Gas-phase oxidation: This method is generally used for multi-walled carbon nanotubes (MWCNTs), more ever this method efficient for the removal of graphitic impurities. A problem identified with this methodology is the poor homogeneity of the gas/solid mixture.[43,44]

3.   Liquid phase oxidation: this method carried out with acid solutions such as HNO3 [45,46]. SWCNTs have generally been oxidized with nitric acid solutions to remove metals and carbon impurities. The acid treatments promote partial destruction of the nanotube sample. The walls of the SWCNTs become damaged, distorted, or even segmented [46].

However, a reproducible purification for especially SWCNTs is still a great challenge, because the purity of CNTs depends on not only purification itself, but also many other factors, including CNT type (SWCNTs or MWCNTs), morphology and structure (defects, whether or not they exist in bundles, diameter), impurity type and their morphology (particle size, defect, curvature, the number and crystallinity of carbon layers wrapping metal particles), purity estimation technique, and so on.

A typical multi-step purification process consist of four steps. A schematic representation of this procedure is shown in Fig.2.10

- ➢ Removal of fullerenes and soluble impurities. Fullerenes can be removed in certain organic solvents, for example using Soxhlet extraction in toluene.

- ➢ A liquid-phase oxidation of amorphous carbon. The amorphous carbon can be eliminated easily, because of its high density of defects, which allow it to be oxidized by upon heating to 350 °C in air or by sonification in H_2O_2.

- ➢ An acid treatment to remove the unprotected metallic particles. , the free metal particles can be removed by heating in a non-oxidizing acid solution (dilute HCl or dilute HNO_3) and filtering afterwards.

- ➢ Separation of the SWCNTs from the graphite impurities and protected catalysts.

- ➢ Polyhedral carbons, having similar oxidation rates to SWNTs, are not easy to remove. Also, metal impurities encapsulated in carbon layers might making them unable to dissolve in acids.
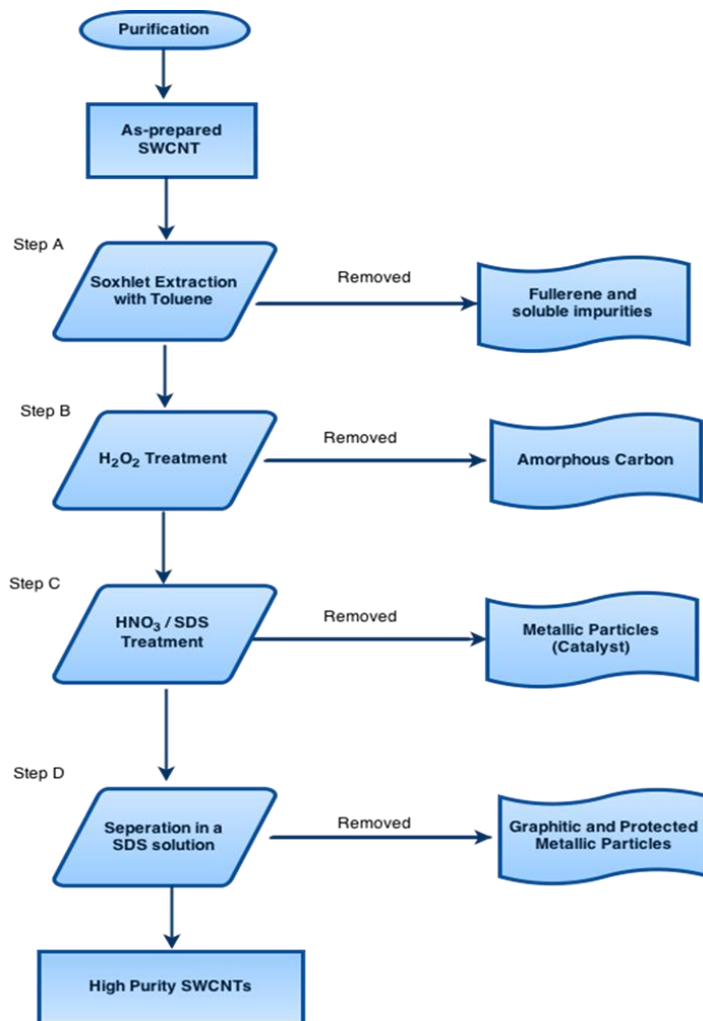
Figure 2.10: Schematic flowchart of the SWCNTs multi-step purification.

2.3.1 Soxhlet extraction

For removing the fullerenes and the soluble impurities, the as-prepared material was surrender to Soxhlet extraction for 6 h in toluene. The sample was then washed and dried at 100 ^{o}C**.**

2.3.2 Liquid-phase oxidation with H_2O_2

The obtained sample was submitted to liquid-phase oxidation with a 10% hydrogen peroxide (H_2O_2) solution. 600 mg of the sample, which obtained from soxhlet extraction, were mixed with 300 mL of a 10% H_2O_2 solution and submitted to ultrasonic for better dispersion. The mixture was refluxed at 100 ^{o}C for 5 h, followed by filtration with a 0.4lm membrane. The sample was then washed with deionized water, and dried in air at 100 ^{o}C.

2.3.3 Acid treatment with an HNO3/SDS mixture

This acid treatment was carried out at room temperature, which minimizes the damage to the SWCNTs. In this process, 300 mg of the result sample were sonicated in 100 mL of an acid mixture: 50 mL HNO3 (98%) and the surfactant SDS (sodium dodecyl sulphate) for 2 h. The surfactant allowed better dispersion of the sample. The dispersion was filtered (0.4lm membrane) and washed with deionized water (to neutral pH), followed by acetone and dried in air at 100 ^{o}C .

2.3.4 Physical separation from the SDS dispersion

The SWCNTs dispersion in SDS solutions is a system that was well studied in the above conditions and below the CMC (critical micellar concentration) [31,38]. Here, approximately 500 mg of the sample, which obtained from acid treatment step was dispersed in 1.0 L of SDS 0.02 M solution by sonication, for 30 min. The dispersion was allowed to stand for 5 h and the supernatant phase was separated and filtered (0.4lm membrane). The material was washed with deionized water and dried in air at 100 ^{o}C.

Methods to analyze the purity of the SWNTs have included thermal gravimetric analysis (TGA), Raman spectroscopy, X-ray diffraction (XRD), transmission electron microscopy (TEM), Scanning electron microscopy (SEM), UV−Vis− Near-IR spectroscopy, and energy dispersive spectroscopy (EDS).
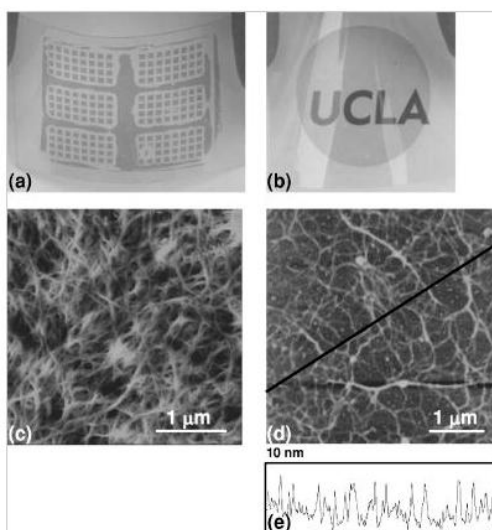
Figure 2.11: (a) Patterned nanotube films on a PET substrate. b) A transparent and homogeneous film (c) AFM image of a nanotube film. (d) AFM image of a sub-monolayer nanotube film. (e) Section analysis of the AFM image in (d) across the black line [16].

Surfactants disperse SWNTs in aqueous solutions mainly through hydrophobic/hydrophilic interactions, in which the hydrophobic tail of the surfactant molecule adsorbs on the surface of SWNT bundles while the hydrophilic head associates with water for dissolution. SWNTs can be encapsulated within cylindrical micelles [Fig.2.12(a)], or covered with either hemispherical micelles [Fig.2.12(b)] or randomly adsorbed molecules [Fig. 2.12(c) [47]

a) cylindrical micelle

b) hemimicelle

c) random adsorption
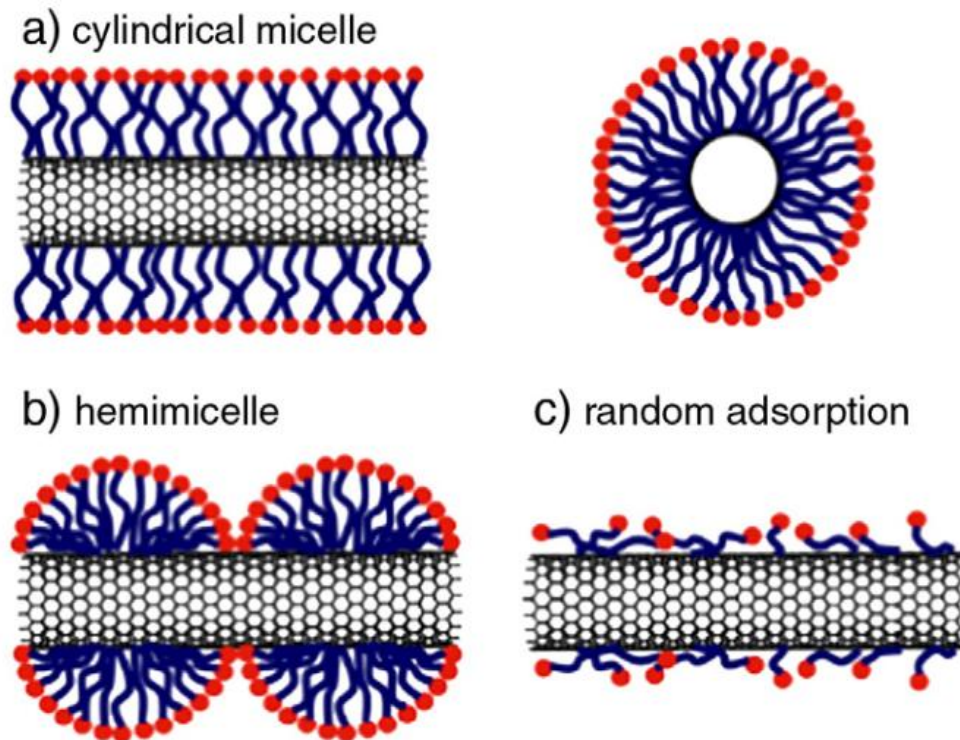
Figure 2.12 : Illustrations of the (a) cylindrical micelle, side and end views, (b) hemimicelle and (c) random adsorption models

Two types of surfactants used for dispersed carbon nano tubes; alkylchain-based surfactants (AS) such as sodium sulfate (SDS), sodium dodecylbenzenesulfonate (SDBS), sodium dodecanoate (SDC) and steroid-based surfactants (SS) such as sodium cholate (SC) and sodium deoxy cholate (SDeC). After casting the solution onto amine-modified substrates, remaining AS in the solution immediately self-assembles into a packed surfactant layer on the substrate. This packed AS layer prohibits the assembly of AS-coated SWCNTs due to repulsive electrostatic forces (Figure 2.13 a).

On the other hand, steroid-based surfactants (SS) allows for the dense assembly of SWCNTs because residual SS cannot form into a packed layer as shown in alkylchain-based surfactants (AS) on amine functionalized surfaces (Figure 2.13

30

b).The rigid nature of the steroid moiety can be attributed as the main reason for its loosely packed structure on the amine surface, in comparison to alkyl moiety's more flexible and therefore tight packing assembled structure.
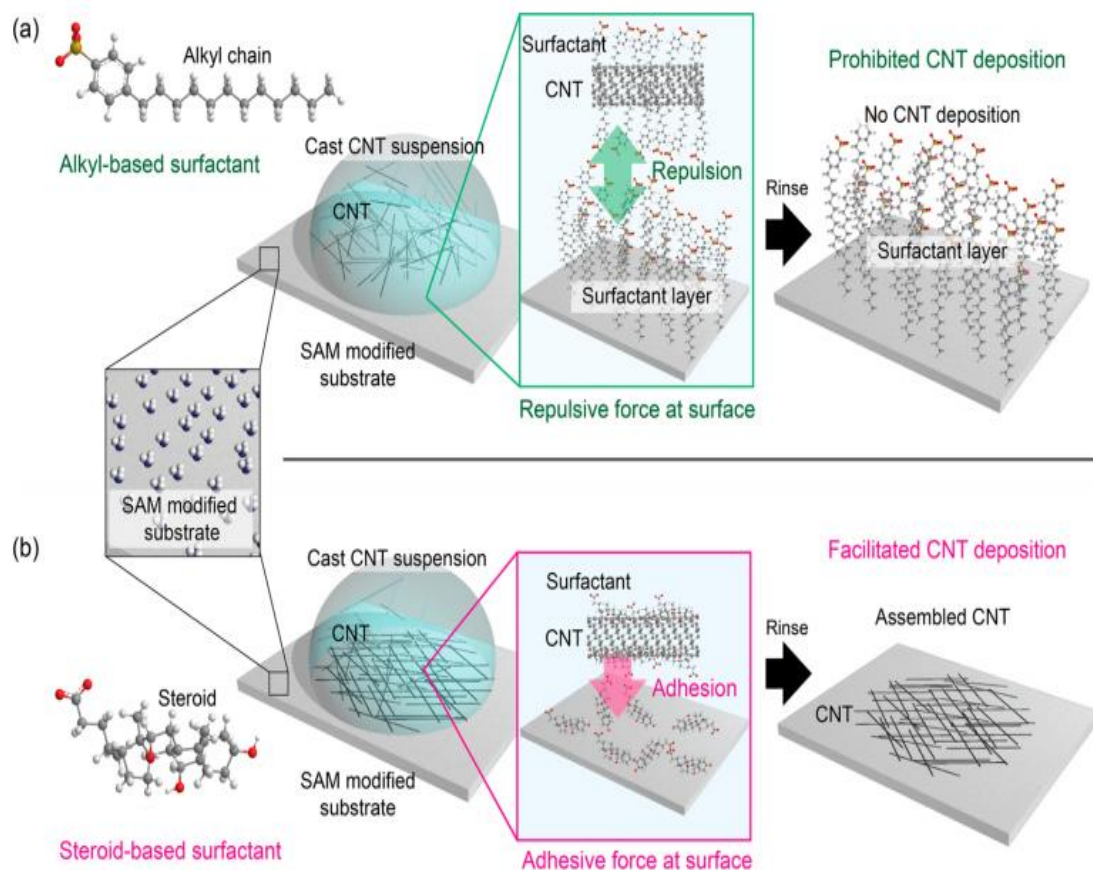
Figure 2.13: Schematic illustration of the solution-based SWCNT assembly process. (a) Deposition of a SWCNT solution with an alkyl-type surfactant(SDBS). (b) Deposition process from a suspension with a steroid type surfactant (SS)

Figure2.14 can reveal that in the cases of SDBS, SDS, and SDC, no SWCNT assembly was observed after the deposition process. The deposition of surfactants followed by washing with DI water and annealing at 200 °C. The deposition time was 10 min at room temperature On the other hand, all SC and SDeC cases show dense SWCNT assemblies. Since the SWCNT surface is also covered with these lipids, the electrostatic repulsion force causes the prohibition of SWCNT assembly when using SDS or SDBS as the surfactants. [48]
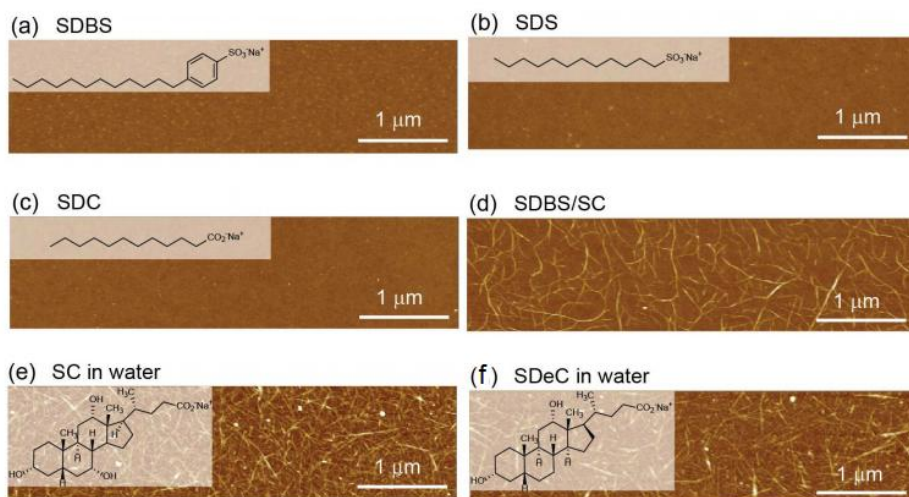
Figure 2.14: AFM images (a) SDBS suspension, (b) SDS suspension, (c) SDC suspension, (d) SDBS/SC suspension, (e) SC suspension, (f) SDeC in DI water

3. CHARACTERIZATION METHODS

In order to probe the morphological and structural characterizations of nanotubes, characterization methods could be used, which are able to characterize CNTs at the individual level such as Thermo-gravimetric analysis or thermal gravimetric analysis (TGA), scanning tunneling microscopy (STM), Raman spectroscopy, scanning tunneling microscopy (STM) and transmission electronic microscopy (TEM), X-ray photoelectron spectroscopy.

3.1   Raman Spectroscopy

Raman spectroscopy is a form of molecular spectroscopy that involves the scattering of electromagnetic radiation by atoms or molecules. It is the shift in wavelength of the in elastically scattered radiation that provides the chemical and structural information. It probes the vibrational, rotational and other low frequency modes of the molecules, the Raman signal is observed as an in elastically scattered light. Stokes radiation occurs at lower energy (longer wavelength) than the Rayleigh radiation, and anti-Stokes radiation has greater energy. The energy increase or decrease is related to the vibrational energy levels in the ground electronic state of the molecule, and as such, the observed Raman shift of the Stokes and anti-Stokes features are a direct measure of the vibrational energies of the molecule. Simplified energy diagram shown in Figure 3.1.
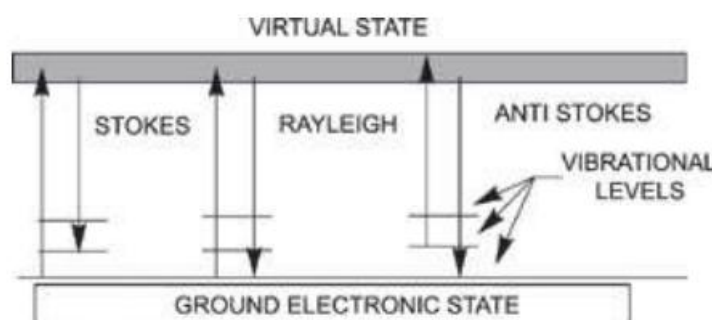
Figure 3.1: Simplified energy diagram

The molecules with high change of the dipoles via polarizability, like benzene, show higher Raman peaks than dipoles like water. Therefore, an advantage of the method is that unlike to FTIR spectroscopy, Raman is insensitive to aqueous absorption bands. Because the samples, investigated in this work were prepared as aqueous dispersions, the Raman method was preferred.
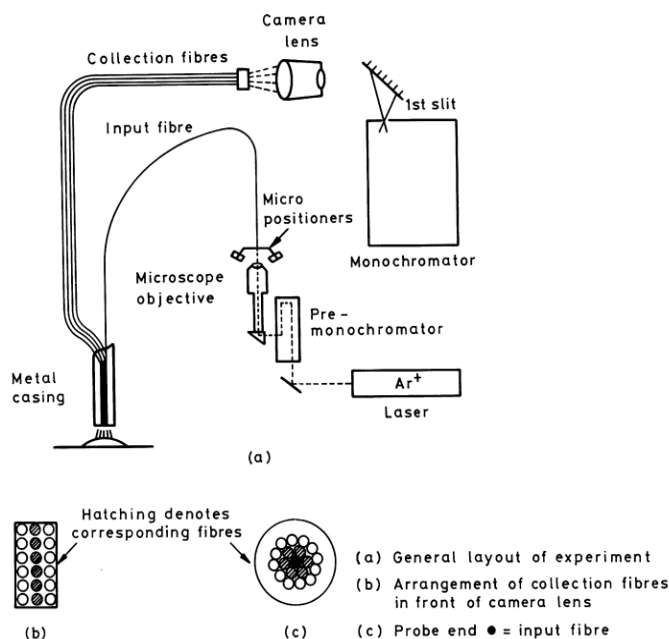
Figure 3.2 : Schematic diagram of a fiber optic probe for Raman spectroscopy.

3.1.1　Raman spectroscopy for CNTs

Raman spectroscopy is one of the most powerful tools for characterization of carbon nanotubes for clarifying the electronic and vibrational structure of SWNTs and to analyze the purity of the materials, without sample preparation, a fast and nondestructive analysis is possible. [51,52]

Raman spectra of graphite and SWNTs can provide us with much information about the exceptional 1D properties of carbon materials, such as their phonon structure and their electronic structure, as well as information about sample imperfections (defects). A general view of the Raman spectra from a sample of single-wall carbon nanotube bundles is shown in figure 3.3.
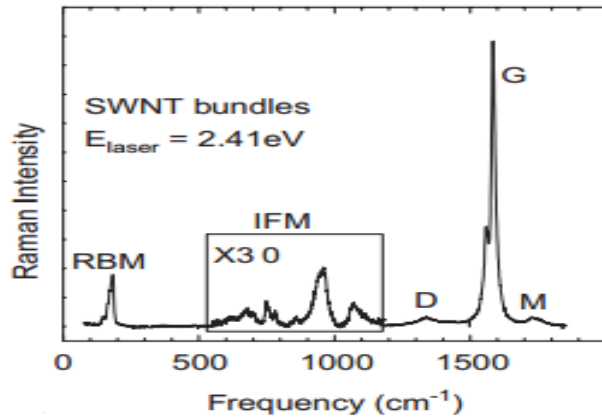
Figure 3.3 : A general view of the Raman spectra from a sample of single-wall carbon nanotube bundles.

The two dominant Raman features are the radial breathing mode (RBM) at low frequencies with A_1 symmetry (below 400 cm^{-1}), and the tangential (G band) multi-feature connect to sp$_2$ bonding in carbon systems (1500–1650 cm^{-1}) consisting of six components with A_1, E_1, and E_2 symmetries arising from the curvature-induced splitting of the E_2 g mode of graphite at higher frequencies. There are weak features too, such as the disorder induced D band at 1250- 1450 cm^{-1}, the M band (an overtone mode).
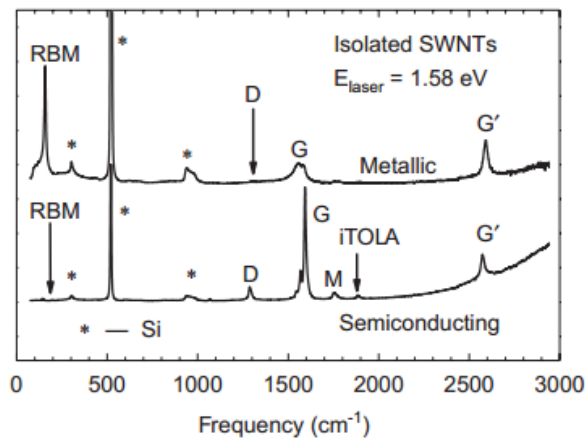
Figure 3.4: Raman spectra from a metallic and a semiconducting SWNT at the single nanotube level.

Figure 3.4   Raman spectra from a metallic (top) and a semiconducting (bottom) SWNT at the single nanotube level. The spectra show the radial breathing modes (RBM),D-band ,G-band And G' band features, in addition to weak double resonance features associated with the M-band and the iTOLA second-order modes[53].

The intensity and the shape of the observed SWNT D-band will therefore be depending on the density of defects and on the amount of carbon impurities. Once the disordered carbon impurities are removed, a sharp dominant D-band feature with a FWHM of about ~ 20 cm^{-1} is observed at 1350 cm^{-1}.Thus, a sharp D-band indicates that the sample has lower impurities and higher crystallinity. As mentioned before, the cleaning steps can introduce defects on the sidewalls of the carbon nanotubes. Although the D-band intensity is small relative to the G-band intensity it is still possible to observe a relative increase in the D-band intensity for the samples to which defects have been introduced during the purifying.

3.2   Thermogravimetric Analysis (TGA)

Thermogravimetric Analysis (TGA) is finding increasing utility in investigations of the pyrolysis and combustion behavior of materials. Such data can provide clues about the number and sequence of reactions, which occur in a pyrolysis process and about such kinetic parameters as the order and activation energy of these reactions. TGA is a method for analyzing the thermal decomposition of materials especially organic polymers. A small sample of material is placed in a platinum "boat" which is suspended from a tiny quartz rod. The quartz rod is one arm of a balance. A thermocouple temperature-measuring device is aligned next to the sample. A quartz tube is slid over the sample with a furnace around it. The sample is heated to decomposition and the weight loss and temperature are recorded.

3.2.1   TGA analysis for carbon structures

It is known that different structural forms of carbon can exhibit different oxidation behavior depending each time on the available reactive sites. Figure 3.3 is Thermogravimetric Analysis of the Oxidation of purified C_{60}, a typical graphite and the mixture of nanotubes and nanoparticles. Because of possible decomposition and oxidation at low temperatures, it is clearly difficult to obtain and measure properties of C_{60} free of irrelevant material. It is clear that the nanotube/nanoparticle sample is more resistant to oxidation than either C_{60} or graphite. The temperature ($\pm$ 5 ^{o}C) of the maximum rate of oxidation (peak in the differential curve) is 695 ^{o}C for the nanotube/nanoparticle sample, 420 ^{o}C for C_{60}, and 645 ^{o}C for graphite (Figure 3.5).
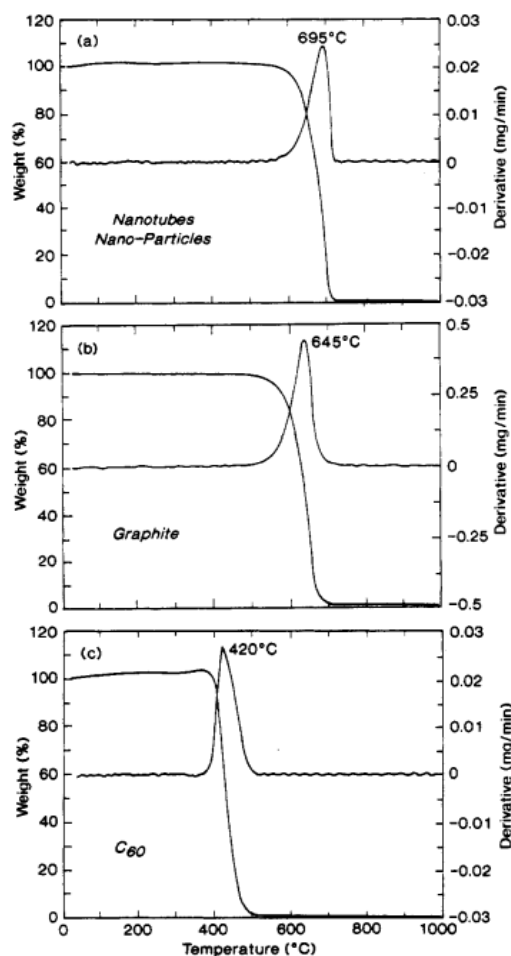
Figure 3.5: Thermogravimetric Analysis of the Oxidation of purified C_{60}, a typical graphite and the mixture of nanotubes and nanoparticles.

TGA used to estimate the purity of the CNTs in terms of metal and metal oxide contents. It should be noted that there is a small difference between the impurity content of the CNTs and the residual weight percent from the oxidation of catalysts in TGA measurements, But the discrepancy is small and can be reasonably neglected when the metal content is very low in the samples. The carbonaceous fractions begin to combust at ~370 ^{o}C and are mostly removed by oxidation below 600 ^{o}C. This temperature is relatively low but presumably, catalyst-assisted dissociation takes place during the process. A small final weight loss beginning at ~650 ^{o}C is due to the oxidation of surviving SWNTs (~4 wt.-%)[55].

The TGA data from acid-refluxed material is also displayed in Figure 3.6. Thermogravimetric analysis of 1±2 mg samples ramped from 25±875 ^{o}C at 5°C per min in a platinum sample pan under 100 sccm flowing air. a) Materials produced at a laser power of ~20 W/cm^{2}, purified crude soot, and crude soot after a 16 h reflux in 3M HNO_3 . The data for the refluxed material was normalized to 100 wt.-% at 100

^oC to compare dry weights. So The sample weight is reduced to approximately zero by 850 ^{o}C since all carbonaceous materials have been removed and very little metal is left [56].
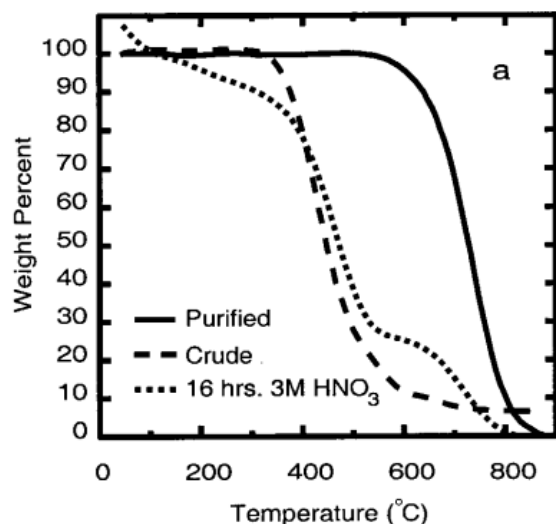
Figure 3.6: Thermogravimetric analysis

Figure 3.7 is shown the TGA graphs of the raw SWCNT sample, and the thermally treated sample, and HCl-treated sample, and HNO$_3$-treated sample. The solid and dot lines correspond to the TG and differentiated TG curves, respectively
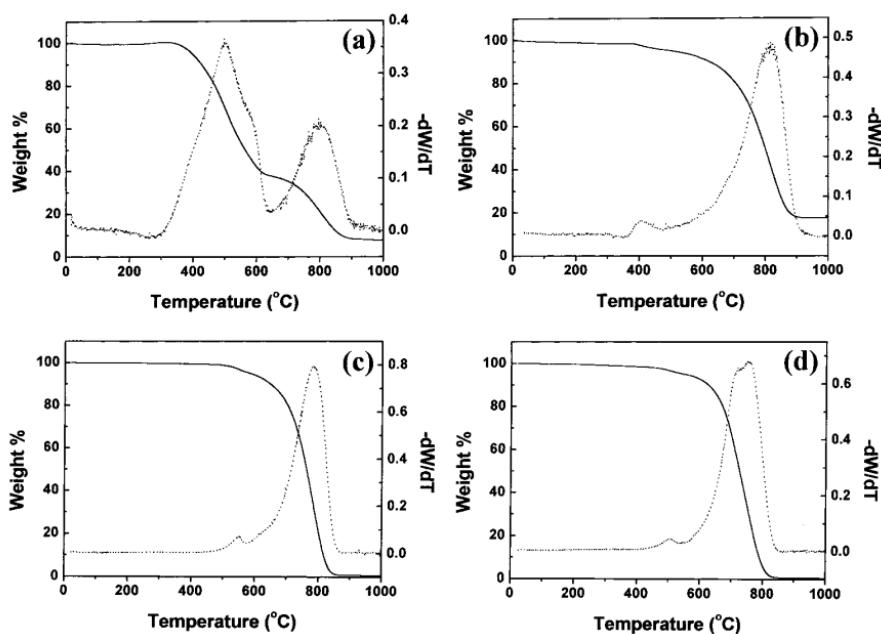
Figure 3.7: TGA graphs of (a) the raw SWCNT sample, (b) the thermally treated sample, (c) HCl-treated sample, and (d) HNO$_3$-treated sample.

3.3   Uv-Vis-NIR Spectroscopy

A spectrophotometer is an instrument which measures the reflection or absorbance characteristics of a sample. Instrument design necessitates that the wavelength of radiation to be studied must be a narrow 'window'. Accordingly, the predetermined electromagnetic radiation wavelengths for ultra-violet (uv), visible (vis) and near infra-red (nir) radiation are defined as follows;

uv radiation   300 to 400nm

Vis radiation   400 to 765mm

nir radiation   765 to 3200nm

Absorption of radiation may occur in a transmission or reflection mode. A diagram of the components of a typical spectrometer are shown in the following diagram.Figure 3.8
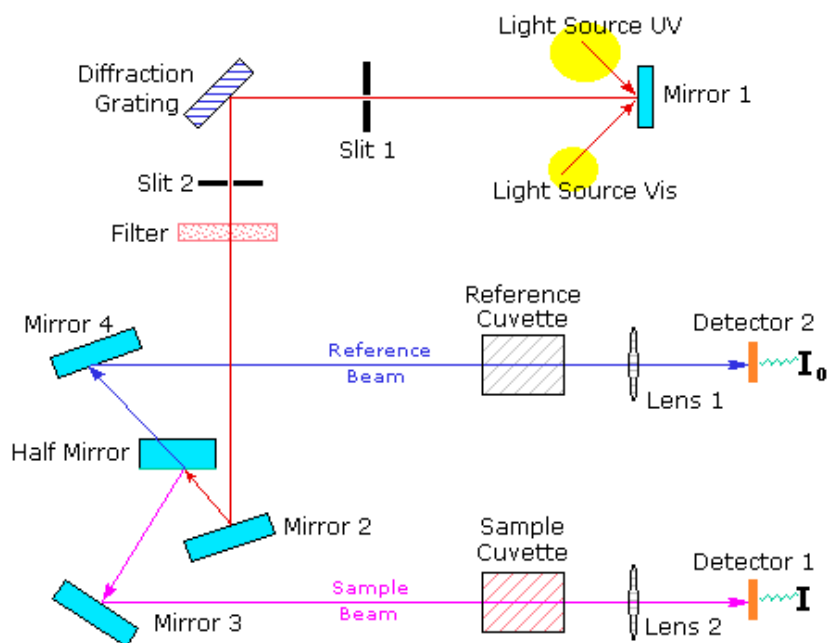
Figure 3.8 : A diagram of the components of a typical spectrometer

A beam of light from a visible and/or UV light source (colored red) is separated into its component wavelengths by a prism or diffraction grating. Each monochromatic (single wavelength) beam in turn is split into two equal intensity beams by a half-mirrored device. One beam, the sample beam (colored magenta), passes through a small transparent container (cuvette) containing a solution of the compound being studied in a transparent solvent. The other beam, the reference (colored blue), passes

through an identical cuvette containing only the solvent. The intensities of these light beams are then measured by electronic detectors and compared. The intensity of the reference beam, which should have suffered little or no light absorption, is defined as I_0. The intensity of the sample beam is defined as I. Over a short period of time, the spectrometer automatically scans all the component wavelengths in the manner described.

3.3.1 Uv-Vis-NIR spectroscopy

Another popular method is UV-Vis absorption spectroscopy for examining the purity. Optical absorption is a powerful technique that can be effectively employed to measure the type and quality of SWCNT in a sample [57], [58], [59] and [60]. The absorption spectrum of SWCNT exhibits the characteristic bands of the 1-dimensional van Hove singularities. Semiconducting SWCNT give rise to transitions between mirror singularities in the electronic density of states termed S_{11}, S_{22}, etc. Integrating intensity of these bands and the spectral background provides a valuable parameter that can be used to estimate the purity of the sample.

To measure the absolute amount of SWCNT in SWCNT soot, a reference SWCNT sample with 100 % purity is required. Figure 3.9 shows UV-VIS-NIR absorption spectrum of the reference. In the figure, semiconducting (S_{11},S_{22}), metallic (M_{11}), and π-plasmon peaks of SWCNT are clearly visible.
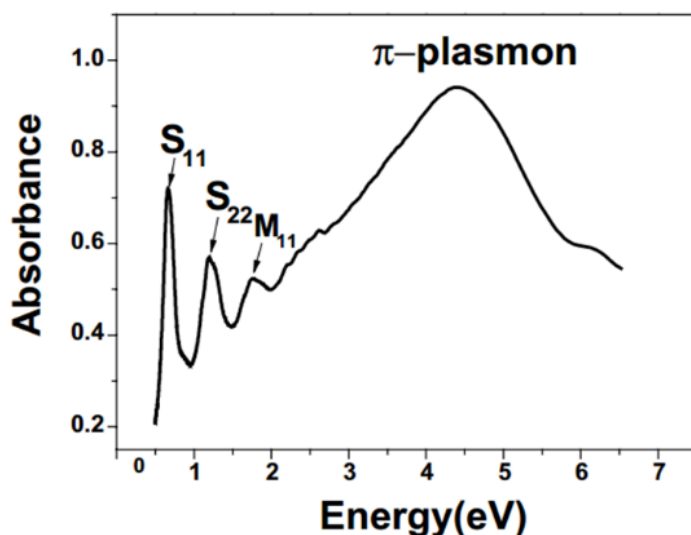
Figure 3.9 : UV-VIS-NIR absorption spectrum of the reference.

The first peak is at around 0.8 eV (S_{11}). The second is at around 1.5 eV (S_{22}). These two peaks correspond to absorption characteristic of semiconducting SWCNT. The

third peak at around 2 eV (M_{11}) corresponds to the valence band to conduction band transition of metallic SWCNT. S_{11} peak is very sensitive to the doping condition and environment because it is near Fermi level. It is well known that the ratio of semiconducting SWCNT and metallic SWCNT takes a variety of different values depending on the synthesizing methods and the chemical processing. Covalent modification of SWCNTs induces changes in the electronic structure that can be probed by optical absorption spectroscopy. With an increasing degree of functionalization, the π-conjugation is increasingly deteriorated.

At low densities of attached groups, the S_{11}, S_{22} and M_{11} transitions can still be discerned in the UV-Vis–NIR spectrum (with diminished intensity). (red trace).Figure 3.10[62-68]. This method applies only to very low concentrations, at odds with the push toward dispersing SWNTs at high loadings. To make suspensions measurable, carbon nanotubes have to be greatly diluted. However, dilution could change both the surfactant aggregates.
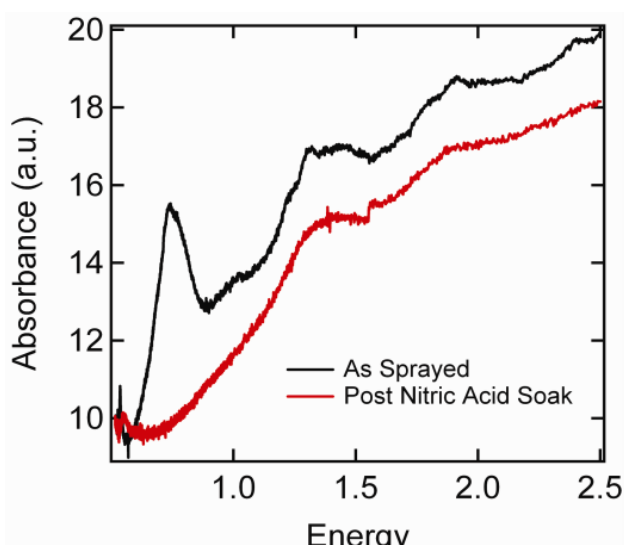
Figure 3.10 : UV-VIS-NIR absorption spectrum of the reference SWCNTs.

Figure 3.11 is shown UV–VIS–NIR spectra of SWNTs at different stages of purification of the same batch of raw SWNTs. Dotted lines are spectra of samples purified by centrifugation. Solid lines are spectra of samples purified by oxidation. The spectrum marked as ''100 %'' corresponds to SWNTs purified by oxidation with subsequent centrifugation. All spectra were normalized at 400 nm to the same absorbance.
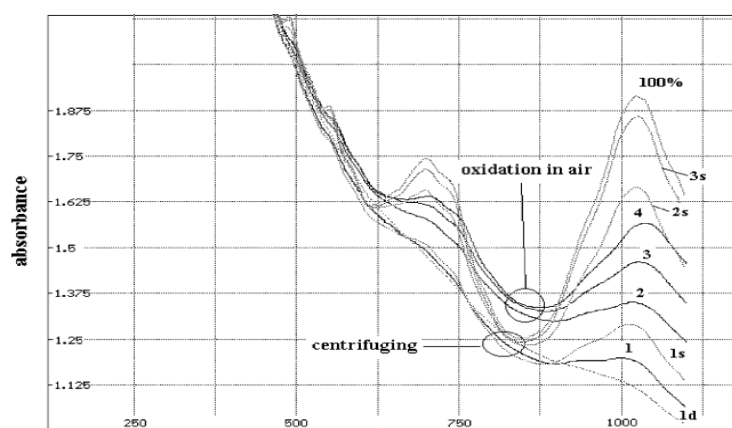
Figure 3.11: UV−VIS−NIR spectra of SWNTs at different stages of purification (1) raw sample, (2–4) samples after first, second and third steps of oxidation.

It is seen that in the course of purification the relative intensity of peaks increases. Peaks are caused by absorption of SWNTs owing to transitions between 1D van-Hove singularities. Fig. 3.11 shows spectrum of first deposit sample 1d with low abundance of SWNTs and low intensity of 1D van-Hove singularities.

The correlation between intensity and abundance may be used for estimation of the abundance of SWNTs from the heights of peaks over the background.

3.4   X-ray Diffraction (XRD)

XRD analysis is based on constructive interference of monochromatic X-rays and a crystalline sample: The X-rays are generated by a cathode ray tube, filtered to produce monochromatic radiation, collimated to concentrate, and directed toward the sample. The interaction of the incident rays with the sample produces constructive interference (and a diffracted ray) when conditions satisfy Bragg's Law ($n\lambda = 2d \sin\theta$). This law relates the wavelength of electromagnetic radiation to the diffraction angle and the lattice spacing in a crystalline sample.The characteristic x-ray diffraction pattern generated in a typical XRD analysis provides a unique "fingerprint" of the crystals present in the sample. When properly interpreted, by comparison with standard reference patterns and measurements, this fingerprint allows identification of the crystalline form.

3.4.1   XRD analysis for CNTs

This characterization method is not cause to ruin of sample. X-ray diffraction was performed in order to determine the effects of chemical treatment and annealing on the nanotubes and their crystalline organization, to follow the evolution of impurity phases throughout the process, and to obtain another estimate of the diameter distribution in fact, it is used to obtain some information on the interlayer spacing, the structural strain and the impurities. However, carbon nanotubes have multiple orientations compared to the X-ray incident beam.

Diameters and chiralities distribution are also observed as well as various number of layers for MWNTs. This leads to a statistical characterization of carbon nanotubes. The main features of X-ray diffraction pattern of CNTs are close to those of graphite. The first family of peaks; the graphite-like (002l) peaks occur at integer multiples of $2\pi/C_o$. Their positions give information on the spacing C_o between the layers, which is systematically found larger than in HOPG. These peaks are nearly symmetric in shape. The slight a symmetry is caused by a continuous decrease of the interlayer distance with increasing diameter of the shells [56]. The second family of peaks due to the honeycomb lattice of the individual layer and comprises the (hk0) reflections of a graphene sheet.
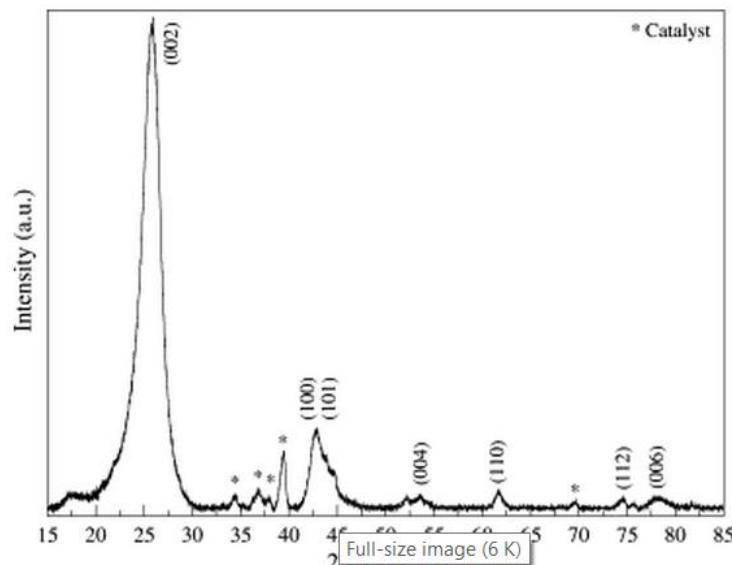
Figure 3.12: XRD pattern of MWNTs synthesized by CVD. The incident X-ray wavelength is λ=0.154056 nm. The most significant Bragg peaks are noticed with Miller indices. The presence of catalysts in the CNT sample is shown by stars.

Consequently, the X-ray diffraction profile is not useful to differentiate microstructural details between the CNTs and the graphite structure but can help to determinate the sample purity (catalyst, functional groups)[57]. A mean diameter of CNTs can be calculated through the use of the Debye–Scherrer relation on (002) peak. There is contributions from both the nanotubes and residual graphite in the (002) peak so the values are calculated from peak decomposition. X-Ray data indicates that acid treatment greatly reduces the background and eliminates the catalysist peaks.
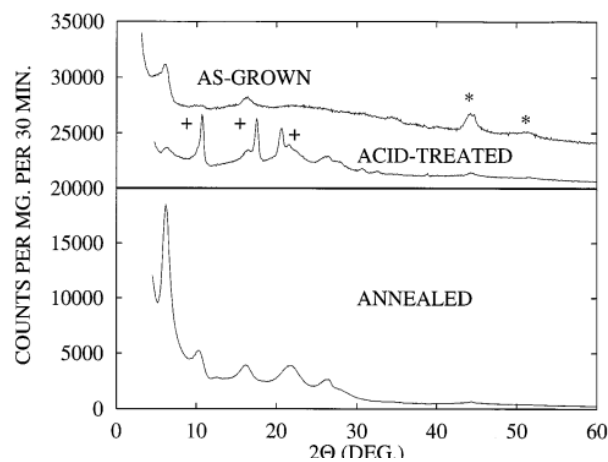
Figure 3.13: X-Ray data for SWNT material. Top (as grown and acid treated material).Bottom (material after annealing)[49]

3.5   Atomic Force Microscope (AFM)

The atomic force microscope (AFM) system has evolved into a useful tool for direct measurements of intermolecular forces with atomic-resolution characterization.
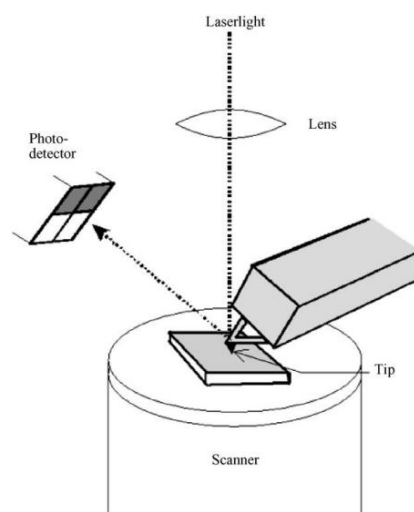
Figure 3.14: Schematic of an atomic force microscope.

A typical AFM system consists of a micro-machined cantilever probe and a sharp tip mounted to a Piezoelectric (PZT) actuator and a position sensitive photo detector for receiving a laser beam reflected off the end-point of the beam to provide cantilever deflection feedback. The principle of AFM operation is to scan the tip over the sample surface with feedback mechanisms that enable the scanners to maintain the tip at a constant force, or constant height above the sample surface. As the tip scans the surface of the sample, moving up and down with the contour of the surface, the laser beam deflected from the cantilever provides measurements of the difference in light intensities between the upper and lower photo detectors. Feedback from the photodiode difference signal, through software control from the computer, enables the tip to maintain either a constant force or constant height above the sample.

Probe artifacts:Images measured with an atomic microscope are always a convolution of the probe geometry and the shape of the features of the images being measured, then the probe-generated artifacts will be minimal and the dimensional measurements derived from the images will be accurate. Avoiding artifacts from probes is achieved by using the optimal probe for the application, for example, if the features that being imaged have feature sizes of interest in the 100 nanometer range, probe as large as 10 nanometers in the diameter will be adequate for getting good images with no artifacts.in some cases, even if the probe is not as sharp as the object being imaged, it is still possible to get accurate information from the image. Common artifacts are:
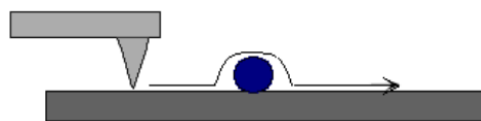
Figure 3.15: Features in an image appear too big

Motion of an AFM probes as it goes over a sphere that is attached to a surface. In such a measurement, the side of the probe will cause a broadening of features in the image.

Figure 3.16: Features in an image appear too small

The motion of an AFM probe as it moves over a hole in a surface. Because of the probe, it does not reach the bottom of the hole.

Scanner artifacts: Scanners that move the probe in an atomic force microscope in the X, Y and Z direction are typically made from piezoelectric ceramics. As electromechanical transducers, piezoelectric ceramic are capable of moving a probe very small distances. However, when a linear voltage ramp is applied to piezoelectric ceramics, the ceramics move in a nonlinear motion. Artifacts can also be introduced into images of the scanner relative to the sample can also create artifacts.

3.6   Contact Angle Measurements

Surface energy and roughness are parameters that can be check up on by contact angle measurements. The most important parameters defining how a liquid will contact a solid are the surface tensions, γ, of the three phases in contact: γ_{LG} (liquid–gas), γ_{LS} (liquid–solid) and γ_{GS} (gas–solid). Depending on the surface energy of a solid, a drop of liquid contacting it will either fully spread or form a defined drop. Full spreading will occur when the surface tension of the solid γ_{GS} is larger and partial spreading when γ_{GS} is smaller than the sum of γ_{LS} and γ_{LG}. the contact angle θ^Y of the drop is only defined by the surface tensions γ in contact.

$$\overline{\qquad\qquad}$$

(3.1)

It is important to recognize that the probing tool of the contact angle measurement is the moving contact line of the liquid, very much like the cantilever tip of an atomic force microscope (AFM).
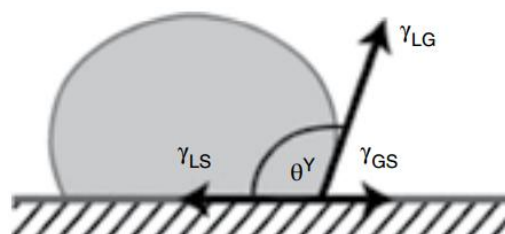
Figure 3.17: Drop on a surface: The force balance between the surface tensions g (G=gas, L=liquid, S=solid) define Young's contact angle θ^Y

3.7 Cyclic Voltammetry

3.7.1 Principles of cyclic voltammetry

To perform cyclic voltammetry (CV) experiments is needed for a three-electrode set-up: a working electrode (WE), a reference electrode (RE), and a counter electrode (CE). Using this set-up, a current–potential polarization curve can be recorded using a potentiostat for 1) controlling the voltage between the WE and the RE and 2) for measuring the current flow between the WE and CE. This principle is shown in fig.
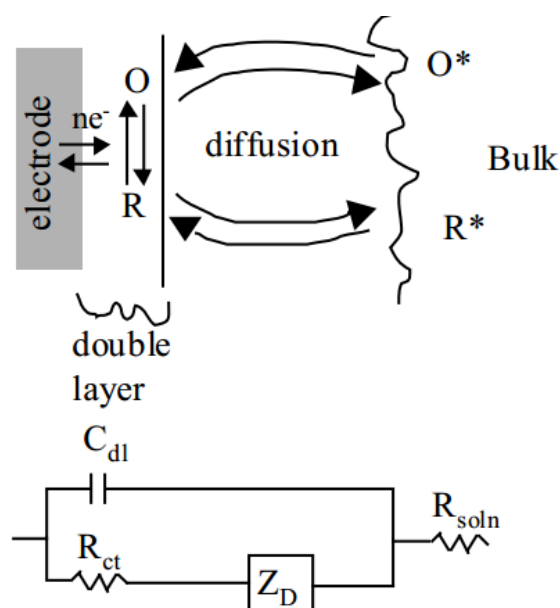
Figure 3.18 : Electrochemical system that includes electron transfer along with its equivalent circuit.

Figure 3.18 describes the process that occurs in simple electrode reactions. In the case of reduction, a species (O) capable of receiving an electron from the electrode diffuses to the surface, receives an electron and diffuses away from the surface. Current at the surface is generated by the transfer of electrons from the electrode to the redox species. In solution, current is carried by migration of ions. A transient current can flow because the electrode-solution interface will behave as a capacitor.

The potential of the working electrode is measured against a reference electrode, which maintains a constant potential, and the resulting applied potential produces an excitation signal such as that of figure. In the forward scan of figure 3.19, the potential first scans negatively, starting from a greater potential (a) and ending at a lower potential (d). The potential extreme (d) is call the switching potential, and is the point where the voltage is sufficient to have caused an oxidation or reduction of

an analytic. The reverse scan occurs from (d) to (g), and is where the potential scans positively. Figure shows a typical reduction occurring from (a) to (d) and an oxidation occurring from (d) to (g). It is important to note that some analyses undergo oxidation first, in which case the potential would first scan positively. This cycle can be repeated, and the scan rate can be varied. The slope of the excitation signal gives the scan rate used.
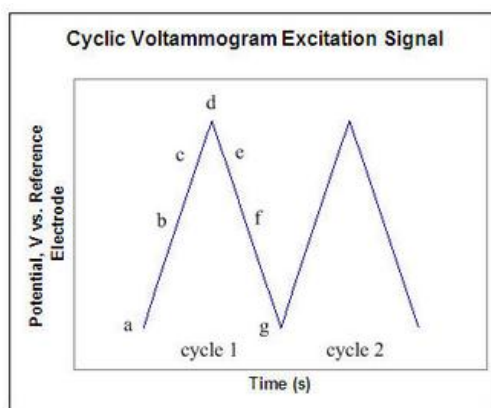
Figure 3. 19 : CV Excitation Signal

About the cast films of SWNTs on Pt and Au electrodes, but the films did not show well-resolved voltammograms. The SWNTs were treated with nitric acid during the purification process. The carboxylic acid groups were introduced on the open ends of the SWNTs [82]. The working electrode was a glassy carbon electrode with a diameter of 4 mm, the auxiliary electrode consisted of a platinum wire, and a saturated calomel electrode (SCE) was used as the reference electrode. Water was triply distilled with a quartz apparatus. High purity nitrogen was used for reaeration. All cyclic voltammetry experiments were carried out at room temperature (about 15°C). When a SWNT film-modified GC electrode was placed into PH 6.9 Britton-Robinson (B-R) buffer solution, a pair of reduction/re-oxidation waves was observed. The peak potentials and peak current remained very stable after the second cycle.
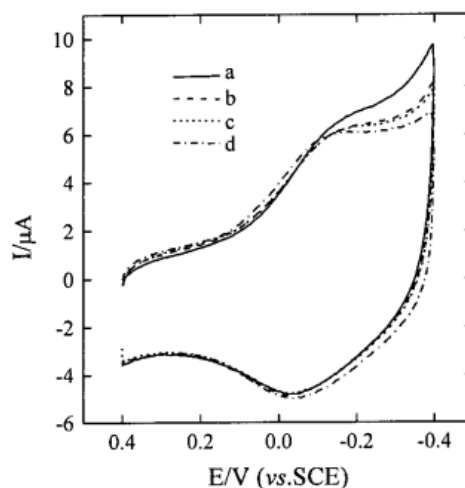
Figure 3.20 : Cyclic voltammograms of the SWNT film on a GC electrode in pH 6.9 B-R buffer, 0.1 V s^{-1} scan rate between 0.4 and -0.4 V. (a) The first, (b) the second, and (c) the third cycle, and (d) after 24 h.

It has been observed, while using individual nanotubes as electrodes, that the nanotubes do not exhibit good wettability. However, when using nanotube based microelectrodes, the electrode has a porous structure and is probably well wetted by the solvent/electrolyte medium. In the context of edge vs basal plane reactivity, it must also be remembered that the surface electronic structure of nanotube layers is not entirely graphite basal-plane-like due to the helicity, low dimensionality, and possible topological defects. The activation energy for the reaction decreases with increasing the electronic interaction width. The structure of the tubes, as well as their different local density of states, might be responsible for the increase of the electronic-energy interaction width.[83-85]

4. CNT DISPERSIONS AND THIN FILM FORMATION

4.1   CNT Dispersions

A uniform and stable dispersion of carbon nanotubes plays an important role, because when submicron or nanometer-sized particles are involved, the surface chemistry controls the dispersion state of the particles within a final product. It is extremely important to learn how to manipulate the surface properties in order to achieve a product with the desired properties. There are some challenge in fabrication of transparent and conductive SWNTs electrodes such as poor solubility of carbon nanotubes and poor uniformity of SWNTs films. In addition, control of films thickness and roughness are some of defiances in produce thin film with acceptable transparency.

There are two types of deposition methods for SWNT films: vacuum process such as CVD and solution-based process. In CVD, a high temperature is needed which is not suitable for plastic substrates; therefore, an additional process is required to transfer the SWNT films onto the plastic substrates. Furthermore, since the as-grown nanotubes include various impurities, the conductivity of as-grown SWNT films is normally low. Solutions based on the deposition method, a process based on nanotube ink, can solve these problems. The dispersion conditions are critically important for the formation of transparent conducting films (TCFs) [73,74]. In order to overcome this difficulty, surfactants or dispersants have been introduced to debundle the large collections of nanotubes into individual nanotubes or to reduce the bundle size. To exploit that, many groups have suspended nanotubes in organic [75] and aqueous media [76-78].

SWNTs can be suspended in aqueous media by non-covalent interactions using surfactants or using non-ionic polymers [79].

For enhancement of dispersion nanotube in water, Surface modification by covalently functionalizing of carbon nanotube walls using aryl-carboxylic acid or aryl-hydroxyl groups (-OH, -Cl, and -NO$_2$) [80] was a successful strategy. The presence of (modified) carboxyl groups leads to a reduction of van der Waals

interactions between the CNTs, which strongly facilitates the separation of nanotube bundles into individual tubes. Additionally, the attachment of suitable groups renders the tubes soluble in aqueous or organic solvents, opening the possibility of further modifications through subsequent solution-based chemistry. A high water solubility of a few tenths of a gram per milliliter has recently been achieved on the basis of the carboxyl-based coupling of hydrophilic polymers such as poly(ethylene glycol) (PEG) [81] SWCNTs with a good solubility in organic solvents can be obtained by covalent[82] or ionic[83] attachment of long-chain aliphatic amines onto the carboxyl groups.

Surprisingly, very low levels of covalent reaction (1-2 groups per 100 carbons) can outweigh the more prevalent SDS coverage in determining the extent of SWNT surface adsorption onto the silicon oxide surface. For aryl chloride, adsorption is enhanced, while the opposite occurs with the aryl nitro and aryl hydroxyl groups. Figure 4.1. Unreacted control-SDS and Cl-SDS samples show the highest level of deposition. All other samples show similar surface coverage. Debris associated with the unpurified SWNT sample is shown.
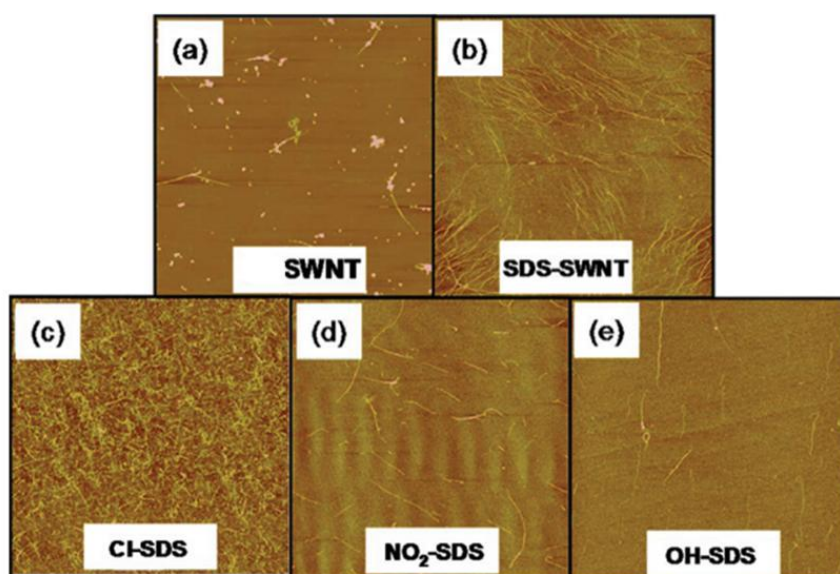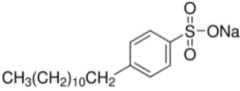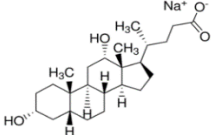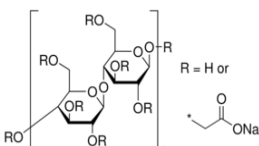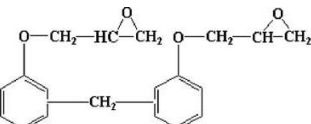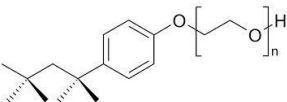
Figure 4.1: Representative AFM images of (a) unreacted SWNT and SDS-suspended carbon nanotube samples, (b) control-SDS, (c) Cl-SDS, (d) NO2-SDS, and (d) OH-SDS.

All these methods create groups at CNT walls, which can act as recombination centers for generated charges. [91,96]. These materials exfoliate nanotubes very efficiently and can disperse nanotubes at reasonably high concentrations. Single-

walled carbon nanotubes have been suspended in aqueous media as individuals surrounded by different surfactant such as sodium dodecyl sulfate (SDS) or sodium dodecylbenzene sulfonate (SDBS) as adsorbed phase. (Table 4.1)

Table 4.1: Surfactants used for the thin film formation of SWNTs in aqueous solutions

Surfactant	Structure	Method
Sodium dodecylbenzenesulfonate (SDBS)		Spray coating/ Acid treatment
Sodium dodecyl sulphate (SDS)	$NaC_{12}H_{25}SO_4$	.Spray coating/ Acid treatment
Sodium deoxycholate (DOC)		.Drop casting/ .Acid treatment
Sodium carboxymethyl cellulose (CMC) average M_w ~70,000, powder		Spray coating/ Acetone treatment
Epoxy resin (Epon 862/EPI Cure W system		Filter method using porous alumina matrix/ .Annealing
Octyl-phenol-ethoxylate (Triton X-100)		pin casting

Three surfactants; sodium deoxycholate (DOC), sodium dodecylbenzenesulfonate (SDBS) and sodium dodecylsulphate (SDS) with decreasing attractive forces to SWNT surfaces lead to three different morphologies of CNT thin films formed by spin casting. The bundle thickness on the formed thin film is expected to depend on the type of surfactant. The dispersion ability varies as DOC > SDBS > SDS, and thus, the attractive force between the SWCNTs is believed to change as SDS > SDBS >DOC. DOC dispersion presents the case of a weak attractive force between CNTs. In this case, an individual random network can be formed being maintained in the dispersion. For the films formed from DOC, fine mesh structures were observed. The thicknesses of the bundles were approximately 1 nm for DOC, respectively. when the attractive force between CNTs increases as in SDBS dispersion, the CNTs begin to align locally in the same direction. Long, bundled ropes formed a homogeneous and

continuous but coarse mesh (approximately 10 μm). For the largest attractive force, such as the SDS dispersion, the CNTs form the thickest bundles. (Figure 4.2b).
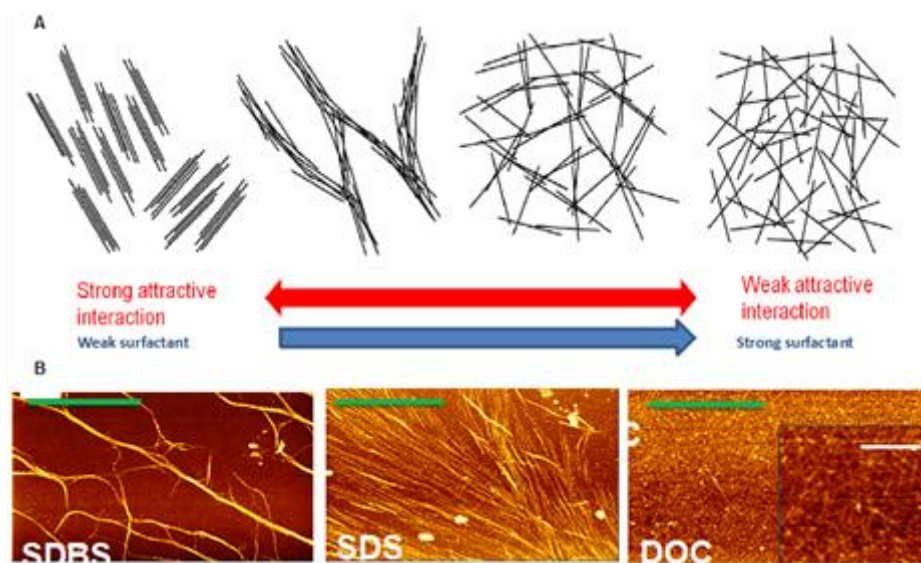
Figure 4.2 : a) Schematic images of the carbon nanotubes with different strength of attractive interactions in solution. b) AFM images of drop casted SWNT layers using SDBS, SDS and DOC as surfactant

A surfactant with a stronger dispersion ability should be in principle better suited to produce CNT electrodes, because it is important to keep the bundles thin to obtain highly transparent electrodes. On the other hand, the surfactant molecules with lower dispersion abilities could adhere not so strongly that the presence of residual surfactant on the CNTs after washing is negligible, leading to low contact resistances. According to conductivity measurements, between DCE, H_2O: SDBS and H_2O: SDS prepared films, SDS is the most favorable surfactant. The SWCNT film prepared with H_2O: SDS demonstrate a sheet resistance of 57 V/sq at 65 % transmittance and a conductivity in excess of 6700 S cm^{-1} [75]. Using the SDS containing CNT inks, smooth electrodes could be prepared using spin-coating and also spray coating techniques. It should be noted, that adding the surfactant into the mixture of CNT in aqueous media often requires processes, such as high-power ultrasonication, which may degrade the nanotube surface and may reduce the average lengths of the tubes. . The surfactant provides sufficient electrostatic repulsion to nearby SWNTs to prevent re-aggregation. With the aid of mechanical sonication to break up SWNT bundles, the hydrophobic tails of the surfactant can attach to individual SWNTs and create stabilized solutions of individual SWNTs in water. Figure 4.3 illustrates this process [86].
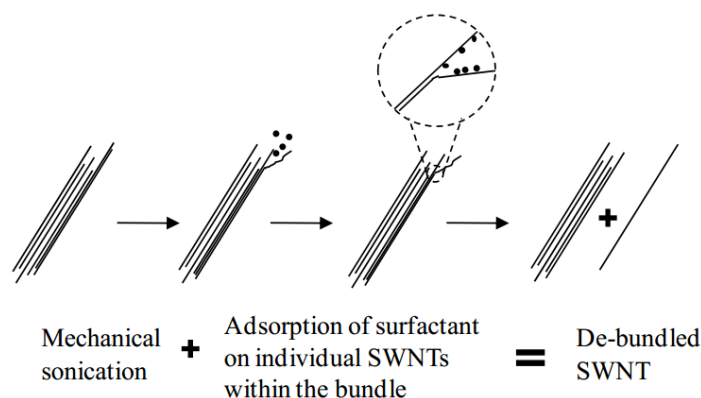
Figure 4.3: Schematic of individual nanotube isolation from bundle via ultra-sonication and surfactant adsorption.
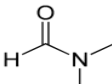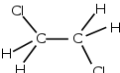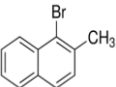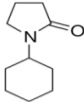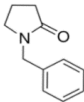
The filter/transfer (FT) approach has the benefit of yielding loosely bundled films that permit easy removal of insulating surfactants by washing in deionized water. This method involves vacuum filtering of a dilute suspension of nanotubes in aqueous solution over a porous alumina filtration membrane. The density of these films can be controlled roughly by controlling the volume of the suspension.

Direct dispersion of CNTs in a suitable solvent is the simplest and the most favorable method especially for p/n junctions in purely organic and in organic-inorganic hybrid bulk heterojunction solar cells. Room temperature solubility of the SWNTs in same organic solvents and the surface tension of the organic solvents are listed in (Table 4.2). [84-87].

For example , 1,2-Dichlorobenzene was found as reasonable solvent for the SWNTs, although the experience show that aggregation in form of small bundles occurs as result of the strong van der Waals interaction between the carbon nanotubes during the storage.

Solvents with electron pair donation, higher polarity and low values of the hydrogen bond donation parameter, such as N-Methyl-2-pyrrolidinone (NMP), dimethyl formamide (DMF), dichlorethan and cyclohexyl pyyrolidon have been identified as the best organic solvents to disperse CNTs to individually separated nanotube particles.

Table 4.2: Solubility parameter of SWCNTs in organic solvents

Solvent	Structure	g/l	Surface tension mN/m
1,3,5-Trimethylbenzene [84]		0.0023	28.80
1,2-Dimethylbenzene [84]		0.0047	30.10
Dimethylformamide [84]		0.0072	37.10
1,2-Dichloroethane [85]		0.0087	38.75
1,2-Dichlorobenzene [85]		0.095	38.75
N-Methyl-2-pyyrolidinone [85]		0.010	40.79
1-Bromo-2-methylnaphthalene [85]		0.023	41.38
1-Cyclohexyl-2-pyrrolidon [86]		3.5	43
1-Methylnaphtalene [85]		0.025	38.60
1-Benzyl-2- pyrrolidinone [87]		3.5	45.00

Nanotubes in NMP spontaneously exfoliate on dilution of SWNT–NMP dispersions, leading to a dynamic equilibrium characterized by significant populations of pristine individual nanotubes and small bundles. Their ability to disperse and exfoliate nanotubes might be reasoned due to the low energetic cost of exfoliation in such solvents. Finally, their relative lack of toxicity makes these solvents much more user-friendly than traditional nanotube solvents such as N-methyl-pyrrolidone or dimethyl-formamide. A disadvantage of this solvents is their high boiling point (Bp of about 150 °C) [89-90].

The most effective method to identify solvents to disperse nanoparticles in solvents depend on conforming the surface energy of the solvent and the surface energy of the nanoparticle, generally. SWNTs have surface energies of about 70 mN/m [86]. For all solvents, the surface tension is about 30 mN/m below the surface energy [87] of the solids. This means that efficient solvents for SWNTs are the one with surface tensions of about 40 mN/m. However, the expected relationship is not approved in praxis. Because of their uniaxial growth, a strong tendency to form bundles occurs because of the strong van der Waals interaction between the tubes

Most of the organic solvents are unable to disperse CNTs at a concentration high enough to be useful for industrial applications (>0.1 mg/mL). After stable nanotube ink is formed, coating methods are applied and Characterization of the nanotube films is done with AFM, SEM, sheet resistance and optical transparency measurement. Much work has been done to deposit carbon nanotube films on various substrates, such as spin coating, filtration and transfer by etching filters, self-assembly, and others. The basic idea of deposition of nanotube films involves two steps: 1) lay down nanotube solution on the substrates and dry; 2) wash away the surfactants. I will focus on four deposition methods for fabricating nanotube films.

4.2 Thin Film Formation

4.2.1 Spin coating

Spin coating is a common laboratory process used to apply uniform thin films to flat substrates. An excess amount of solution is placed on the substrate that is subsequently rotated at high speeds to produce a centrifugal force that spreads the

fluid uniformly over the substrate. The SWNT film thickness was controlled by the number of times a spin-coated layer was allowed to dry to have a successive layer spin coated on top of it. Kim et al. [91] were dispersed the dried SWCNTs (2 mg) in DCE (200 mL). the SWCNT/solvent mixtures were subjected to ultrasonic agitation (100 W) for a period of 12 h. High-speed (15 000 rpm) centrifugation was then used to induce sedimentation of large SWCNT bundles, after which homogeneous dispersions of the SWCNTs were obtained by decanting the upper 50% of the supernatant. Glass substrates (12 mm×12 mm) were cleaned with ethanol and detergent and then dried in a stream of nitrogen gas, prior to baking for 30 min in an oven (1008 ^{o}C). The substrates were then coated with SWCNTs ink. The SWCNT films shows sheet resistances around 100Vsq^{-1} at reasonable transmission 128±2 V.sq^{-1} at 90   25 nm.
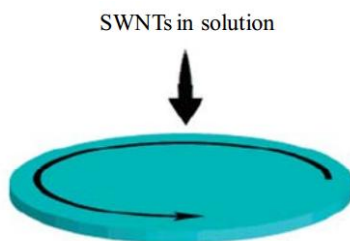
Fig 4.4: Schematic process of SWNT spin coating procedure.
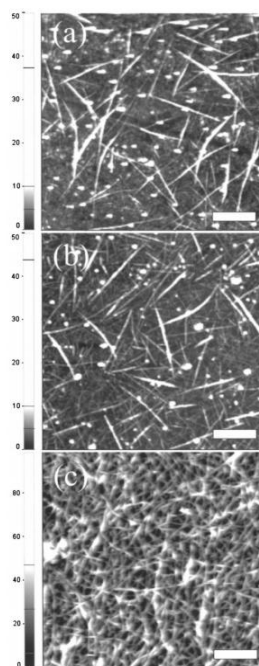
Figure 4.5 : Typical AFM images of SWCNT films on glass substrates: single spin coating using (a) poor and (b) good dispersion, and (c) after repeating spin coating 100 times. The scale bar is 1 μm.

4.2.2 Spray coating

In this simple approach, SWNT solutions are directly sprayed onto substrates via an airbrush pistol or spray tools. Before the spraying, the substrates such as glass and silicon wafers need to be silane treated, which is done either by soaking the substrates in 1% silane solution in water for 5 minutes or putting them into the silane vapor chamber for 10 minutes. The substrate is kept hot during the process (ca. 100°C) to accelerate drying of the fine solution droplets on the surface. After one spray, the substrate is immersed in DI water (room temperature) or Methanol for 1 minute, then is sprayed again, and immersed in water. The spraying and immersion in water are repeated multiple times until the desired sheet resistance is achieved. Washing multiple times is essential here. It could increase the conductivity of the network by removing the SDS surfactant between the SWNTs. Furthermore, the washing between each brief spray results in more homogenous films without observable dots. Figure 4.6 shows the spray setup schematic.
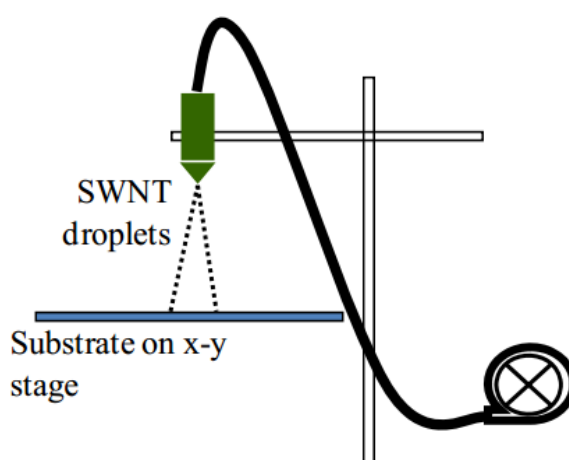
Figure 4.6: Schematic of spray coating method.

Spray coating technique provides a simple and quick method to create various film thickness, but important heterogeneity on the nanometer scale can find.in Figure 4.7 which reported by Kaempgen et al.[98] large error bars for film transparency in versus thickness can observe.
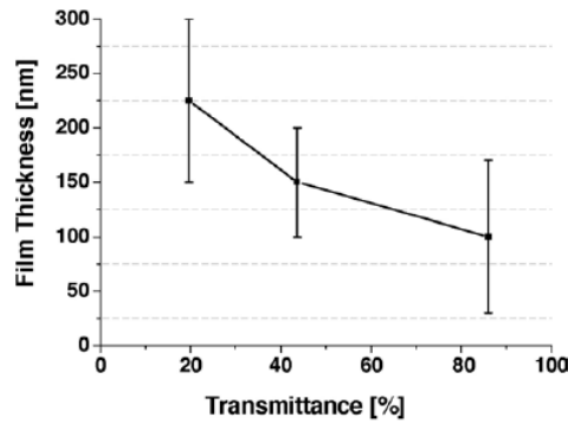
Figure 4.7: Transmittance (at 550 nm) versus film thickness of SWNT networks determined by AFM at step edges.

4.2.3 Dip-coating

The dip-coating method for depositing nanotube films has been reported by Tsukruk et al[100] However, because of the lack of control over the drying, large domain structures formed in the coated films due to the agglomeration in the long drying process. we will report here a much better method for dip coating nanotube films, which can be applied to any nanostructure fabrication. The method involves first depositing a solution of SWNTs in a solvent (with or without a surfactant) on a substrate. The solvent is subsequently flash-dried from the solution in a uniform manner. Such flash drying begins on one side of the substrate, and sweeps across the substrate in a "drying wave." Heat can be applied in various Manners Additionally, solvent evaporation may be aided by air-flow blow drying, and the substrate may undergo subsequent water rinsing to remove surfactant. To achieve a coat o f a desired thickness, this process can be repeated multiple times. Factors that determine the number of cycles required for a certain film thickness include the concentration of nanostructures in the solution. Advantages of the method of the present invention include its simple design, ability to produce relatively uniform nanostructure-films, large scale processing potential, and compatibility with established Meyer rod technology. Figure 4.8 shows Schematic drawing of the dip-coating method.
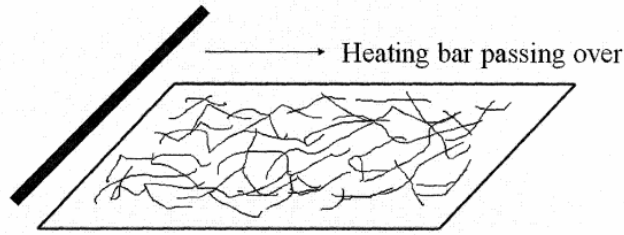
Figure 4.8 : Schematic drawing of the dip-coating method.

4.2.4 Self-assembly

Self-assembly have been used for depositing nanotube networks for transistor applications. The nanotube ink is either in an organic solvent such as dichlorobenzene [101]. Since self-assembly can only lead to monolayer thick nanotube networks, this deposition method is used mainly for evaluation of the characteristics of nanotube source such as the length and bundle size, and for the solution-based transistor fabrications using the self-assembled sub-monolayer nanotube network as the active channel of transistors. Various substrates have been tested for this method, including glass, silicon wafer and ITO/PET substrates. As in the dip coating method, substrates including glass, silicon, ITO and gold need to be treated with silane gas or solution; other substrates, mainly polymer substrates, including PET, PEN, and polycarbonate, need no treatment. Usually, 0.1 mg/mL purified nanotube solution after centrifuge is used. The substrate is soaked in the solution for around 2-10 minutes, and blown to dry. Then the substrate is soaked in pure DI water for 20 minutes to remove the surfactants, and blown dry with N_2. The cross section of the image indicates the bundle size of nanotubes is 3-5 nm. Although many groups have claimed that SDS or NaDDBS surfactants can lead to individually suspended nanotubes in solution from the featured fluorescence spectra, it is observed that the nanotubes form bundles during the self-assembly process.

5. EXPERIMENTAL

5.1 Production of Carbon Nanotubes by Nickel Catalyst

CVD-made SWCNTs supplied by Energy Institute Material Production and Preparation Laboratory used.[102] CNT production experiments were conducted with CVD methods on a fluidized-bed system and synthesis of acetylene (C_2H_2) on a magnesium oxide (MgO) powder impregnated with nikel nitrate $Ni(NO_3)_2.6H_2O$. The CVD apparatus consists of a vertical furnace and a quartz glass tube with a diameter of 3 cm in which in the middle a quartz filter (Fig. 5.1). A magnesium oxide (100 m^2 g^{-1}) supported iron oxide powder produced by impregnation in an iron nitrate ethanol solution is used as precursor powder. To get a precursor with a MgO to Fe weight ratio of 5%, MgO were suspended in ethanol and nickel nitrate previously dissolved in 100 ml ethanol was stirred together and sonicated for 20 min in order to homogenize the mixture. Afterward the precursor was dried and grinded into a fine powder. For one deposition, typically, 0.6 g of precursor powder was filled in the quartz tube and the atmosphere was purged with argon for 5 min. Then the furnace was heated to the synthesis temperature (800 °C). By heating up the precursor, powder nickel oxide clusters were formed due to the thermal decomposition of the iron nitrate at 125 °C. The synthesis was started with the introduction acetylene mixed with argon for 60 min. After synthesis, the CNTs were cooled in inert gas (argon).
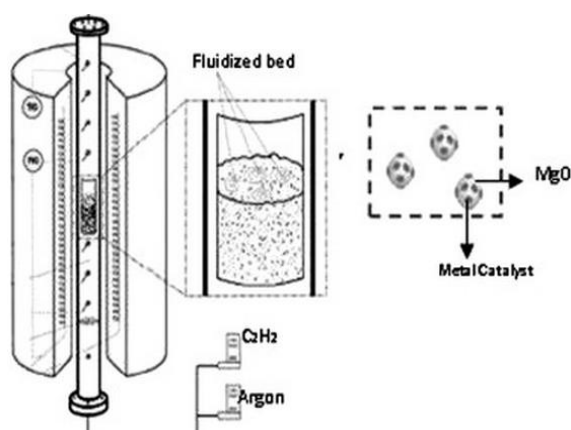
Figure 5.1: Schema of the fluidized-bed reactor [102]

5.2 Multi-step Purification

5.2.1 Treatment with toluene

The as-prepared material was stirring with toluene for 6 h. This procedure was used to remove the fullerenes and the soluble impurities. The sample was then washed with acetone and dried in air at 110 $^{\circ}$C.

5.2.2 Liquid-phase oxidation with H_2O_2

The step one sample was submitted to liquid-phase oxidation with a 10 % hydrogen peroxide (H_2O_2) solution. Preliminary results obtained with acidic peroxide solutions or in high concentration (20 % and 30 %) indicated a more intense damage to the structure of the SWCNTs. The conditions detailed here were optimized to minimize damage to the SWCNTs and to allow the complete removal of amorphous carbon. In a typical treatment, 600 mg of the step one sample were mixed with 300 mL of a 10 % H_2O_2 solution and submitted to ultrasonic horn for better dispersion. The mixture was refluxed at 100 $^{\circ}$C for 5 h, followed by filtration with a 0.4lm membrane under vacuum. The sample was then was washed with deionized water, followed by acetone, and dried in air at 110 $^{\circ}$C.

5.2.3 Acid treatment with an HNO3/SDS mixture

This acid treatment was carried out at room temperature, which minimizes the damage to the SWCNTs. In this process, 300 mg of the second step sample were sonicated in 100 mL of a mixture: 50 mL HNO_3 (98 %) and the surfactant SDS (sodium dodecyl sulphate) for 2 h. The surfactant allowed better dispersion of the sample, favoring the attack to the catalysts. The dispersion was filtered (0.4 lm membrane) and washed abundantly with deionized water (to neutral pH), followed by acetone and dried in air at 110 $^{\circ}$C.

5.2.4 Physical separation from the SDS dispersion

Approximately 500 mg of the third step sample was dispersed in 1.0 L of SDS 0.02 M solution by sonication, for 30 min. The dispersion was allowed to stand for 5 h and the supernatant phase was separated and filtered (0.4lm membrane). The material was abundantly washed with deionized water, followed by acetone and dried in air at 110 $^{\circ}$C.

With using Thermogravimetric Analysis (TGA), X-ray (X-ray) and Raman measurement method at the end of purification steps properties of changing material were evaluated.

5.3 Characterization

5.3.1 X-ray analysis

After synthesis and the step D purification of Produced CNT, X-ray analysis was conducted. X-ray peaks was observed MgO (111), MgO (200), MgO (311), MgO (222) of Produced CNT, however these peaks completely disappeared after purification of the step D. (111) of Co, 2θ X-ray peak (44 °) was reduced to almost nothing is shown in figure 5.2. From these results, it is seen that the purification method was successful.
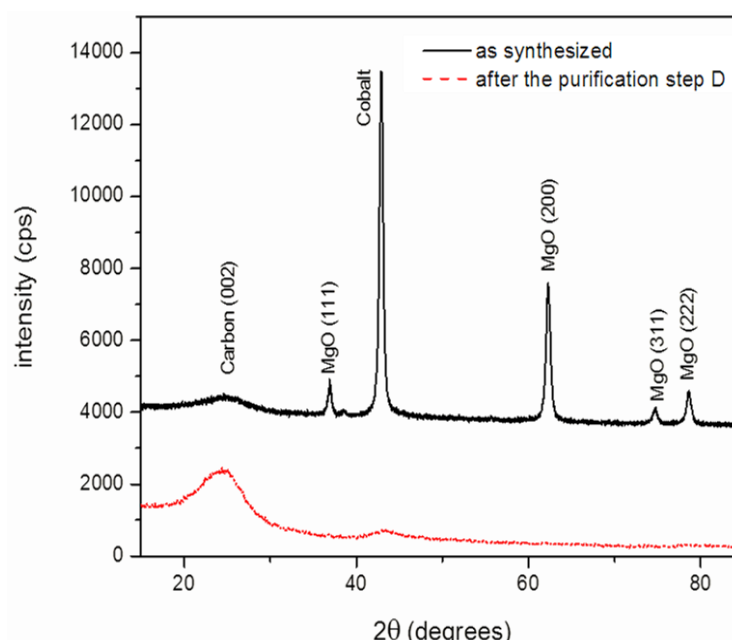
Figure 5.2 : XRD analysis of the synthesized CNT structure in different purification steps metallic elements are removed after purification, the broad peak of carbon (around $2\theta=26$) reveals that there are defects in the crystal structure of SWCNTs.

5.3.2 TGA analysis

Thermo-gravimetric analysis (TGA) is used to characterize the total carbon loading and determine the residual metallic catalyst. The resulting combustion enthalpy shows the oxidation of the carbon structure. The amorphous carbon is completely oxidized at temperatures below 350°C and graphite burns above 750°C. The

oxidation temperatures of the SWNTs depend on the nanotube type. As shown in figure 5.3, has high metal content (about 58%) and 42% compounds containing metal catalyst remaining back. In other words, under the synthesis conditions, only 58 % of manufactured material containing carbon nanotube. In step A The material is washed with toluene for 6h, so material was removed of the fullerenes and the soluble impurities. (Step toluene) in TGA analysis can observed that only 52 % of analyzed materials have been destroyed by fire. Compared synthesized material, and the remaining material from Step A, realized that in synthesis conditions, the ratio of fullerene and carbon based materials is estimated to be roughly near 6 %. The used acid in Step B for purification, although the metal catalyst used in the purification process, since there is no counter ion to form metal salts, it is obvious that the purification effect is too low. In Step B of the purification method, the measured material with TGA includes 64 % CNT and 36 % components of the metal catalyst. At the end of purification steps C and D, 100 % combustion has occurred the TGA analysis to contain 100 % pure CNT material, which is shown in figure 5.3. The surface-active material used in Step C, effectively opened the bundles of carbon nanotubes and tucked metal catalyst component is oxidized in the acid environment, it was concluded that the removed from the mixture. This diagnosis is supported by the X-ray measurements.
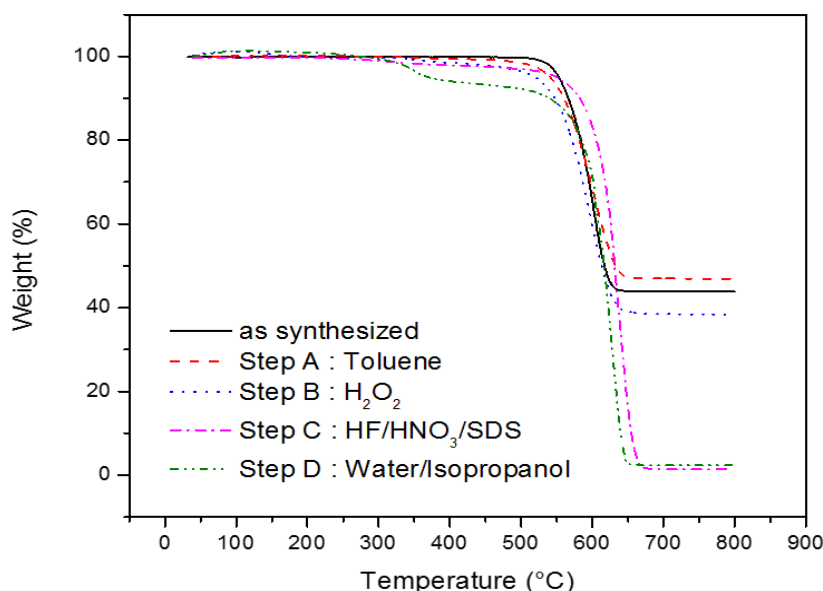
Figure 5.3: TGA analysis of the synthesized CNT structure realized after different purification steps

TGA in air Ramp 10.00 °C/min from 38 to 800.00 °C. By purification, the amount of the CNT remaining after 650 °C is nearly zero.

5.3.3   Raman spectroscopy analysis

In Raman spectroscopy of CNT structures, The G'-bands are associated with sp^2 bonding in carbon systems and occur and frequencies are around 1500 cm^{-1} – 1650cm^{-1} and it provides information to distinguish between metallic and semiconducting SWNTs. A disorder-induced band (D-band) occur at 1250- 1450 cm^{-1} and it depends on the amount of carbon impurities and on the density of surface defects. The radial breathing mode (RBM) Raman features are unique for SWNTs and occur between 120 and 350 cm^{-1}. After synthesis and purified CNT materials, G-band peak was observed around 1576-1580 cm^{-1}. There is also a slight ridge around 1540 cm^{-1}. In references, this asymmetric peak structure was usually observed for metallic CNT structure. This evaluation shows that it has metallic properties in the material, which used. D/G ratio has increased after purification.it increased from 0.3 to 0.4, which demonstrate that the materials used during the purification, modified the CNT surface.it means that defects have increased. It was estimated that on acidic environment, COO- groups formed on the surface of CNT, which is the type of s of 'error's and it caused to have increased the intensity of the D band near to 30 %.
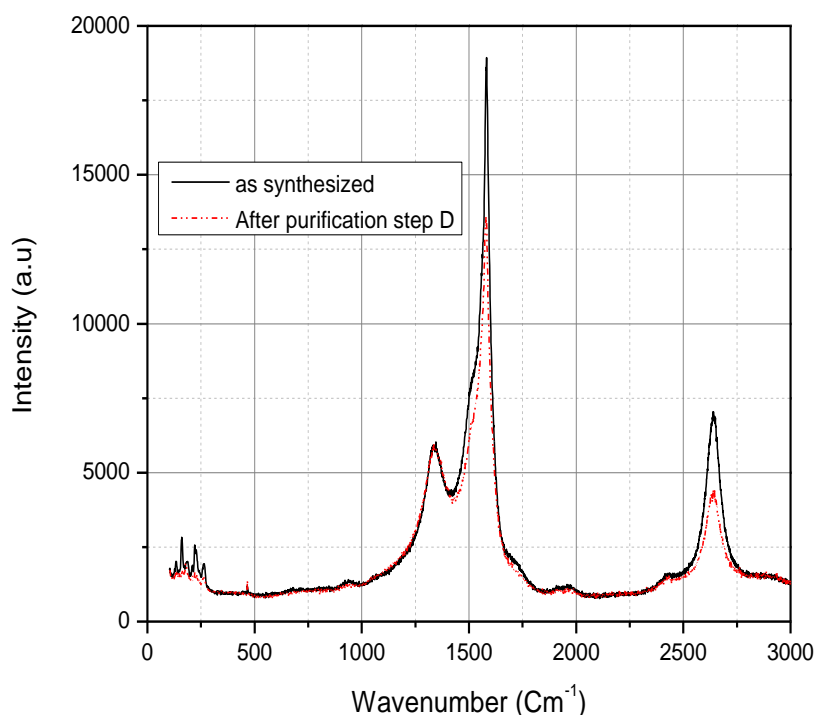
Figure 5.4 : Raman Spectroscopy analysis of the synthesized CNT structure in the different purification steps
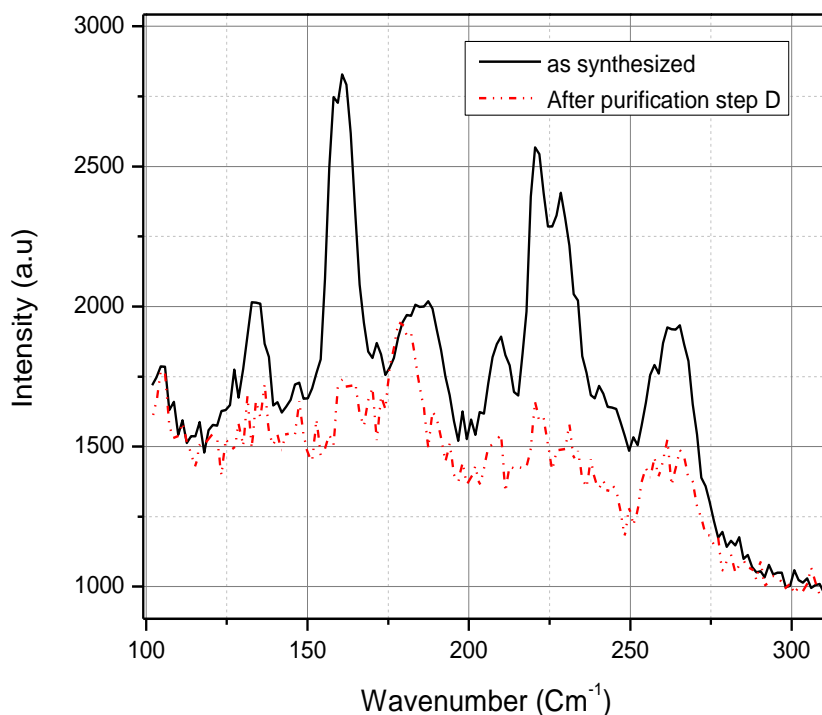
Figure 5.5 : RBM region of SWCNTs.

These peaks in the RBM region, confirms SWCNTs existence before and after purification.

5.4 Preparation of CNT inks

Surfactants,CNT and water in order to prepare the ink for forming thin films by spin-coating method, first the surfaces of pure CNTs were functionalized by adding polar groups. to this end, $K_2S_2O_8$ which is strong oxidizing material dissolved in distilled water.

A 100 mL flask was charged with a magnetic stirring bar,

1)   2.0 g of DOC, 20 mg of purified SWNT and 30 mL of water.

2)   2.0 g of SDS, 20 mg of purified SWNT and 30 mL of water.

3)   2.0 g of SDBS, 20 mg of purified SWNT and 30 mL of water.

After stirring for 10 h at room temperature, 20 mg of $K_2S_2O_8$ was added, and the mixture was degassed by azote cycles. The flask was heated at 65 ºC under stirring to start polymerization. After 48 h the reaction was stopped by cooling to room temperature and opening the flask to air.

 Expected reaction stream is like it:

(5.1)

The mixture was diluted to 250 mL with water, bath sonicated for 1 h, and centrifuged at 6,000 X g for 8h. The homogenous black supernatant was removed.

In figure 5.6 which is Schematic illustrating the process of SWCNT electrode fabrication; involves the following key steps: dry CVD-made SWCNTs were added to a solvent or surfactant and water (H_2O:DOC, H_2O:SDS or H_2O:SDBS) and subjected to high-speed centrifugation; the upper 50% of the supernatant was retained; SWCNT films were deposited by spin-coating and patterned by selective oxygen-plasma treatment.
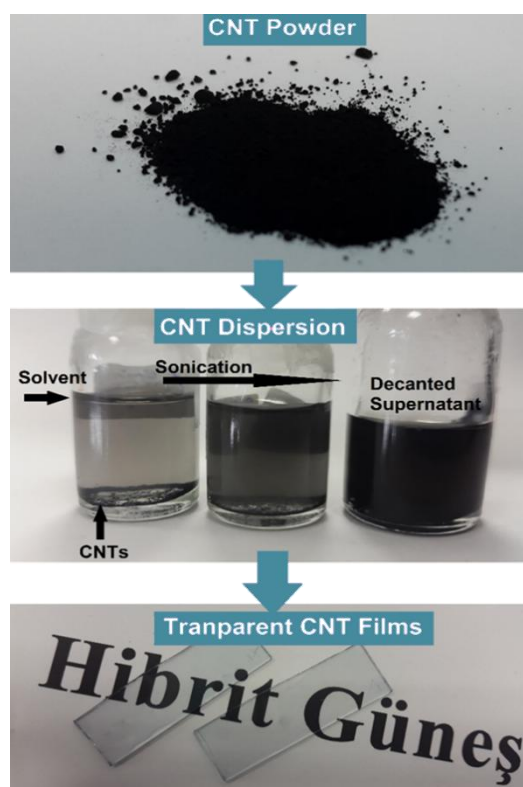
Figure 5.6 : Schematic illustrating the process of SWCNT electrode fabrication.

The resulting mixture of Glass substrates (15mm X 15mm) were cleaned with acetone and propanol each one for 15min in Ultrasonic Bath and then dried in a stream ozone gas, and were placed at UVO cleaner for 15min.

For provide etch ITO coated on glass We take the ITO coated glass, protected by plating tape, and dip it into the acid etch. Our etch mixture is 300mL deionized water, 225mL hydrochloric acid (HCl), and 75mL nitric acid (HNO_3). The etch time for our ~150nm thick ITO is 15 minutes under vigorous stirring at room temperature. We then rinse off the acid under DI water.

Poly (3, 4-ethylenedioxythiophene) (PEDOT) can be filtered by syringe filters in this work we use 0.45 um and 0.22um PVDF.

Filtered PEDOT were mixed with our three different SWCNT dissolution.

1.   Blend of SWCNT/SDS and PEDOT 1:2 (10 μL of SWCNT/SDS dissolution mixed with SDS: 20 μL PEDOT)

2.   Blend of SWCNT/SDBS and PEDOT 1:2 (10 μL SWCNT/SDBS dissolution mixed with SDBS: 20 μL PEDOT)

3.   Blend of SWCNT/DOC and PEDOT 1:2 (10 μL SWCNT/DOC dissolution mixed with DOC: 20 μL PEDOT)

5.4.1 contact angle analysis

As shown in Table 5.1 and Figure 5.7, generally, the coating on poly (3,4-ethylenedioxy-thiophene)-poly(styrene sulfonate) PEDOT:PSS surface are expected to be more successful than coating on glass substrate. Because when the contact angle of the ink on glass varies between 20-28 °, on the other hand, the contact angle of PEDOT: PSS is between 3-10 degrees. SDBS and DOC, compared with SDS, CNT's on PEDOT: PSS shows more effective coating, however this order is the exactly opposite on the glass surface. The solvent NMP (N-methyl pyrrolidone) where in acts similarly to the coating properties of DOC and SDBS coating properties.

Table 5.1: The contact angle measurements of Different surfactant / CNT inks coated on PEDOT:PSS and glass surface

#	Sample Solution	Tension	Glass Substrate		PEDOT:PSS Coated glass	
			left	Right	Left	Right
1	PEDOT:PSS	27,8	6,5	6,5	3,5	3,5
2	SWNT/PEDOT:PSS					
3	DOC/SWNT	46,85	25,9	24,9	~3	~3
4	SDBS/SWNT	32,4	27,6	29	3,8	3,8
5	SWCNT+NMP	39,6	27,5	26,8	4,6	4,5
6	SWCNT+SDS	44,97	19,6	20,6	10,6	10,9
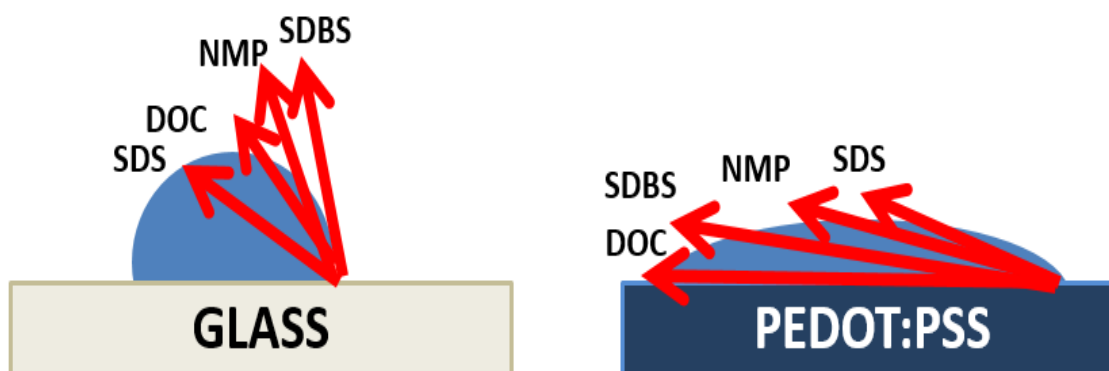
Figure 5.7 : Schematic of contact angle of different surfactant/ SWCNT inks was coated on glass and PEDOT:PSS surface**.**

5.4.2 UV spectroscopy

The sonication-driven exfoliation of aggregates and bundles of single-wall carbon nanotubes (SWNTs) in an aqueous surfactant solution can be easily monitored by UV-vis spectroscopy. The maximum achievable exfoliation (which does not mean that 100% of the NTs are effectively exfoliated) corresponds to the maximum UV-vis absorbance of the CNT solution. Bundled carbon nanotubes are not active in the UV–vis region and only individual carbon nanotubes absorb in this region. During SDBS sonication, the provided mechanical energy can indeed overcome the van der Waals interactions in the SWNT bundles and lead to CNT exfoliation. Simultaneously, surfactant molecules can adsorb on the surface of the SWNTs. As a result, a dispersion of CNTs with adsorbed surfactant molecules is obtained. Bundled CNTs are hardly active in the wavelength region between 200 and 1200 nm. The absorption of SWNTs and surfactant s appeared at 200-350 nm. In addition, absorption amount are 200,800 and 600 for SDS, SDBS and DOC respectively. The increasing amount of exfoliated CNTs results in an increasing area below the lines representing the absorbance. Therefore, it can be understand that amount of SWNT exfoliated in aqueous area are higher for SDBS and less amount for SDS.
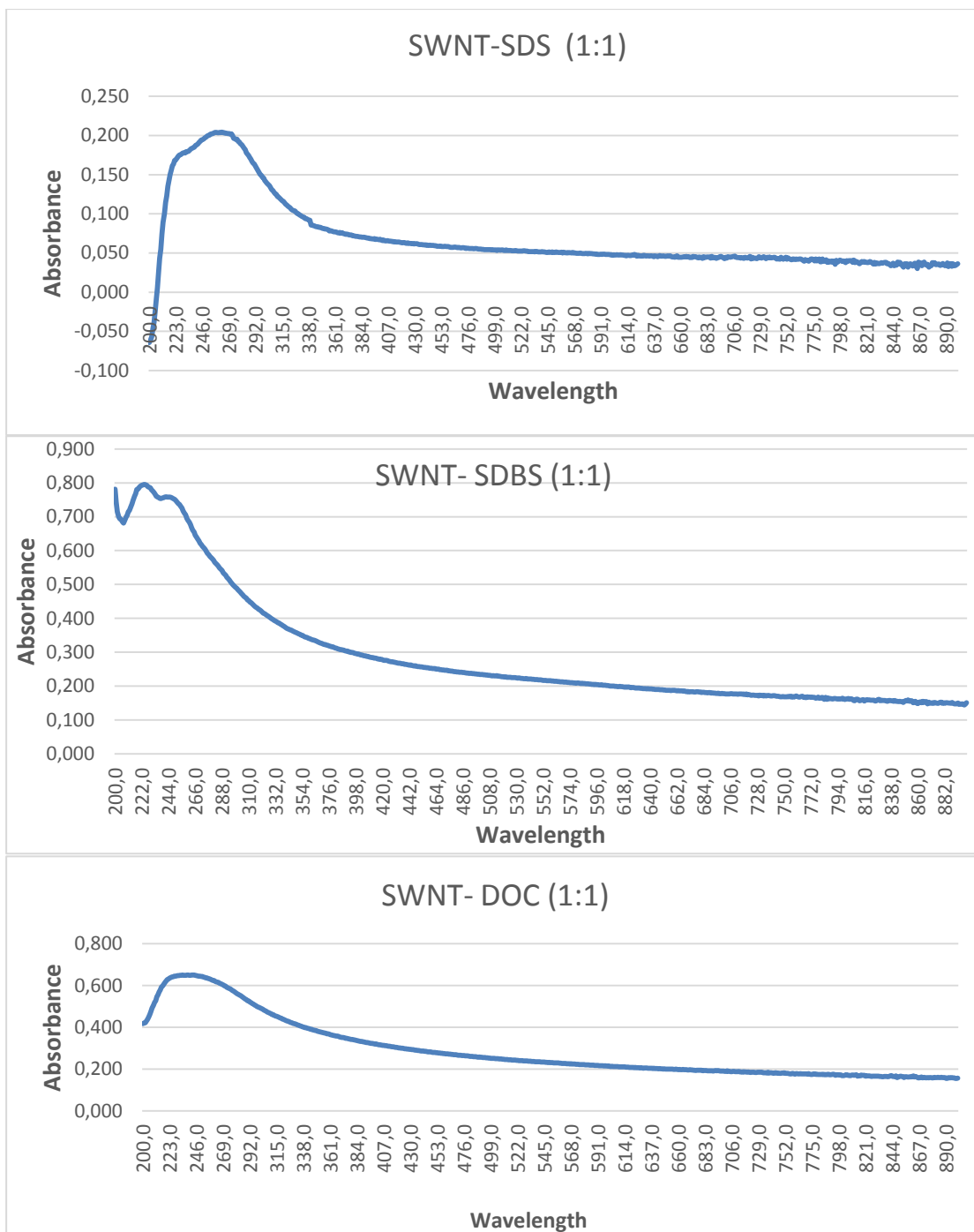
Figure 5.8 : UV–vis spectrum of SWNTs in aqueous solution with using SDS, SDBS and DOC as surfactant.

5.5   Preparation of CNT Thin Film And morphology analysis

The etch ITO coated glass substrates were coated with spin coating from each one of prepared inks at room temperature (figure 5.6). As shown in Figure 5.9, the glass substrate AFM image at 5 μm.

For comparison, we coated different kind of films too. PEDOT spin coated to etch ITO coated glass for one time and annealed in 110 ^{o}C for 1h (Figure 5.10) and again coated with our three SWCNT and surfactants mixtures for 5 times and annealed overnight in 110 ^{o}C. The morphology of the formed thin films were examined with atomic force microscope (AFM). SDS / SWCNT containing ink spin coated for 5 times with spin coating methods on PEDOT:PSS surface (Figure 5.11- 5.12), and observed that the thickness of films were about 23-44 nm. The surface roughness of these films is about 3.45-3.68 nm. The patterned SWCNT films were immersed in 4 M HNO$_3$ overnight and soaked in 14.5 M HNO$_3$ for 30 min, rinsed thoroughly with deionized water, and finally dried at 80 ^{o}C for 30 min in a hot oven as shown in Figure 5.13. Thin film thickness decreased to around 18.8 nm and observed less roughness (average 1.46 nm). This enhancement was attributed to the removal of remaining SDS and the subsequent densified film formation to improve the cross-junction resistance between SWCNT networks and enhanced metallicity of SWCNTs, whereas the chemical doping effect was negligible.
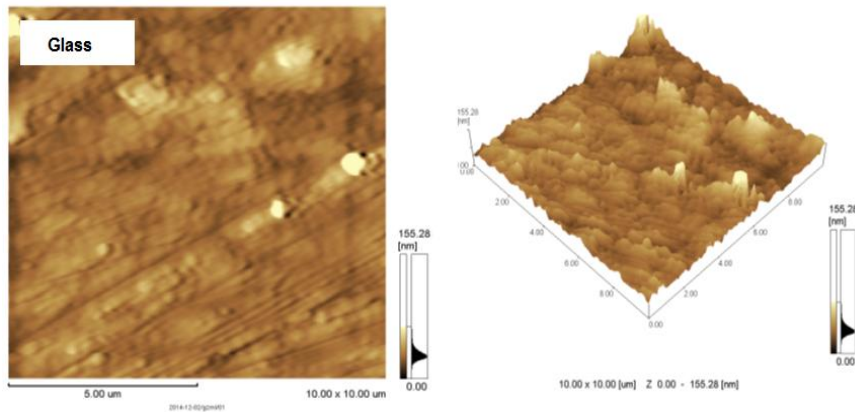
Figure 5.9 : AFM images of the glass substrate.

Figure 5.10: Spin cast glass substrate with PEDOT: PSS for 5 times and annealed at

$$100\,^{o}\,C$$

Figure 5.11: The AFM image of PEDOT:PSS coated glass, then spin casted for 5 times with SWCNT and SDS mixture and has annealed at $110\,^{o}C$.

Figure 5.12: The second area AFM image of PEDOT:PSS coated glass, then spin casted for 5 times with SWCNT and SDS mixture and has annealed at $110\,^{o}C$.
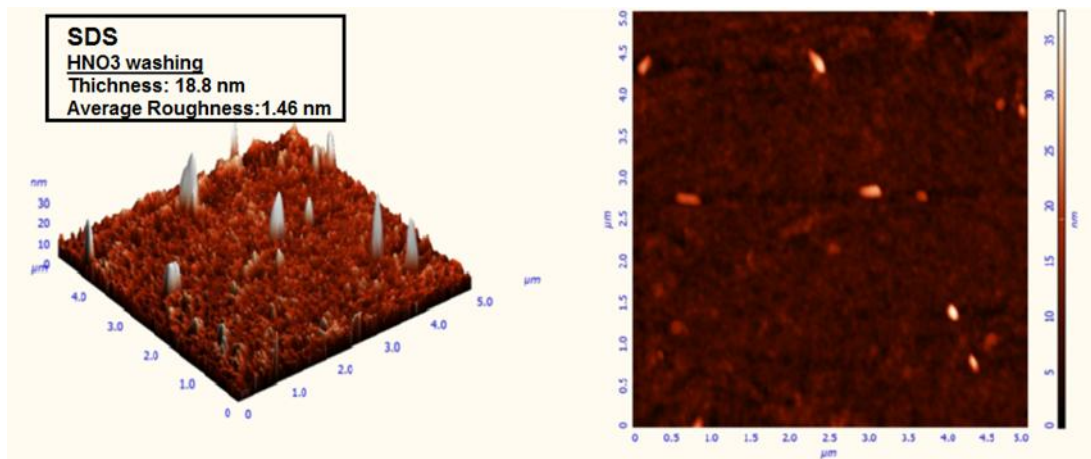
Figure 5.13 : The AFM image of PEDOT:PSS coated glass, then spin casted with SWCNT and SDS mixture and immersed at 4M HNO_3 overnight.

DOC / SWCNT containing ink spin coated for 5 times with spin coating methods on PEDOT:PSS surface (Figure 5.14- 5.15), and observed that the thickness of films were about 20- 22 nm. The surface roughness of these films is about 3.2 -3.4 nm. The patterned SWCNT films were immersed in 4M HNO_3 overnight and soaked in 14.5 M HNO_3 for 30 min, rinsed thoroughly with deionized water, and finally dried at 80 ^{o}C for 30 min in a hot oven as shown in Figure 5.16. Thin film thickness decreased to around 13 nm and observed less roughness (average 1.43 nm). This enhancement was attributed to the removal of remaining DOC and the subsequent densified film formation to improve the cross-junction resistance between SWCNT networks and enhanced metallicity of SWCNTs, whereas the chemical doping effect was negligible.
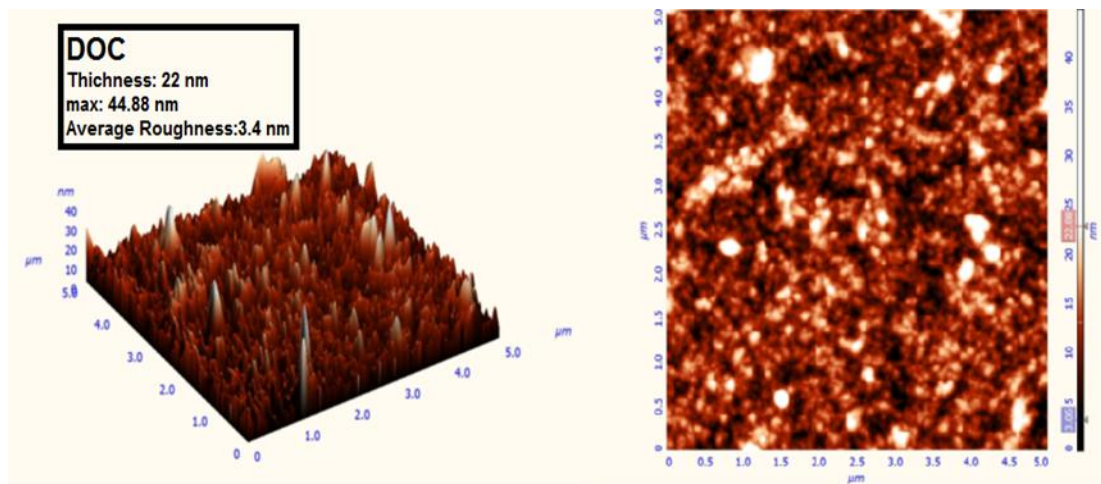
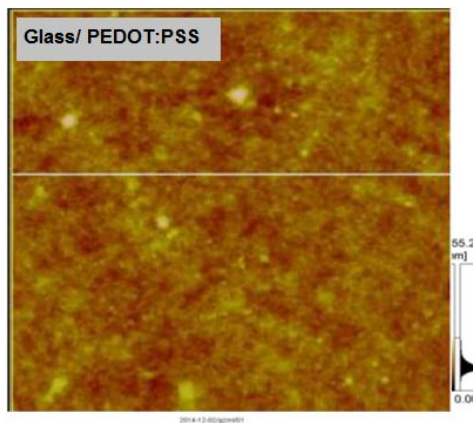**Figure 5.14:** The AFM image of PEDOT: PSS coated glass, then spin casted for 5 times with SWCNT and DOC mixture and has annealed at 110 ^{o}C .
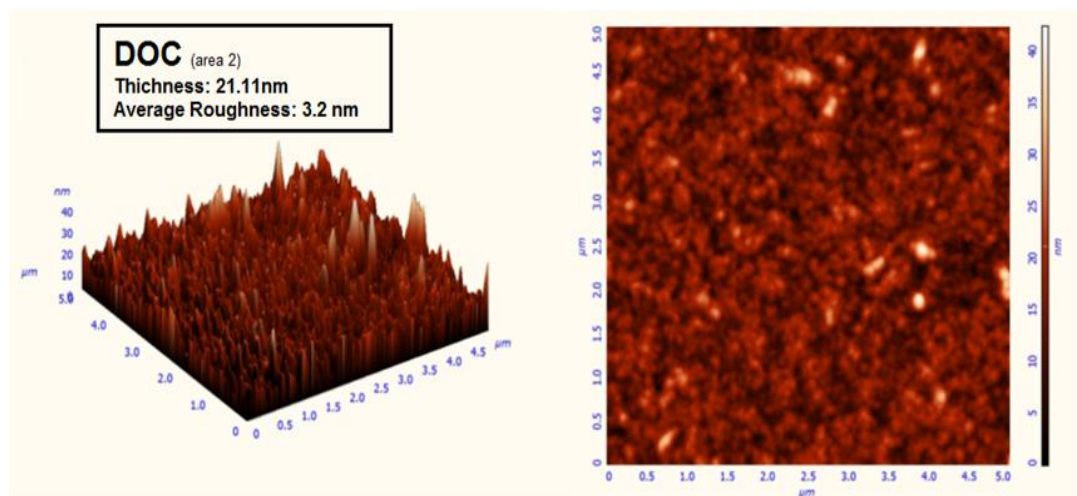
Figure 5.15 : The second AFM image of PEDOT:PSS coated glass, then spin casted for 5 times with WCNT and DOC mixture and has annealed at 110 ^{o}C .
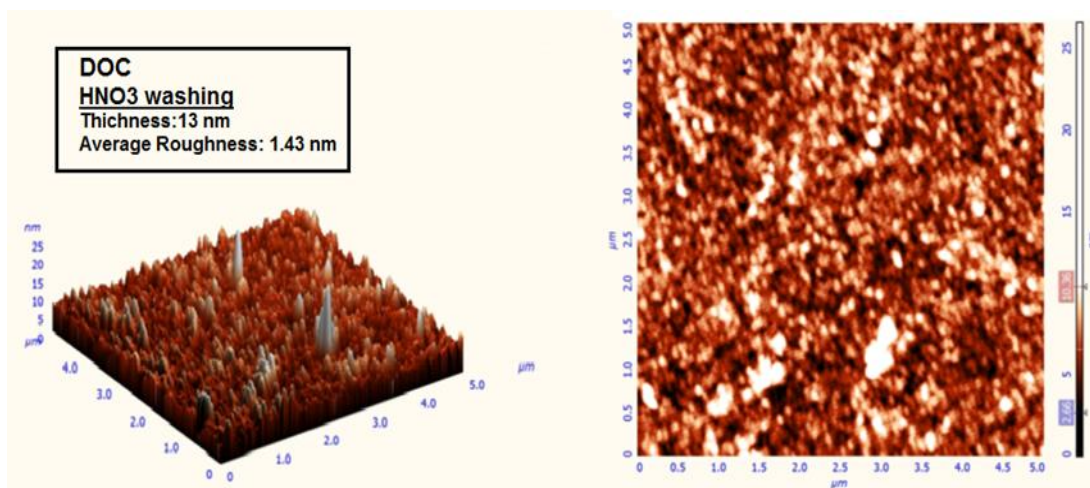
Figure 5.16 : The AFM image of PEDOT:PSS coated glass, then spin casted with SWCNT and DOC mixture and immersed at 4M HNO_3 overnight.

Similarly, CNT films were formed with using SDBS and NMP (N-methyl pyrrolidones) and were immersed in 4M HNO_3 overnight and soaked in 14.5M HNO_3 for 30 min, rinsed thoroughly with deionized water.

The surface roughness of films, which prepared with SDBS as surfactant is about 30-45 nm and there average roughness is near to 3.75 nm as shown in figure 5.17. After immersed films in 4 M HNO_3 overnight and soaked in 14.5 M HNO_3 for 30 min, rinsed thoroughly with deionized water, and finally dried at 80 ^{o}C for 30 min in a hot oven as shown in Figure 5.18. Thin film thickness decreased to around 12.15 nm and observed less roughness (average 1.28 nm)
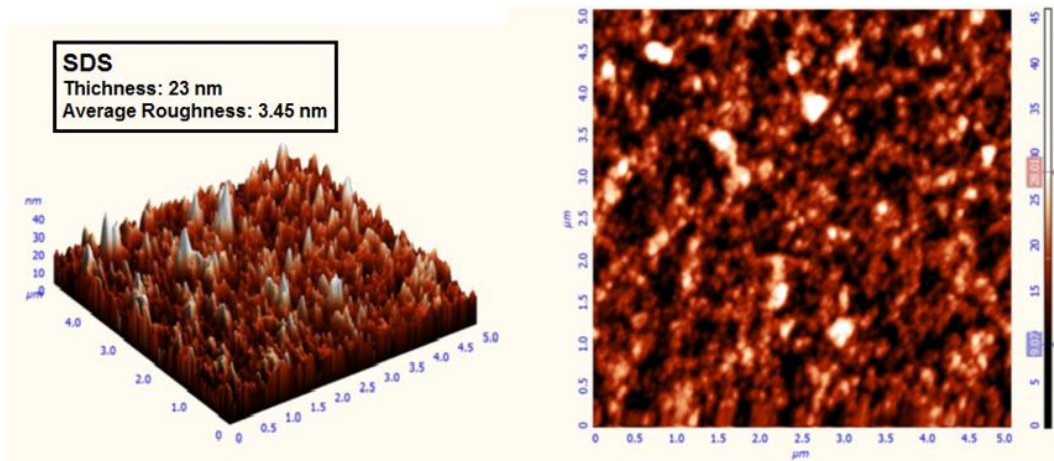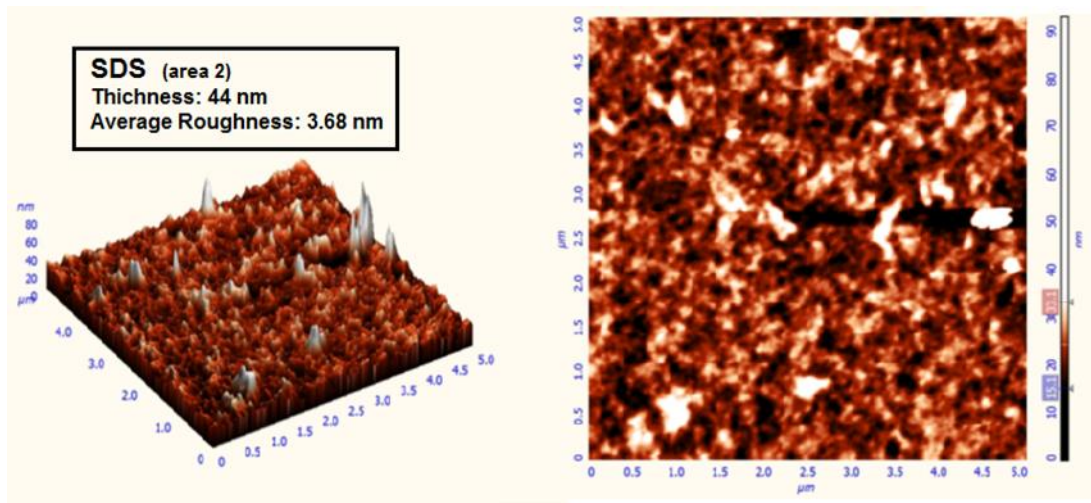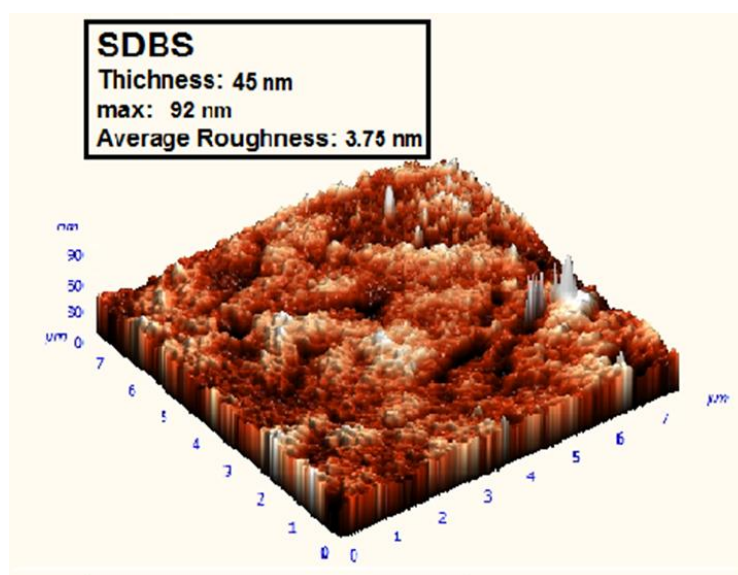

Figure 5.17: The AFM image of PEDOT:PSS coated glass, then spin casted for 5 times with SWCNT and DOC mixture and has annealed at 110 ^{o}C .

76
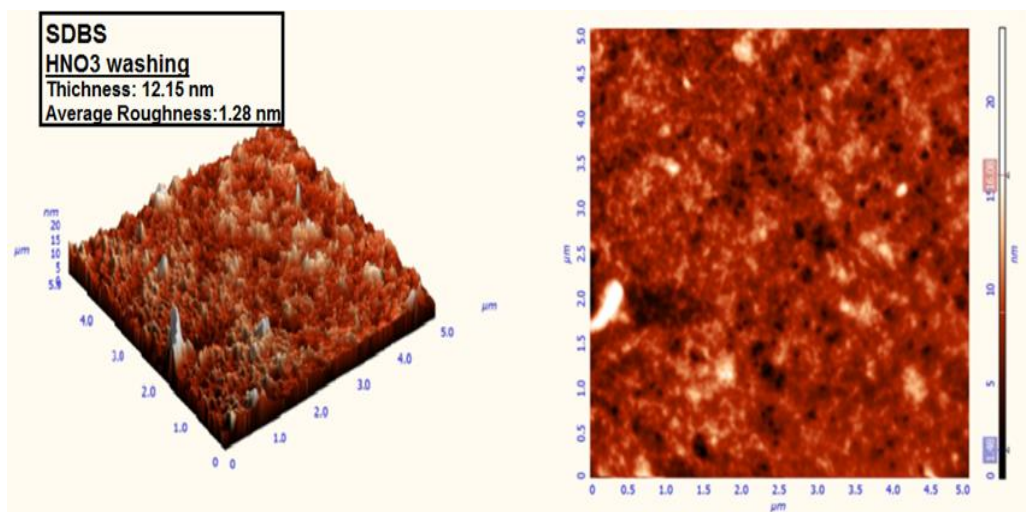
Figure 5.18: The morphology of CNT/SDBS films washed with HNO_3

The morphology of CNT film's that prepared on the glass/PEDOT: PSS surface with spin coating method was compared between DOC,SDS and SDBS / CNT mixtures. Contact angle on the surface of DOC/CNT compared to SDS/CNT is much lower (3° for DOC/CNT mixture) (10° for SDS/CNT mixture). Two film morphology when compared (Figure 5.19), SDS / CNTs were observed to form thicker bundles. DOC is bulky than SDS, thereby CNT aggregates are a material susceptible to inhibit growth of the diffusion channel. Due to this difference, our prediction is that DOC/CNT is form thinner film, while SDS / CNT is form thicker bundles.
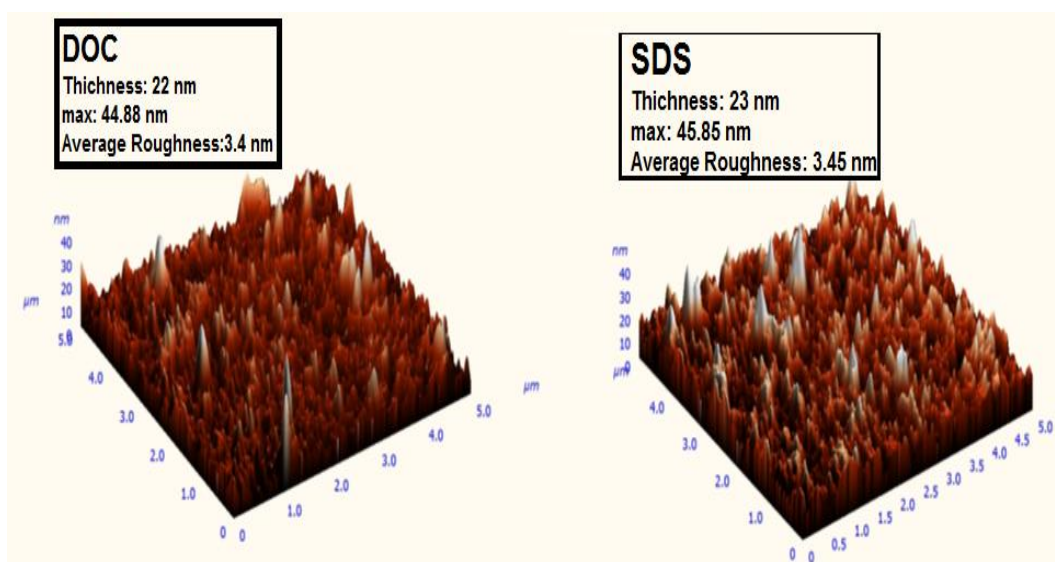
Figure 5.19: Thin films formed with SDS / CNT and DOC / CNT dispersions AFM images

Comparison of Fig 5.11-19 with reveals the change of the morphology for the as-prepared CNT film before and after HNO_3 treatment and annealing. It was observed

that when The NMP solvent is used, the obtained surface is inclusive the smoothest CNT films as shown in figure 5.20. However because does not occur any ionic bond or OH group between CNT in NMP, doesn't homogeneous films were produced on 5×5 μm. The thickness of the CNT films created from the NMP is about 3-5 nm and surface roughness is 0.3 nm. The thickness of the films formed using with SDS as surfactant, after acid treatment, had decreased to 18-20 nm, while the surface roughness is 1.46 nm. Due to the contact angle formed by the SDS on PEDOT: PSS surface is highest; SDS is known of the weakest material which holding above PEDOT: PSS. Therefore, acid treatment for films that prepared with SDS occurred in the most unsuccessful way. In DOC and SDS mixtures, after the washing step with HNO_3, On the surface of films that estimated to be surfactants, the ruins have accumulated more intense.
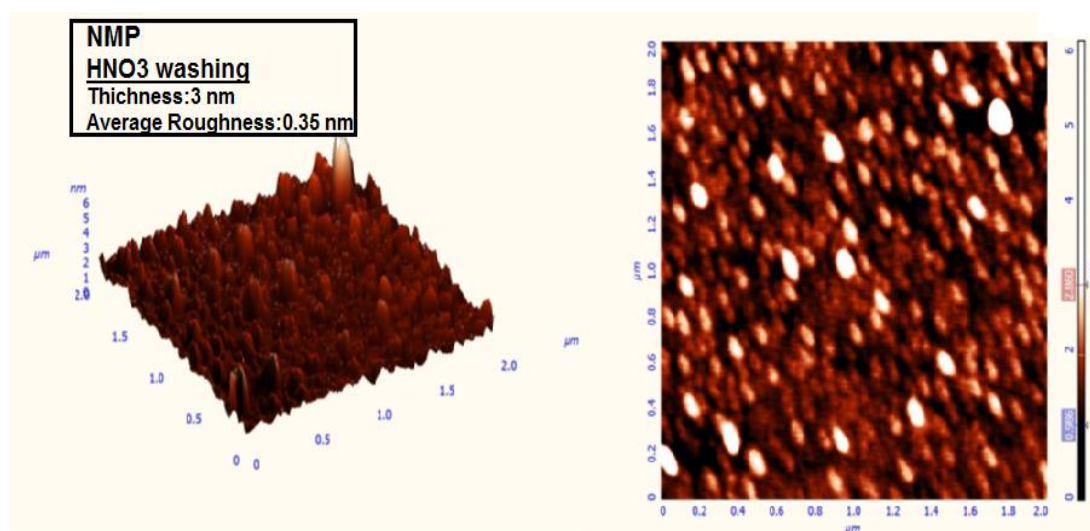
Figure 5.20: The morphology of SWCNT/NMP film washed with HNO_3

5.6 Cyclic voltammetry on prepared SWNTs electrode surface

For comparison, we coated different kind of films for cyclic voltammetry analysis.
- PEDOT/PSS
- PEDOT/PSS: CNT-B/SDS=1:1
- PEDOT/PSS: CNT-B/SDS=1:1 (HNO_3 treatment)

Thin films is used as the electrode material in 0.5 wt. % of ferrocene carboxylic acid circular voltammetry measurements. Platin is used as counter and ferrocene redox used as potential measured material. Expected reaction stream is like figure 5. Moreover, it will be a reversible reaction in the absence abrasion on the electrodes.
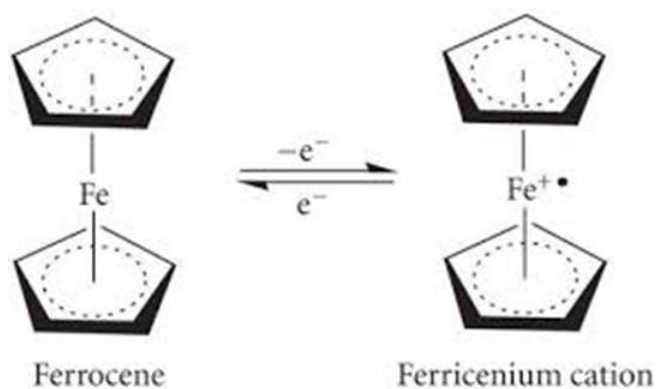
Figure 5.21 : Structure of ferrocene and ferricenium cation

When Glass / PEDOT: PSS and Glass / PEDOT: PSS (HNO3 treatment) is used, the reaction reversible but when Glass / CNT / SDS: PEDOT / PSS (1:1) films is used the reaction was measured as irreversible. It can be understood irreversibility of films is as result of films low thickness. In addition, current for the CNT / SDS co-voltage were 10 times smaller as shown in figure 5.22.
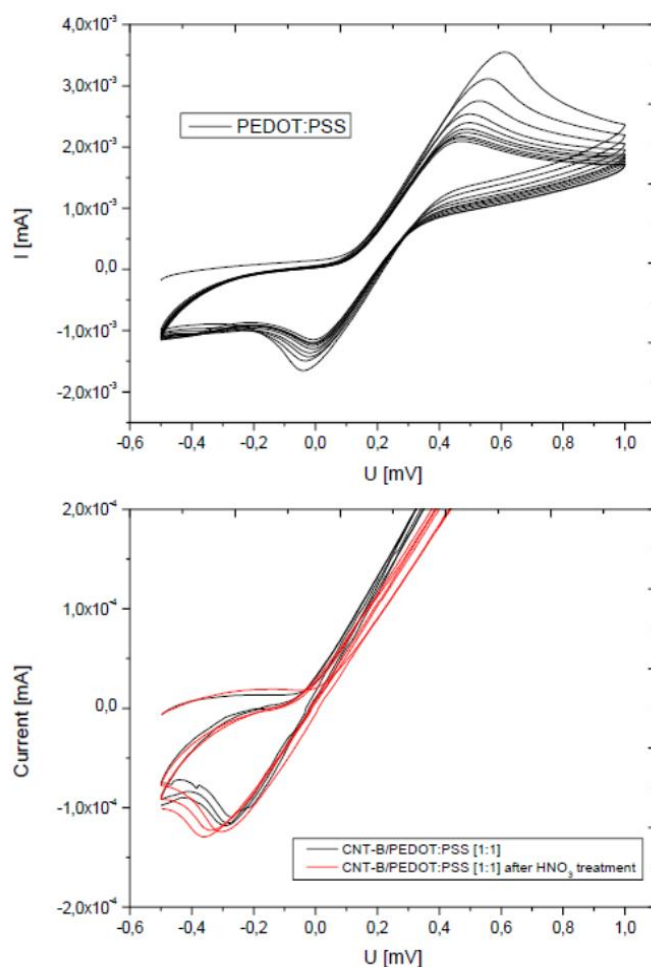
Figure 5.22: Comparison CV measurements of ferrocene , PEDOT: PSS and CNT-B/SDS as electrode.

Thin films thickness increased with using drop-casting method and prepared SWCNT and three different surfactant mixture electrode and acid treatment of each electrode for propose of removing surfactant from surface of electrode, for CV measurement analysis. The electrochemical properties of electrodes was analyzed by CV in 5 mM $K_3Fe(CN)_6$ and 0.1 M KCl solution in a three compartment cell. A Pt wire and an Ag wire electrode were used as a counter electrode and a reference electrode, respectively. The CV curves are exhibited in figure 5.23 for PEDOT: PSS electrodes in different scan rate.
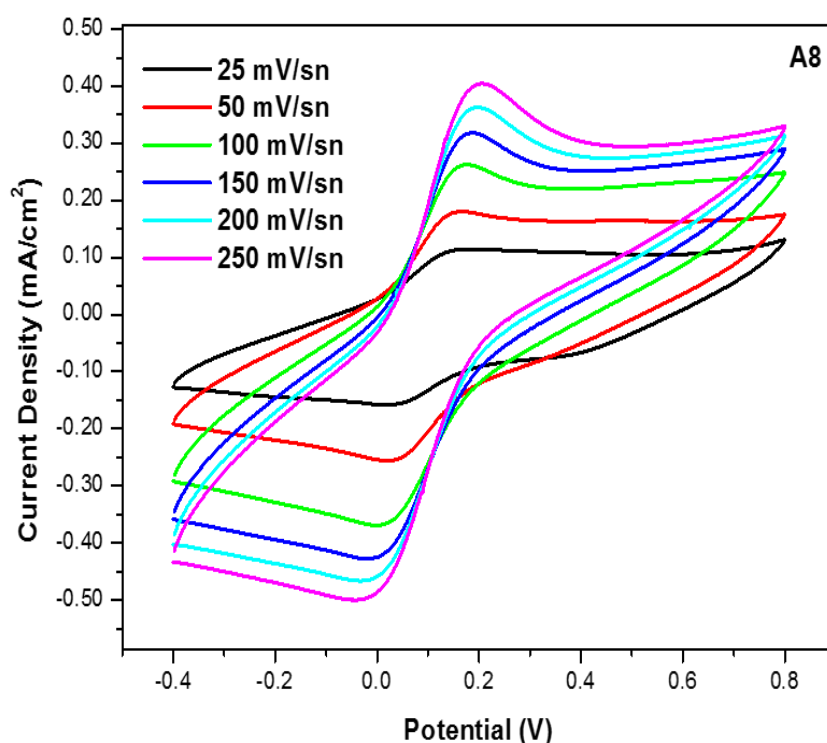
Figure 5.23: CV curves of 5 mM $K_3Fe(CN)_6$ and 0.1 M KCl solution for PEDOT:PSS

The CV curves of SDS/SWNT, SDBS/SWNT and DOC /SWNT coated electrodes before and after acid treatment are exhibited in figure 5.23-5.
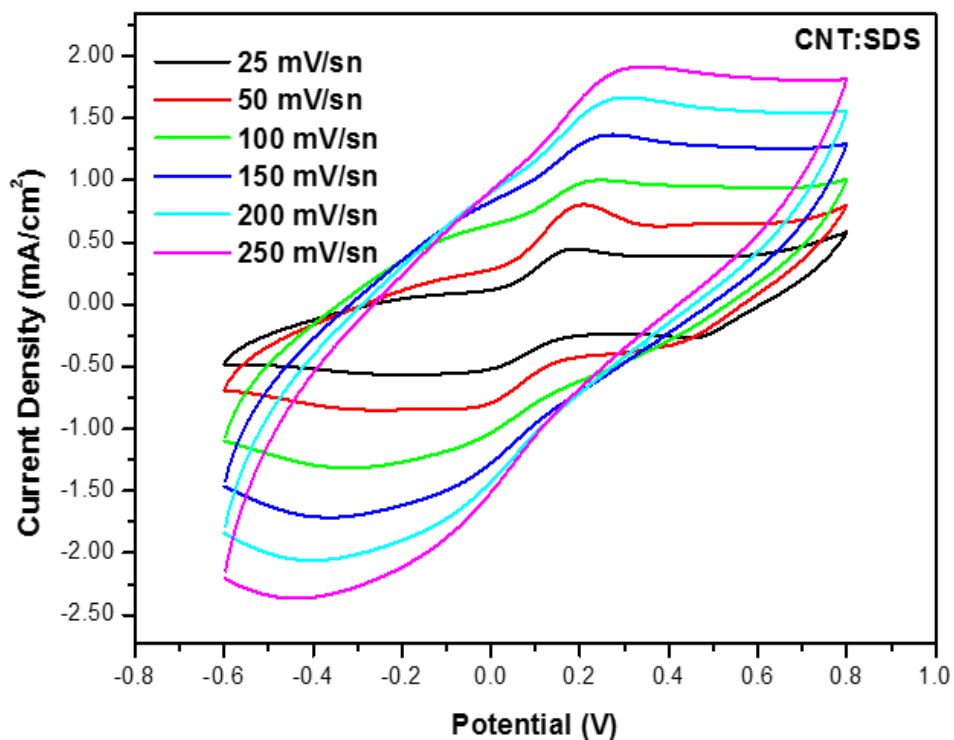
Figure 5.24 : CV curves of 5 mM $K_3Fe(CN)_6$ and 0.1 M KCl solution for SWNT/ SDS electrode
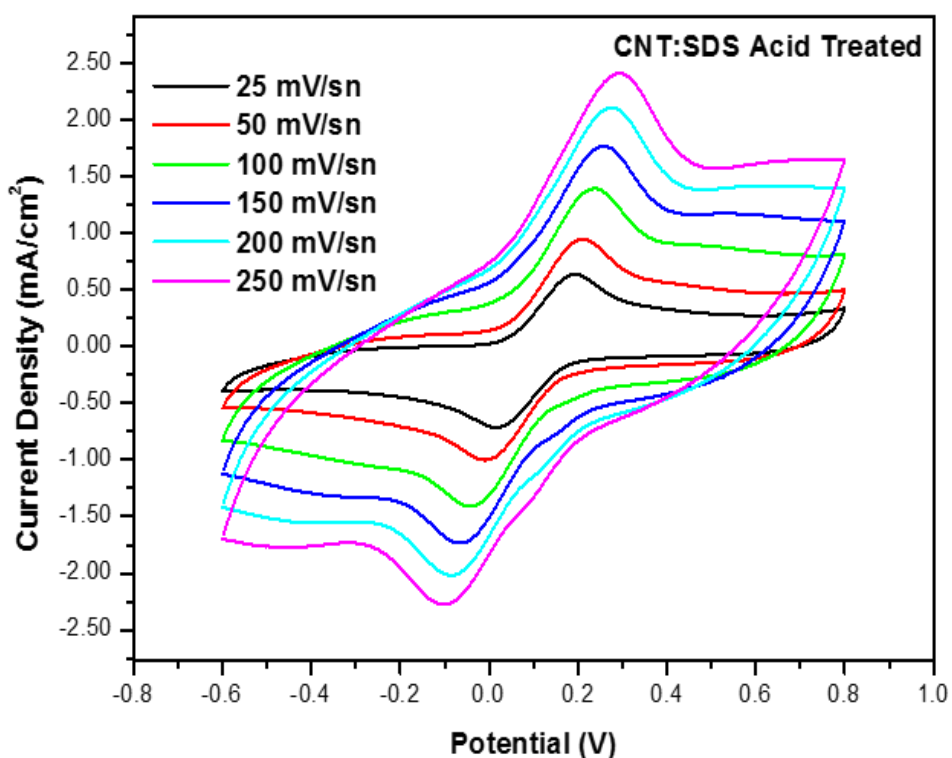
Figure 5.25: CV curves of 5 mM $K_3Fe(CN)_6$ and 0.1 M KCl solution for SWNT/ SDS electrode after acid treatment.
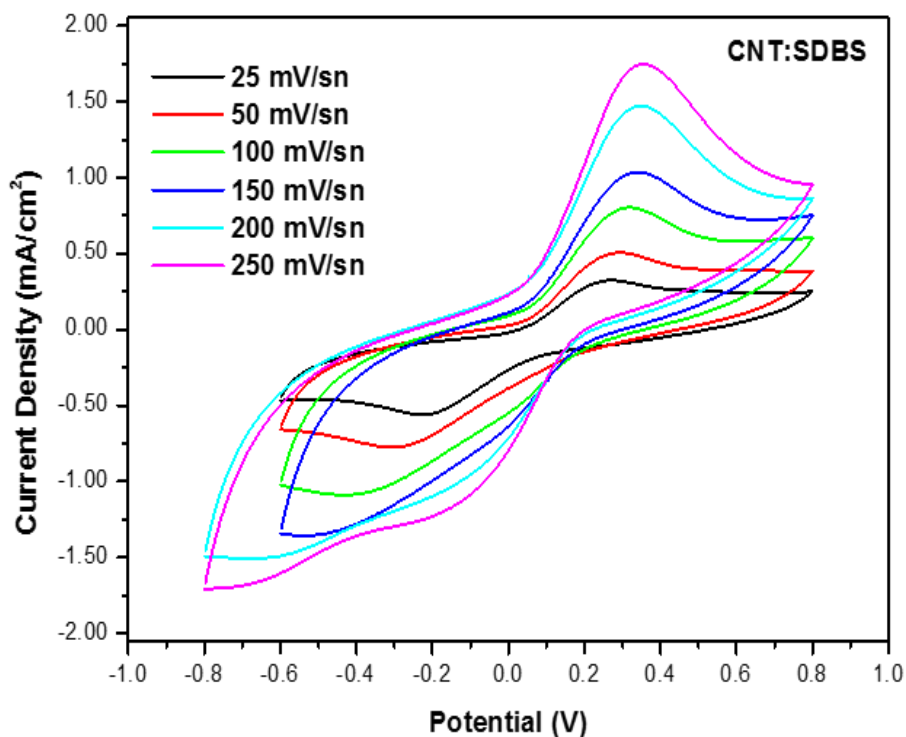
Figure 5.26 : CV curves of 5 mM $K_3Fe(CN)_6$ and 0.1 M KCl solution for SWNT/ SDBS electrode
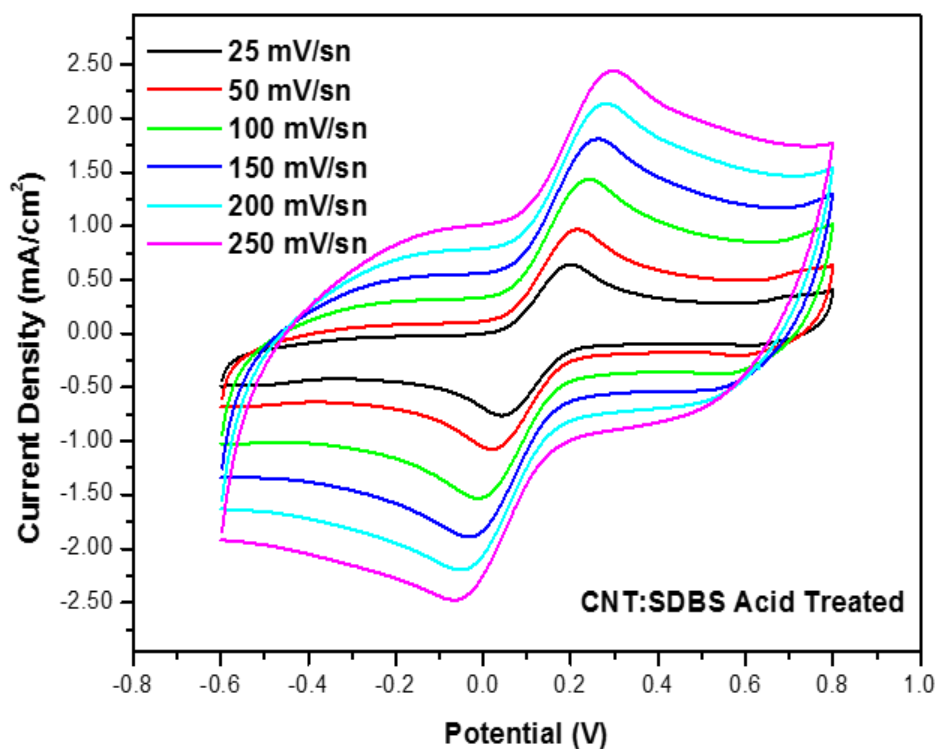
Figure 5.27 : CV curves of 5 mM $K_3Fe(CN)_6$ and 0.1 M KCl solution for SWNT/ SDBS electrode after acid treatment.
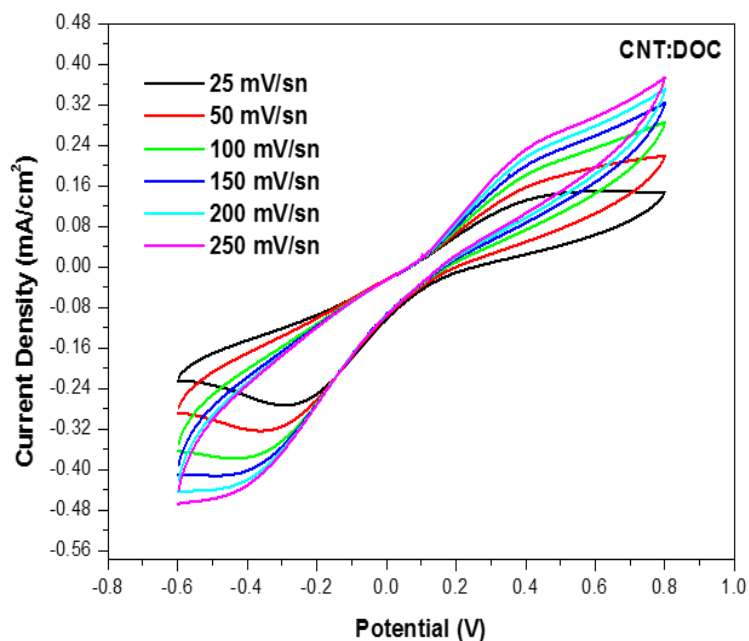
Figure 5.28 : CV curves of 5 mM K3Fe(CN)6 and 0.1 M KCl solution for SWNT/ SDS electrode
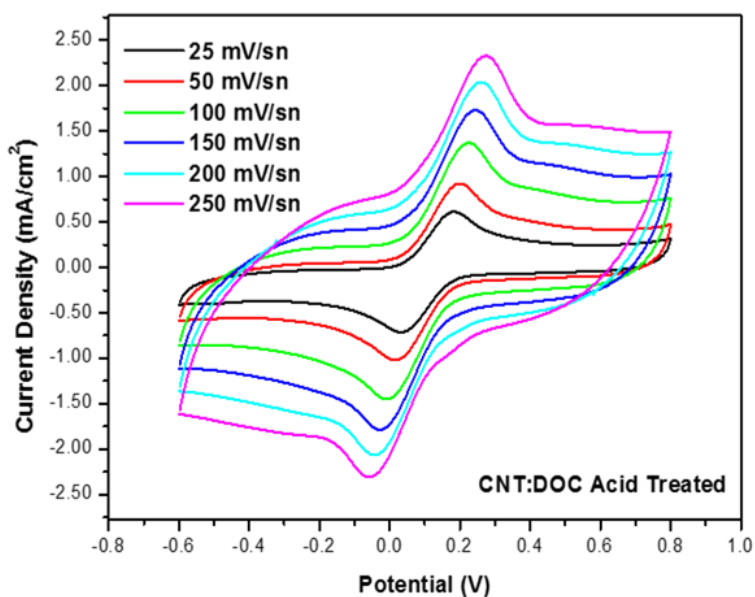
Figure 5.29 : CV curves of 5 mM K3Fe(CN)6 and 0.1 M KCl solution for SWNT/ SDS electrode after acid treatment

The compare CV curves for three surfactant and SWNT mixture I 25mv/s exhibited in figure 5.30. Dependence of the current density on the scan rate of CV measurement for SWNT and surfactant mixture deposited films after acid treatment shown in figure 5.31.
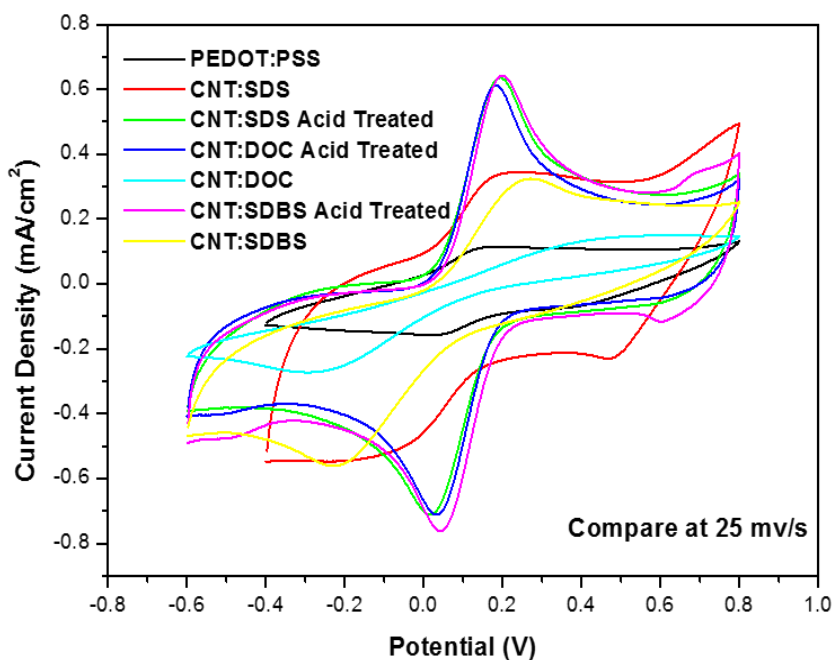
Figure 5.30 : Cyclic voltammetric curves of different surfactant and SWNT mixture electrode measured in 5 mM $K_3Fe(CN)_6$ and 0.1 M KCl solution at a scan rate of 25 mV/s
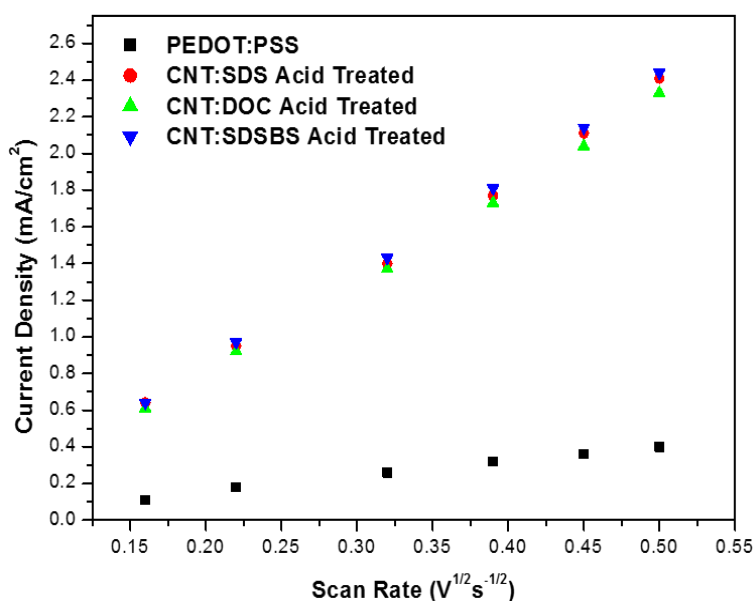
Figure 5.31: Dependence of the current density on the scan rate of CV measurement for SWNT and surfactant mixture deposited films after acid treatment

It can be seen that the current density of reduction peak of composites films significantly increased after addition of SWCNT into the PEDOT:PSS matrix except SWNT:DOC sample. The increase of current density after SWCNT addition is due to the enlargement of the film active area and/or lower film resistance. Also, current density didn't change with the increasing number of cycles, this indicates that producing electrodes are stable (figure 5.32)
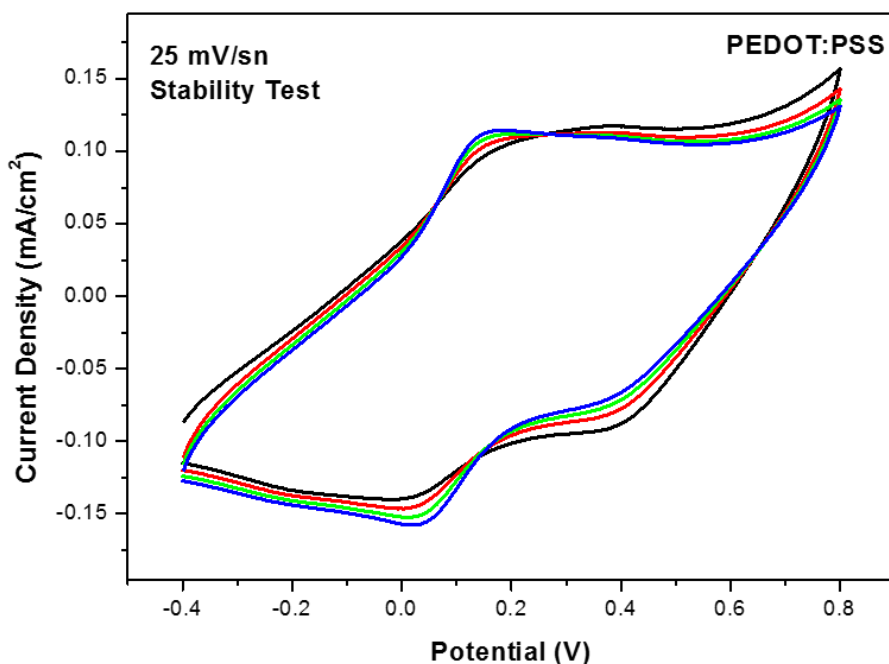
Figure 5.32: lifetime testing of the fabricated electrodes.

In addition, we note that after acid treatment of electrodes in order to remove surfactant from the samples, the reduction and oxidation peaks of $K_3Fe(CN)_6$ became sharper and current density of these peaks increased. This because, the elimination of surfactant from the surface probably provides higher surface area and better connectivity between SWNT, thus conductivity of electrodes increased. The amount of current density of reduction peaks of acid treated composites electrodes are about the same figure 5.30 .To estimate the film active area of PEDOT: PSS, SWNT:SDS, SWNT:DOC and SWNT:SDBS samples different scanning rates were used in 5 mM $K_3Fe(CN)_6$ and 0.1 M KCl solution. Figures which can be seen above shows the current density versus applied voltage of the electrodes. It is seen that current density increases with scanning rate. The reduction current density of $Fe(CN)_6^{-3/-4}$ vs. the square root of the scanning rate curves of pure and acid treated composited samples (other electrodes are not shown) can be seen in figure 5.31

The curves are fitted according to the Randles-Sevcik equation. The magnitude of the reduction slopes of the acid treated composite films (slope: 5.14) is higher than that of the pure PEDOT:PSS film (slope:0.83). Thus, the slope of curves varies only with the film active area. The increase of slopes of the acid treated composite films confirms the enlargement of their active areas [103,104].

6. CONCLUSION

Generally, the coating on poly(3,4-ethylenedioxy-thiophene)-poly(styrene sulfonate) PEDOT:PSS surface are expected to be more successful than coating on glass substrate. Because when the contact angle of the ink on glass varies between 20-28 ° ,on the other hand, the contact angle of PEDOT: PSS is between 3-10 degrees. SDBS and DOC, compared with SDS, SWCNT's on PEDOT: PSS shows more effective coating. Contact angle on the surface of DOC/SWCNT compared to SDS/SWCNT is much lower (3° for DOC/SWCNT mixture) (10° for SDS/SWCNT mixture). The solvent NMP (N-methyl pyrrolidone) where in acts similarly to the coating properties of DOC and SDBS coating properties.

SDS / SWCNT containing ink spin coated for 5 times with spin coating methods on PEDOT:PSS surface, and observed that the thickness of films were about 25-40 mm. The surface roughness of these films is about 3-4 nm. The thickness of patterned SWCNT films which treatment with HNO_3, decreased to around 18-20 nm and observed less roughness (average 1.4 nm). SDS / SWCNTs thin films were observed to form thicker bundles. DOC is bulky than SDS, thereby SWCNT aggregates are a material susceptible to inhibit growth of the diffusion channel. Due to this difference, our prediction is that DOC/SWCNT is form thinner, while SDS / SWCNT is form thicker bundles. When The NMP solvent is used, the obtained surface is inclusive the smoothest CNT films. However because does not occur any ionic bond or OH group between SWCNT in NMP, does not homogeneous films. The thickness of the SWCNT films created from the NMP is about 3-4 nm and surface roughness is 0.3 nm. When Glass / PEDOT: PSS and Glass / PEDOT: PSS (HNO3 treatment) is used, the reaction reversible in CV measurement but when Glass / CNT / SDS: PEDOT / PSS (1:1) films is used the reaction was measured as irreversible. In addition, current for the CNT / SDS co-voltage were 10 times smaller

Acid treatment for films that prepared with SDS occurred in the most unsuccessful way.

The current density of reduction peak of composites films significantly increased after addition of SWCNT into the PEDOT: PSS matrix. The increase of current

density after SWCNT addition is due to the enlargement of the film active area and/or lower film resistance. In addition, current density did not change with the increasing number of cycles; this indicates that producing electrodes are stable. After acid treatment of electrodes in order to remove surfactant from the samples, the reduction and oxidation peaks of $K_3Fe(CN)_6$ became sharper and current density of these peaks increased. This because, the elimination of surfactant from the surface probably provides higher surface area and better connectivity between SWNT, thus conductivity of electrodes increased.

REFERENCES

[1] **Conibeer, G.** (2007). Third-generation photovoltaics. *Materials today*, *10*(11), 42-50.

[2] **Balasubramanian, U.** (2004). *Indium oxide as a high resistivity buffer layer for CdTe/CdS thin film solar cells* (Doctoral dissertation, University of South Florida).

[3] **Günes, S., Neugebauer, H., & Sariciftci, N. S.** (2007). Conjugated polymer-based organic solar cells. *Chemical reviews*, *107*(4), 1324-1338.

[4] **Yeh, N., & Yeh, P.** (2013). Organic solar cells: Their developments and potentials. *Renewable and Sustainable Energy Reviews*, *21*, 421-431.

[5] **Ginley, D. S., & Bright, C.** (2000). Transparent conducting oxides. Mrs Bulletin, 25(08), 15-18.

[6] **Tang, C. W.** (1986). Two-layer organic photovoltaic cell. Applied Physics Letters, 48(2), 183-185.

[7] **Groenendaal, L., Jonas, F., Freitag, D., Pielartzik, H., & Reynolds, J. R**. (2000). Poly (3, 4-ethylenedioxythiophene) and its derivatives: past, present, and future. *Advanced Materials*, *12*(7), 481-494.

[8] **Kirchmeyer, S., & Reuter, K.** (2005). Scientific importance, properties and growing applications of poly (3, 4-ethylenedioxythiophene). *Journal of Materials Chemistry*, *15*(21), 2077-2088.

[9] **Hecht, D. S., Hu, L., & Irvin, G.** (2011). Emerging transparent electrodes based on thin films of carbon nanotubes, graphene, and metallic nanostructures.*Advanced Materials*, *23*(13), 1482-1513.

[10] **Wu, Z., Chen, Z., Du, X., Logan, J. M., Sippel, J., Nikolou, M., ... & Rinzler, A. G.** (2004). Transparent, conductive carbon nanotube films. *Science*, *305*(5688), 1273-1276.

[11] **Hu, L., Hecht, D. S., & Grüner, G.** (2004). Percolation in transparent and conducting carbon nanotube networks. *Nano Letters*, *4*(12), 2513-2517.

[12] **Saran, N., Parikh, K., Suh, D. S., Munoz, E., Kolla, H., & Manohar, S. K.** (2004). Fabrication and characterization of thin films of single-walled carbon nanotube bundles on flexible plastic substrates. *Journal of the American Chemical Society*, *126*(14), 4462-4463.

[13] **Kaempgen, M., Duesberg, G. S., & Roth, S**. (2005). Transparent carbon nanotube coatings. *Applied Surface Science*, *252*(2), 425-429.

[14] **Bekyarova, E., Itkis, M. E., Cabrera, N., Zhao, B., Yu, A., Gao, J., & Haddon, R. C. (2005).** Electronic properties of single-walled carbon

nanotube networks.*Journal of the American Chemical Society*, *127*(16), 5990-5995.

[15]**Kim, S., Yim, J., Wang, X., Bradley, D. D., Lee, S., & deMello, J. C.** (2010). Spin-and Spray-Deposited Single-Walled Carbon-Nanotube Electrodes for Organic Solar Cells. *Advanced Functional Materials*, *20*(14), 2310-2316.

[16] **Zhou, Y., Hu, L., & Grüner, G.** (2006). A method of printing carbon nanotube thin films. *Applied Physics Letters*, *88*(12), 123109.

[17] Iijima, S. (1991). Helical microtubules of graphitic carbon. *nature*, *354*(6348), 56-58.

[18] **Saito, R. Dresselhaus, G. Dresselhaus, MS.** (1998).Physical properties of carbon nanotubes. London: Imperial College Press.

[19] **Jorio, A., Dresselhaus, G., & Dresselhaus, M. S.** (2007). *Carbon nanotubes: advanced topics in the synthesis, structure, properties and applications* (Vol. 111). Springer.

[20] **Asada, Y., Nihey, F., Ohmori, S., Shinohara, H., & Saito, T.** (2011). Diameter-Dependent Performance of Single-Walled Carbon Nanotube Thin-Film Transistors. *Advanced Materials*, *23*(40), 4631-4635.

[21] **Kataura, H., Kumazawa, Y., Maniwa, Y., Umezu, I., Suzuki, S., Ohtsuka, Y., & Achiba, Y.** (1999). Optical properties of single-wall carbon nanotubes. *Synthetic Metals*, *103*(1), 2555-2558.

[22] **Jorio, A.; Saito, R.; Hafner, J. H.; Lieber, C. M.; Hunter, M.;McClure, T.; Dresselhaus, G.; Dresselhaus, M. S.** (2001) Structural(n,m) Determination of Isolated Single-Wall Carbon Nanotubes by Resonant Raman Scattering.Phys. Rev. Lett.2001,86, 1118–1121

[23] **Ando, Y., & Zhao, X.** (2006). Synthesis of carbon nanotubes by arc-discharge method. *New Diamond and Frontier Carbon Technology*, *16*(3), 123-138.

[24] **Ebbesen, T. W., & Ajayan, P. M.** (1992). Large-scale synthesis of carbon nanotubes. *Nature*, *358*(6383), 220-222.

[25] **Laurent, C., Flahaut, E., Peigney, A., & Rousset**, A. (1998). Metal nanoparticles for the catalytic synthesis of carbon nanotubes. *New J. Chem.*,*22*(11), 1229-1237.

[26] **Guo, T., Nikolaev, P., Rinzler, A. G., Tomanek, D., Colbert, D. T., & Smalley, R. E.** (1995). Self-assembly of tubular fullerenes. The Journal of Physical Chemistry, 99(27), 10694-10697.

[27] **Dai, H., Rinzler, A. G., Nikolaev**, P., **Thess**, A., **Colbert**, D. T., & **Smalley**, R. E. (1996). Single-wall nanotubes produced by metal-catalyzed disproportionation of carbon monoxide. *Chemical Physics Letters*, *260*(3), 471-475.

[28] **Terrones, M.** (2003). Science and technology of the twenty-first century: synthesis, properties, and applications of carbon nanotubes. *Annual review of materials research*, *33*(1), 419-501.

[29] **Arepalli, S., Holmes, W. A., Nikolaev, P., Hadjiev, V. G., & Scott, C. D.** (2004). A parametric study of single-wall carbon nanotube growth by laser ablation.*Journal of nanoscience and nanotechnology*, *4*(7), 762-773.

[30] **Popov, V. N.** (2004). Carbon nanotubes: properties and application. *Materials Science and Engineering: R: Reports*, *43*(3), 61-102.

[31] **Dai, H.** (2001). Nanotube growth and characterization. In *Carbon Nanotubes*(pp. 29-53). Springer Berlin Heidelberg.

[32] **Thostenson, E. T., Ren, Z., & Chou, T. W.** (2001). Advances in the science and technology of carbon nanotubes and their composites: a review.*Composites science and technology*, *61*(13), 1899-1912.

[33] **Dai, H**. (2002). Carbon nanotubes: opportunities and challenges. *Surface Science*, *500*(1), 218-241.

[34] **Chen**, R. J., **Zhang**, Y., **Wang**, D., & **Dai**, H. (2001). Noncovalent sidewall functionalization of single-walled carbon nanotubes for protein immobilization.*Journal of the American Chemical Society*, *123*(16), 3838-3839.

[35] **Kong, J., Soh, H. T., Cassell, A. M., Quate, C. F., & Dai, H**. (1998). Synthesis of individual single-walled carbon nanotubes on patterned silicon wafers.*Nature*, *395*(6705), 878-881.

[36] **Kong, J., Soh, H. T., Cassell, A. M., Quate, C. F., & Dai, H.** (1998). Synthesis of individual single-walled carbon nanotubes on patterned silicon wafers.*Nature*, *395*(6705), 878-881.

[37] **Cassell, A. M., Raymakers, J. A., Kong, J., & Dai, H**. (1999). Large scale CVD synthesis of single-walled carbon nanotubes. *The Journal of Physical Chemistry B*, *103*(31), 6484-6492.

[38] **Kong, J., Cassell, A. M., & Dai, H.** (1998). Chemical vapor deposition of methane for single-walled carbon nanotubes. *Chemical Physics Letters*, *292*(4), 567-574.

[39] **Hu, H., Bhowmik, P., Zhao, B., Hamon, M. A., Itkis, M. E., & Haddon, R. C.** (2001). Determination of the acidic sites of purified single-walled carbon nanotubes by acid–base titration. *Chemical Physics Letters*, *345*(1), 25-28.

[40] **Hou, P. X., Liu, C., & Cheng, H. M.** (2008). Purification of carbon nanotubes.*Carbon*, *46*(15), 2003-2025.

[41] **Montoro**, L. A., & **Rosole**n, J. M. (2006). A multi-step treatment to effective purification of single-walled carbon nanotubes. *Carbon*, *44*(15), 3293-3301.

[42] **Duesberg, G. S., Muster, J., Byrne, H. J., Roth, S., & Burghard, M.** (1999). Towards processing of carbon nanotubes for technical applications. *Applied Physics A*, *69*(3), 269-274.

[43] **Hu, H., Bhowmik, P., Zhao, B., Hamon, M. A., Itkis, M. E., & Haddon, R. C.** (2001). Determination of the acidic sites of purified single-walled

carbon nanotubes by acid–base titration. *Chemical Physics Letters*, *345*(1), 25-28.

[44] **Zimmerman, J. L., Bradley, R. K., Huffman, C. B., Hauge, R. H., & Margrave, J. L.** (2000). Gas-phase purification of single-wall carbon nanotubes. *Chemistry of Materials*, *12*(5), 1361-1366.

[45] **Hiura, H., Ebbesen, T. W., & Tanigaki, K.** (1995). Opening and purification of carbon nanotubes in high yields. *Advanced Materials*, *7*(3), 275-276.

[46] **Monthioux, M., Smith, B. W., Burteaux, B., Claye, A., Fischer, J. E., & Luzzi, D. E.** (2001). Sensitivity of single-wall carbon nanotubes to chemical processing: an electron microscopy investigation. *Carbon*, *39*(8), 1251-1272.

[47] **Wallace, E. J., & Sansom, M. S.** (2009). Carbon nanotube self-assembly with lipids and detergent: a molecular dynamics study. *Nanotechnology*, *20*(4), 045101.

[48] **Tenent, R. C., Barnes, T. M., Bergeson, J. D., Ferguson, A. J., To, B., Gedvilas, L. M., ... & Blackburn, J. L.** (2009). Ultrasmooth, Large-Area, High-Uniformity, Conductive Transparent Single-Walled-Carbon-Nanotube Films for Photovoltaics Produced by Ultrasonic Spraying. *Advanced materials*, *21*(31), 3210-3216.

[49] **Dujardin, E., Ebbesen, T. W., Krishnan, A., & Treacy, M. M**. (1998). Purification of single-shell nanotubes. *Advanced materials*, *10*(8), 611-613.

[50] **Bonard, J. M., Stora, T., Salvetat,** J. P., **Maier,** F., **Stöckli**, T., **Duschl, C., ... & Châtelain, A.** (1997). Purification and size-selection of carbon nanotubes.*Advanced Materials*, *9*(10), 827-831.

[51] **Mayhew, E., & Prakash, V.** (2013). Thermal conductivity of individual carbon nanofibers. *Carbon*, *62*, 493-500.

[52] **Rao,** A. M., **Richter**, E., **Bandow, S., Chase,** B., **Eklund,** P. C., **Williams, K. A., ... & Dresselhaus, M. S.** (1997). Diameter-selective Raman scattering from vibrational modes in carbon nanotubes. *Science*, *275*(5297), 187-191.

[53] **Brar**, V. W., Samsonidze, G. G., Dresselhaus, M. S., Dresselhaus, G., Saito, R., Swan, A. K., ... & Jorio, A. (2002). Second-order harmonic and combination modes in graphite, single-wall carbon nanotube bundles, and isolated single-wall carbon nanotubes. *Physical Review B*, *66*(15), 155418.

[54] **Dillon, A. C., Parilla, P. A., Jones, K. M., Riker, G., & Heben, M. J.** (1998, January). A comparison of single-wall carbon nanotube production using continuous wave and pulsed laser vaporization. In *MRS Proceedings* (Vol. 526, p. 403). Cambridge University Press.

[55] **Lambin, P., Loiseau, A., Culot, C., & Biro, L. P.** (2002). Structure of carbon nanotubes probed by local and global probes. *Carbon*, *40*(10), 1635-1648.

[56] **Attal, S., Thiruvengadathan, R., & Regev, O.** (2006). Determination of the concentration of single-walled carbon nanotubes in aqueous dispersions using UV-visible absorption spectroscopy. *Analytical chemistry*, *78*(23), 8098-8104.

[57] **Landi, B. J., Ruf, H. J., Evans, C. M., Cress, C. D., & Raffaelle, R. P.** (2005). Purity assessment of single-wall carbon nanotubes, using optical absorption spectroscopy. *The Journal of Physical Chemistry B*, *109*(20), 9952-9965.

[58] **Landi, B. J., Ruf, H. J., Worman, J. J., & Raffaelle, R. P.** (2004). Effects of alkyl amide solvents on the dispersion of single-wall carbon nanotubes. *The Journal of Physical Chemistry B*, *108*(44), 17089-17095.

[59] **Ryabenko, A. G., Dorofeeva, T. V., & Zvereva, G. I**. (2004). UV–VIS–NIR spectroscopy study of sensitivity of single-wall carbon nanotubes to chemical processing and Van-der-Waals SWNT/SWNT interaction. Verification of the SWNT content measurements by absorption spectroscopy. *Carbon*, *42*(8), 1523-1535.

[60] **Zhu, W. Z., Miser, D. E., Chan, W. G., & Hajaligol, M. R**. (2003). Characterization of multiwalled carbon nanotubes prepared by carbon arc cathode deposit. *Materials chemistry and physics*, *82*(3), 638-647.

[61] **Rinzler, A. G., Liu, J., Dai, H., Nikolaev, P., Huffman, C. B., Rodriguez-Macias, F. J., ... & Smalley, R. E.** (1998). Large-scale purification of single-wall carbon nanotubes: process, product, and characterization. *Applied Physics A: Materials Science & Processing*, *67*(1), 29-37.

[62] **Jiang**, L., **Gao, L., & Sun, J.** (2003). Production of aqueous colloidal dispersions of carbon nanotubes. *Journal of Colloid and Interface Science*,*260*(1), 89-94.

[63] **Freiman, S., Hooker, S., Migler, K., Arepalli, S.** (2008) Measurement issues in single wall carbon nanotubes. *NIST Special Publication*, 960-19.

[64] **Lee, J. U., Huh, J., Kim, K. H., Park, C., & Jo, W. H**. (2007). Aqueous suspension of carbon nanotubes via non-covalent functionalization with oligothiophene-terminated poly (ethylene glycol). *Carbon*, *45*(5), 1051-1057.

[65] **Marsh, D. H., Rance, G. A., Zaka, M. H., Whitby, R. J., & Khlobystov, A. N.** (2007). Comparison of the stability of multiwalled carbon nanotube dispersions in water. *Physical Chemistry Chemical Physics*, *9*(40), 5490-5496.

[66] **Rastogi, R., Kaushal, R., Tripathi, S. K., Sharma, A. L., Kaur, I., & Bharadwaj, L. M.** (2008). Comparative study of carbon nanotube dispersion using surfactants. *Journal of colloid and interface science*, *328*(2), 421-428.

[67] **Shen, J., Hu, Y., Qin, C., Li, C., & Ye, M.** (2008). Dispersion behavior of single-walled carbon nanotubes by grafting of amphiphilic block

copolymer.*Composites Part A: Applied Science and Manufacturing*, *39*(10), 1679-1683.

[68] **Yu, J., Grossiord, N., Koning, C. E., & Loos, J.** (2007). Controlling the dispersion of multi-wall carbon nanotubes in aqueous surfactant solution.*Carbon*, *45*(3), 618-623.

[69] **Zhao, Y., & Li, W.** (2010). Effect of annealing and HNO3-treatment on the electrical properties of transparent conducting carbon nanotube films.*Microelectronic Engineering*, *87*(4), 576-579.

[70] **Ajayan, P. M.** (1999). Nanotubes from carbon. *Chemical reviews*, *99*(7), 1787-1800

[71] **Dujardin, E., Ebbesen, T. W., Hiura, H., & Tanigaki, K.** (1994). Capillarity and wetting of carbon nanotubes. *Science*, *265*(5180), 1850-1852.

[72] **Nugent, J. M., Santhanam, K. S. V., Rubio, A., & Ajayan, P. M.** (2001). Fast electron transfer kinetics on multiwalled carbon nanotube microbundle electrodes. *Nano Letters*, *1*(2), 87-91.

[73] **Geng, H. Z., Kim, K. K., Lee, K., Kim, G. Y., Choi, H. K., Lee, D. S., ... & Lee, Y. J.** (2007). Dependence of material quality on performance of flexible transparent conducting films with single-walled carbon nanotubes. *Nano*, *2*(03), 157-167.

[74] **Wang, X., Zhi, L., Tsao, N., Tomović, Ž., Li, J., & Müllen, K.** (2008). Transparent carbon films as electrodes in organic solar cells. *Angewandte Chemie*, *120*(16), 3032-3034.

[75] **Ausman, K. D., Piner, R., Lourie, O., Ruoff, R. S., & Korobov, M.** (2000). Organic solvent dispersions of single-walled carbon nanotubes: toward solutions of pristine nanotubes. *The Journal of Physical Chemistry B*, *104*(38), 8911-8915.

[76] **Islam, M. F., Rojas, E., Bergey, D. M., Johnson, A. T., & Yodh**, A. G. (2003). High weight fraction surfactant solubilization of single-wall carbon nanotubes in water. *Nano Letters*, *3*(2), 269-273.

[77] **O'connell, M. J., Bachilo, S. M., Huffman, C. B., Moore, V. C., Strano, M. S., Haroz, E. H., ... & Smalley, R. E.** (2002). Band gap fluorescence from individual single-walled carbon nanotubes. *Science*, *297*(5581), 593-596.

[78] **O'Connell, M. J., Boul, P., Ericson, L. M., Huffman, C., Wang, Y., Haroz, E., ... & Smalley, R. E.** (2001). Reversible water-solubilization of single-walled carbon nanotubes by polymer wrapping. *Chemical Physics Letters*, *342*(3), 265-271.

[79] **Strano, M. S., Moore, V. C., Miller, M. K., Allen, M. J., Haroz, E. H., Kittrell, C., ... & Smalley, R. E.** (2003). The role of surfactant adsorption during ultrasonication in the dispersion of single-walled carbon nanotubes. *Journal of Nanoscience and Nanotechnology*, *3*(1-2), 1-2.

[80] **Usrey, M. L., Chaffee, A., Jeng, E. S., & Strano, M. S.** (2009). Application of polymer solubility theory to solution phase dispersion of single-walled

carbon nanotubes. *The Journal of Physical Chemistry C*, *113*(22), 9532-9540.

[81] **Shiral Fernando, K. A., Lin, Y., & Sun, Y. P.** (2004). High aqueous solubility of functionalized single-walled carbon nanotubes. *Langmuir*, *20*(11), 4777-4778.

[82] **Hamon, M. A., Chen, J., Hu, H., Chen, Y., Itkis, M. E., Rao, A. M., ... & Haddon, R. C.** (1999). Dissolution of single-walled carbon nanotubes. *Advanced Materials*, *11*(10), 834-840.

[83] **Chen, J., Rao, A. M., Lyuksyutov, S., Itkis, M. E., Hamon, M. A., Hu, H., ... & Haddon, R. C.** (2001). Dissolution of full-length single-walled carbon nanotubes. *The Journal of Physical Chemistry B*, *105*(13), 2525-2528.

[84] **Bahr, J. L., Mickelson, E. T., Bronikowski, M. J., Smalley, R. E., & Tour, J. M.** (2001). Dissolution of small diameter single-wall carbon nanotubes in organic solvents?. *Chem. Commun.*, (2), 193-194.

[85] **Kim, K. K., Bae, D. J., Yang, C. M., An, K. H., Lee, J. Y., & Lee, Y. H.** (2005). Nanodispersion of single-walled carbon nanotubes using dichloroethane. *Journal of nanoscience and nanotechnology*, *5*(7), 1055-1059.

[86] **Bergin, S. D., Sun, Z., Rickard, D., Streich, P. V., Hamilton, J. P., & Coleman, J. N.** (2009). Multicomponent solubility parameters for single-walled carbon nanotube− solvent mixtures. *Acs Nano*, *3*(8), 2340-2350.

[87] **Bergin, S. D., Sun, Z., Streich, P., Hamilton, J., & Coleman, J. N.** (2009). New solvents for nanotubes: approaching the dispersibility of surfactants. *The Journal of Physical Chemistry C*, *114*(1), 231-237.

[88] **Usrey, M. L., & Strano, M. S.** (2009). Controlling single-walled carbon nanotube surface adsorption with covalent and noncovalent functionalization. *The Journal of Physical Chemistry C*, *113*(28), 12443-12453.

[89] **Bahr, J. L., Mickelson, E. T., Bronikowski, M. J., Smalley, R. E., & Tour, J. M.** (2001). Dissolution of small diameter single-wall carbon nanotubes in organic solvents?. *Chem. Commun.*, (2), 193-194.

[90] **Bergin, S. D., Sun, Z., Rickard, D., Streich, P. V., Hamilton, J. P., & Coleman, J. N.** (2009). Multicomponent solubility parameters for single-walled carbon nanotube− solvent mixtures. *Acs Nano*, *3*(8), 2340-2350.

[91] **Kim, S., Yim, J., Wang, X., Bradley, D. D., Lee, S., & deMello, J. C.** (2010). Spin-and Spray-Deposited Single-Walled Carbon-Nanotube Electrodes for Organic Solar Cells. *Advanced Functional Materials*, *20*(14), 2310-2316.

[92] **Kane, C., Balents, L., & Fisher, M. P.** (1997). Coulomb interactions and mesoscopic effects in carbon nanotubes. *Physical review letters*, *79*(25), 5086.

[93] **Geng, H. Z., Kim, K. K., So, K. P., Lee, Y. S., Chang, Y., & Lee, Y. H.** (2007). Effect of acid treatment on carbon nanotube-based flexible transparent conducting films. *Journal of the American Chemical Society*, *129*(25), 7758-7759.

[94] **Wu, Z., Chen, Z., Du, X., Logan, J. M., Sippel, J., Nikolou, M., ... & Rinzler, A. G.** (2004). Transparent, conductive carbon nanotube films. *Science*, *305*(5688), 1273-1276.

[95] **Geng, H. Z., Kim, K. K., Lee, K., Kim, G. Y., Choi, H. K., Lee, D. S., ... & Lee, Y. J.** (2007). Dependence of material quality on performance of flexible transparent conducting films with single-walled carbon nanotubes. *Nano*, *2*(03), 157-167.

[96] **Kiriya, D., Chen, K., Ota, H., Lin, Y., Zhao, P., Yu, Z., ... & Javey, A.** (2014). Design of Surfactant–Substrate Interactions for Roll-to-Roll Assembly of Carbon Nanotubes for Thin-Film Transistors. *Journal of the American Chemical Society*, *136*(31), 11188-11194.

[97] **Usrey, M. L., Chaffee, A., Jeng, E. S., & Strano, M. S**. (2009). Application of polymer solubility theory to solution phase dispersion of single-walled carbon nanotubes. *The Journal of Physical Chemistry C*, *113*(22), 9532-9540.

[98] **Kaempgen, M., Duesberg, G. S., & Roth, S.** (2005). Transparent carbon nanotube coatings. *Applied Surface Science*, *252*(2), 425-429

[100] **Ko, H., & Tsukruk, V. V.** (2006). Liquid-crystalline processing of highly oriented carbon nanotube arrays for thin-film transistors. *Nano letters*, *6*(7), 1443-1448.

[101] **Kilbride, B. E., Coleman, J. N., Fraysse, J., Fournet, P., Cadek, M., Drury, A., ... & Blau, W. J.** (2002). Experimental observation of scaling laws for alternating current and direct current conductivity in polymer-carbon nanotube composite thin films. *Journal of Applied Physics*, *92*(7), 4024-4030.

[102] **Karatepe, N., & Yuca, N.** (2011). Hydrogen adsorption on carbon nanotubes purified by different methods. *International journal of hydrogen energy*, *36*(17), 11467-11473.

[103] **Maiaugree, W., Pimanpang, S., Towannang, M., Saekow, S., Jarernboon, W., & Amornkitbamrung, V.** (2012). Optimization of TiO 2 nanoparticle mixed PEDOT–PSS counter electrodes for high efficiency dye sensitized solar cell.*Journal of Non-Crystalline Solids*, *358*(17), 2489-2495.

[104] **Yun, D. J., Ra, H., & Rhee, S. W.** (2013). Concentration effect of multiwalled carbon nanotube and poly (3, 4-ethylenedioxythiophene) polymerized with poly (4-styrenesulfonate) conjugated film on the catalytic activity for counter electrode in dye sensitized solar cells. *Renewable Energy*, *50*, 692-700.

CURRICULUM VITAE

Name Surname	:Mozhgan LAKI
Place and Date of Birth	: Iran 1989
E-Mail	:laki.mojgan@gmail.com

EDUCATION:

B.Sc.	: Optics and Laser Engineering
	Islamic Azad University, Science and Research Branch

PROFESSIONAL EXPERIENCE:

Project Assistant at Energy Institute of Istanbul Technical University

Project Title: "Development of Carbon Nanotube Based Organic Solar Cells with High efficiency" Supported by: The Scientific and Technological Research Council of Turkey (TUBITAK)

PUBLICATIONS, PRESENTATIONS AND PATENTS ON THE THESIS:

- **LAKI, M.**, TABATABAİ A., YAVUZ, N., ARICI E."High Purity Single Walled Carbon Nanotubes as Transparent Electrode Materials*" 3rd Turkish Solar Electricity Conference and Exhibition*, 27-29 April 2015 Middle East Technical University, Ankara

- **LAKI, M.**, TABATABAİ A., YAVUZ, N., ARICI E.""Carbon nanotubes as electrodes for solar cells". *1st Ulusal Karbon Konferansı* 12-13 Mart, 2015 Istanbul Technical university, Istanbul